RWTH AACHEN UNIVERSITY

HELMHOLTZ-INSTITUTE FOR BIOMEDICAL ENGINEERING
RWTH AACHEN

CHAIR FOR MEDICAL INFORMATION TECHNOLOGY
Univ.-Prof. Dr.-Ing. Dr. med. Steffen Leonhardt

Development of a Capacitive Bioimpedance Measurement System

Daniel Gomez Abad

Supervisors: Dipl.-Ing. Benjamin Eilebrecht
M.Sc. Guillermo Medrano

24. August 2009

Pauwelsstraße 20
D-52074 Aachen

Phone: +49 (0)241 80 -23211
Fax: +49 (0)241 80 -82442
E-Mail: medit@hia.rwth-aachen.de

Declaration

I declare that, to the best of my knowledge and belief, this assignment is my own work, all sources have been properly acknowledged, and the assignment contains no plagiarism. I did not use any other medium than the ones quoted by me.

Place, Date

Signature

A mi familia y amigos

'If I have seen further, it is by standing on the shoulders of giants'.
Sir Isaac Newton (1643-1727)

Abstract

Bioelectrical impedance spectroscopy (BIS) is a well-established and non-invasive method to determine and monitor body composition. Commercially available bioelectrical impedance systems use coated hydrogel-aluminium electrodes, where the hydrogel acts as an adhesive and as an electrolytic medium. The gel/adhesive is physiologically inert over short periods. However, when used over longer periods, hydrogel-aluminium electrodes present limitations, which capacitive electrodes may overcome. First measurements using capacitive electrodes have shown that commercial devices are not designed to work with these kind of electrodes. The presented high impedance, specially at low frequencies (e.g. 5kHz), presents a challenge for the current injection and therefore for the design of the current source. Within this project, a bioimpedance spectroscopy (BIS) system to perform measurements using capacitive electrodes has been developed. The system has been tested in the critical frequency range, namely in the lower frequency range (5 kHz - 43 kHz). Measurements have been performed using dummy electrical models, which simulate different values of skin and electrode impedance. The results obtained show the better performance of the device in comparison to a commercial device (Xitron Hydra 4200, Xitron Technologies) for that frequency range. An important item in this thesis has been the design of a multi-frequency current source able to perform measurements using capacitive electrodes.

Keywords:

Bioimpedance spectroscopy, capacitive measurement, capacitive electrodes, multi-frequency current source.

Contents

List of Abbreviations and Symbols

Symbol	Meaning
A	Cross sectional Area of a Cylinder $[m^2]$
A_C	Area of condensator $[m^2]$
BIS	Bioimpedance Spectroscopy
C	Capacitance $[F]$
c	Volumetric concentration of nonconductive spheres in a suspension
C_a	Circumference of an arm$[m]$
C_c	Circumference of a cylinder $[m]$
C_{elec}, C_e	Electrode Capacitance $[F]$
C_l	Circumference of a leg$[m]$
C_m	Membrance Cell Capacitance $[F]$
C_s	Capacitance presented by the skin $[F]$
C_t	Circumference of the trunk$[m]$
d	Width of the dielectric $[m]$
E_{cm}	Common mode Voltage $[V]$
E_d	Differential Voltage $[V]$
ECW	Extracellular Water $[l]$
ϵ_0	Dielectric constant $[As/Vm]$
ϵ_r	Relative dielectric constant
EIT	Electrical Impedance Tomography
f	Frequency $[Hz]$
f_c	Characteristic frequency $[Hz]$
F_c	Cut-off frequency $[Hz]$
f_s	Sampling frequency $[Hz]$
GND	Ground
H	Body height $[m]$
$I(j\omega), I(t), i(t)$	Electrical current $[A]$
ICW	Intracellular Water $[l]$
K_b	Correction factor
L	Length of a cylinder $[m]$
L_a	Length of an arm $[m]$
L_l	Length of a leg $[m]$
L_t	Length of the trunk $[m]$
Q	Quantization interval
$q(t)$	Electric Charge $[C]$
R	Resistance $[\Omega]$
R_c	Resistance of a cylinder $[\Omega]$
$R_e, R_{e(ECW)}$	Extracellular resistance $[\Omega]$
$R_i, R_{e(ICW)}$	Intracellular resistance $[\Omega]$
R_r, R_{wire}	Resistance presented by the wires $[\Omega]$

Symbol	Meaning
R_s	Resistance presented by the skin $[\Omega]$
R_k	Resistance presented by the electrode $[\Omega]$
R_0	Bioimpedance for $f \to 0$ $[\Omega]$
R_∞	Bioimpedance for $f \to \infty$ $[\Omega]$
rms	Root mean square
ρ	Specific resistivity $[\Omega m]$
ρ_a	Effective specific resistivity of a medium composed of a conductive medium with embedded non conductive spheres $[\Omega m]$
t	Time $[s]$
TBW	Total Body Water $[l]$
Θ	Phase $[rad]$
$V(j\omega), V(t), v(t)$	Electrical voltage $[V]$
V_{ECW}	Extracellular Water $[l]$
V_{ICW}	Intracellular Water $[l]$
V_{TBW}	Total Body Water $[l]$
V_b	Body Volume $[l]$
V_c	Cylinder Volume $[l]$
$Z(j\omega), Z, Z_{body}$	Impedence of the body $[\Omega]$
$Z_{electrode}$	Impedence presented by the electrode $[\Omega]$
$Z_{electrode-skin}$	Skin-Electrode Impedence $[\Omega]$
$Z_{contact}$	Resistance of the contact gel and the wires $[\Omega]$
Z_{skin}	Impedence of the skin $[\Omega]$
ω	Angular frequency $[rad]$

1 Introduction

Bioelectrical impedance spectroscopy (BIS) is a well-established and non-invasive method to determine and monitor body composition, which includes the percentage of fat, bone, muscle and fluid levels in the human body.

BIS is used to determine the bioelectrical impedance, which is a measure of the opposition of tissue to the flow of an electrically applied current. In body composition analysis, bioelectrical impedance is commonly used with custom equations (i.e. equations derived from Hanai mixture theory) to calculate Total Body Water (TBW) and its compartments intracellular water (ICW) and extracellular water (ECW).

For the measurement of the bioimpedance of the whole body, typically two electrodes will be placed on the wrist and other two placed on the ankle. Other techniques imply the measurements of segments of the body. This technique allows to study and monitor physiological variables like respiratory rate, (by means of impedance pneumography [OV70]), or tissue state [Kus92]. Furthermore, it is applied in a wide range of areas like detection of ischemia (a restriction in blood supply) [Gen05], tumours and skin cancer ([SHSP04], [Åbe04] and [BKZS04]), meningitis (an inflammation of the protective membranes covering the brain and spinal cord) [VK01] or brain cellular oedemas (an excess accumulation of water in the intracellular and/or extracellular spaces of the brain) [LDH$^+$03] and [Seo05]. The proper study and control of the mentioned health diseases point out the necessity of an exact monitoring of physiological variables.

Monitoring physiological variables during everyday life could be useful to monitor the health state of subjects suffering from determined diseases. Long-term monitoring could also be helpful to estimate the effects of treatments at home and to observe deviations in health status. Current electrodes, for BIS, ECG, etc., consist of aluminium and are covered with hydro gel, which serves as an adhesive, as well as an electrolytic medium. To maintain reliable contact to the skin, the electrolytic paste or the conductive adhesive is usually required. The gel/adhesive is physiologically inert over short periods. However, when used over long periods, it presents limitations as its interaction with the skin may produce irritation and discomfort, or in more severe cases, it can cause skin allergy and inflammation [Whe62]. Additionally, bacterial and fungal growth can take place under electrodes worn for extended periods [MDK67].

A possible solution to this problem is the use of capacitive electrodes. Due to the absence of hydro gel, capacitive electrodes feature different characteristics concerning the skin contact. They present a higher electrode-skin impedance resulting in technical limitations for existent commercial bioimpedance devices. Within the present project a system to perform BIS measurements using capacitive electrodes has been designed and implemented in order to overcome actual technological limitations.

2 Theoretical Background of Bioelectrical Impedance Spectroscopy (BIS) and Electrodes.

BIS is a technique for the determination of body composition analysis (which means the estimation of fat, bone, muscle and fluid levels in the human body). Measurements are carried out with the help of two or four conductive electrodes directly attached to the body, injecting a current into the tissue and measuring the produced difference of potential (Figure 2.1). BIS enables to study and monitor physiological variables, e.g. the fluid distribution in the body, which could be associated with different disseases, namely: tumours, meningitis or brain cellular oedema, etc.

So far, dilution methods have been the 'gold standard' for the determination of body composition, some of them are the isotopic deuterium or the bromide dilution method. Deuterium oxide (D_2O) dilution method for example is done by administering a dose of D_2O, by injection or orally, to the patient. The dose will be diluted and mixed in body water. Results are obtained by dint of analyzing the concentrations of D_2O in the body water in samples of blood, saliva or urine. This technique is invasive, expensive and cannot be repeated frequently. On the other hand, BIS is an attractive method for measuring body fluids as the procedure is simple, non-invasive, inexpensive, and the results are obtained rapidly.

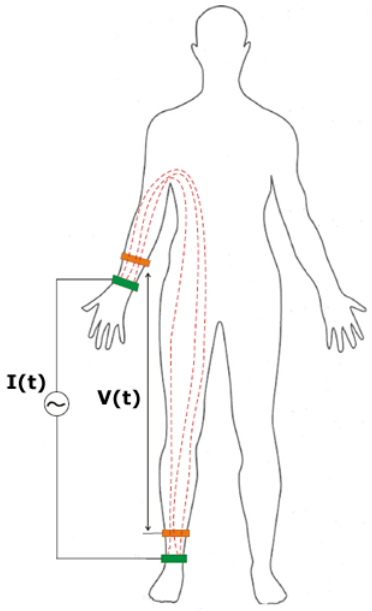

Figure 2.1: Setup of a 4-point BIS measurement, where I(t) is the injected current and V(t) the measured voltage.

2.1 Determination of Body Components

In this section it is examined how impedance can be used to actually quantify the body composition. BIS measurements usually calculate the total body water (TBW), a measure

of all the water in the body (TBW can be devided into its intracellular (ICW) and extracellular (ECW) components). From TBW again other parameters can be calculated, namely fat-free mass (FFM) and body fat.

BIS is performed in two clearly defined steps. In the first step, model parameters are obtained from an electrical equivalent model of the body. In the second step, those parameters are used in equations to predict the intra- and extracellular water content and thus the total water content of the body.

2.1.1 First Step: Modelling. The Cole-Cole Model

Modelling serves to analyse the individual components of the body. As described previously, impedance (Z) could be represented as a combination of two components, resistance (R, real part of Z) and reactance (X_c, imaginary part of Z). The components of the body may show a resistive or reactive behaviour. While the cellular membrane, due to its lipid layer presents a capacitive/reactive behaviour, components like blood, muscle, extracellular and intracellular fluid, will each show a predominantly resistive behaviour.

Focusing on the TBW, the content of water in human tissue can be divided into intra- and extracellular fluid, separated by the cellular membrane. According to this definition and the resistive and reactive behaviour of each component, the conduction of the current will be different for low and high frequencies. At low frequencies, current will flow around the cells, while at high frequencies current will pass through the cells, as shown in figure 2.2.

The Cole's model takes into account this behaviour and defines three different ways of representing tissue's behaviour: an equivalent electrical circuit, the corresponding equation and its complex Z plot.

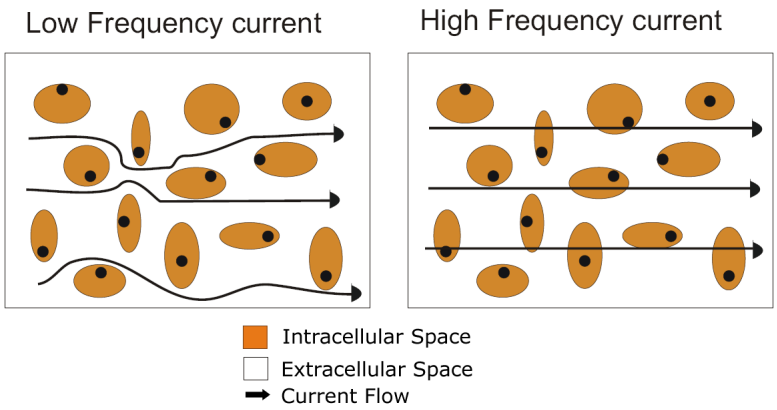

Figure 2.2: Cell behaviour in frequency.

The Equivalent Electrical Circuit

In the equivalent circuit, the resistive and capacitive behaviour of the tissue is represented by the combination of two resistors, R_i and R_e, which correspond to the ICW and ECW

respectively, and one capacitor, C_m, which represents the cell membrane. The equivalent circuit is shown in figure 2.3:

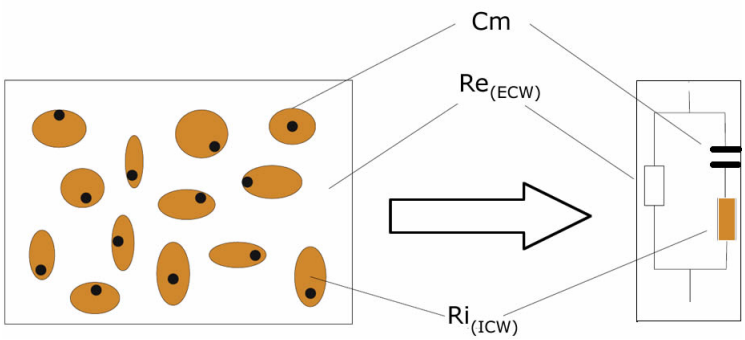

Figure 2.3: Cole-Cole Electrical Model.

The Equation

Equation 2.1 mathematically defines the relation between impedance $Z(j\omega)$ and the values of the electrical model R_e, R_i and C_m. These values can be determined by measuring body's impedance at different frequencies (ω) and solving the equation for the parallel circuit (see figure 2.3 right).

$$Z(j\omega) = \frac{R_e \times (R_i + \frac{1}{j\omega C_m})}{R_e + (R_i + \frac{1}{j\omega C_m})} \tag{2.1}$$

At DC level or low frequencies ($\omega \rightarrow 0$), current does not penetrate the cell membrane, which acts as an insulator. Hence, the capacitor behaves as an open circuit, and therefore the current only flows through the extracellular fluid, obtaining equation 2.2. At very high frequencies ($\omega \rightarrow \infty$) the capacitor behaves as a short circuit, and thus the impedance reflects the effect of the intra R_i and extracellular R_e fluid (equation 2.3). The value of R_i is obtained from equation 2.4.

$$R_e = lim_{\omega \rightarrow 0} Z(j\omega) = R_0 \tag{2.2}$$

$$R_\infty = lim_{\omega \rightarrow \infty} Z(j\omega) = \frac{R_e Ri}{Re + Ri} \tag{2.3}$$

$$R_i = lim_{\omega \rightarrow \infty} \frac{R_e \Delta Z(j\omega)}{R_e - Z(j\omega)} \tag{2.4}$$

The Complex Impedance Plot

If the impedance of the body tissue is measured over a frequency range varing from low to high frequencies, a series of complex values is obtained. The curve formed by these points

in the Real-Imaginary plane is a semicircle of complex impedance (figure 2.4), and its shape is a result of the electrical and structural characteristics of the tissue.

The complex plot depicts the behaviour of the equivalent circuit. At DC level the current would only flow through the ECW, hence the impedance value $R_e = R_0$ is obtained. At the characteristic frequency (f_c), X_c reaches the maximum value. At infinite frequency, the limit resistance R_∞ is obtained where the current would flow through both ICW and ECW solution.

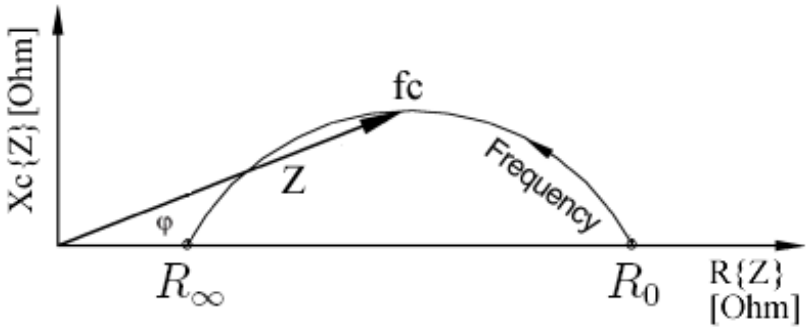

Figure 2.4: The Complex Plot

In order to calculate the parameters R_e, R_i and C_m, frequencies between 5 kHz and 1 MHz are used instead 0 and ∞. In addition, extrapolation and curve fitting methods (see figure 2.5) are used to calculate the parameters of the Cole-Cole model.

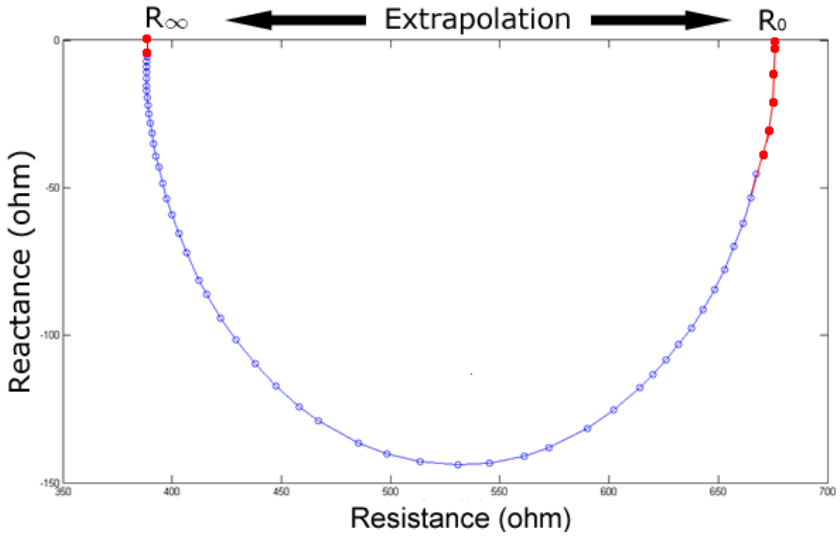

Figure 2.5: Extrapolation and curve fitting methods

2.1.2 Second Step: Determination of ECW and ICW

In order to determine the ECW and ICW, and subsequently to obtain the TBW, using bioimpedance methods, volumes are estimated from the modelled R_e and R_i using equations formulated from Hanai's theory (equation 2.6).

Firstly, the human body is modelled as the sum of five cylindrical volumes (figure 2.6 left): two representing the legs, two the arms and one the trunk [DLAMW97]. Although the parts of the body are not uniform cylinders and their conductivities are not constant, a relationship can be established between the impedance and the water volume. The cylinder model establishes a relation (equation 2.5) between its geometry and its resistance (R_c). In this model, the impedance of a cylinder is proportional to its length (L) and inversely proportional to its cross sectional area (A) (see figure 2.6 right).

$$R_c \propto \frac{L}{A} = \frac{L^2}{V_c} \tag{2.5}$$

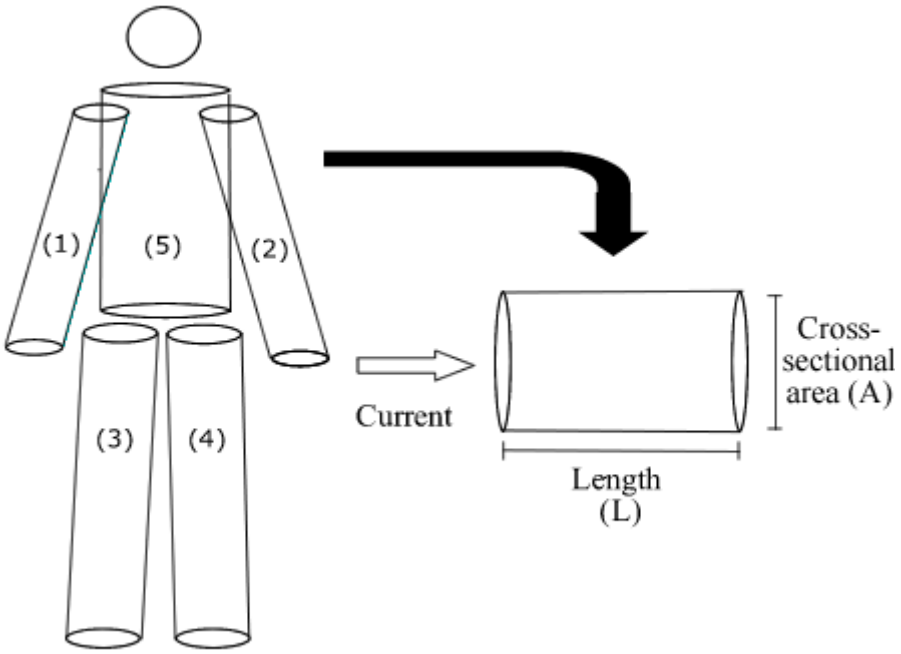

Figure 2.6: Left: Representation of the body as five cylinder. Right: Geometric parameters of a cylinder.

According to Hanai's theory, the effective specific resistivity of a medium composed of a conductive medium with embedded non conductive spheres (ρ_a) will be affected by the partial volume (c) occupied by the non conductive spheres:

$$\rho_a = \frac{\rho}{(1-c)^{\frac{3}{2}}} \tag{2.6}$$

Where ρ is the specific resistivity of the conductive medium (Ωm) and c is the volumetric concentration of the nonconductive material in the mixture.

Thus the resistance of a single cylinder (equation 2.5) can be expressed more precisely, if the specific resistivity of the cylinder (ρ_a) is included. Then, the resistance is expressed by equation 2.7.

$$R_c = \rho_a \times \frac{L}{A} = \rho_a \frac{L^2}{V_c} \tag{2.7}$$

Where V_c represents the cylinder volume.

Hence, the body volume in terms of impedance is defined as:

$$V_b = \rho_a \frac{L^2}{Z} \tag{2.8}$$

If now the whole body is considered with the five cylinder model, equation 2.9 is obtained from equation 2.7 in terms of the cylinder length and circumference.

$$R = \rho_a \frac{4\pi L}{C_c^2} \tag{2.9}$$

Where 'C_c' is the circumference of the cylinder and 'L' its length. The volume of the cylinder is given by:

$$V_c = \frac{LC_c^2}{4\pi} \tag{2.10}$$

If we consider the body to be formed by five cylinders (legs, arms and trunk), then its volume can be expressed by:

$$V_b = 2(\frac{L_a C_a^2}{4\pi}) + 2(\frac{L_l C_l^2}{4\pi}) + 2(\frac{L_t C_t^2}{4\pi}) \tag{2.11}$$

Where V_b is the body volume in m^3,L_a and C_a are the length and circumference of an arm, L_l and C_l are the length and circumference of a leg, and L_t and C_t are the length and circumference of the trunk.

Equation 2.11 is a complex equation dependending on arm, leg and trunk parameters. In [DLAMW97], a simplified equation for this application is described. It uses a dimensionless shape factor K_b, which relates the relative proportions of the leg, arm, torso and height. Using this new factor the impedance-volume equation turns into:

$$Z = K_b \rho_a \frac{H^2}{V_b} \tag{2.12}$$

Where H is the body height. K_b can be set according to standard anthropometric ratios and is not dependent on the electrical parameters of the body.

Total Body Water, Extra and Intra Cellular Water

In this last step, ECW and ICW are obtained from the combination of all the previously explained concepts: Cole-Cole models, Hanai Theory [HAN68] and the five cylindrical volume concept of the human body.

In order to calculate V_{ECW}, first it is needed to express equation 2.6 for low frequencies, obtaining:

$$\rho_a = \rho_{ECW}(\frac{V_b}{V_{ECW}})^{\frac{3}{2}} \tag{2.13}$$

Finally, from equation 2.13 and the volume fraction of nonconducting elements in the body at low frequency (equation 2.14), the value of V_{ECW} is calculated with equation 2.15.

$$c = 1 - \frac{V_{ECW}}{V_b} \tag{2.14}$$

$$V_{ECW} = (K_b \rho_{ECW} \frac{H^2}{R_e})^{\frac{2}{3}} V_b^{\frac{1}{3}} \tag{2.15}$$

Where R_e is the value of the fitted model parameter (Ω), H is the body height, K_b is an anthropometric factor and V_b is the body volume.

Similarly, V_{ICW} can be obtained from the combination and substitution of ρ_a of TBW, c and the resistance of the body equations at high frequencies. The relation of V_{ECW} and V_{ICW} is described by:

$$(1 + \frac{V_{ICW}}{V_{ECW}})^{\frac{5}{2}} = \frac{R_e + R_i}{R_i}(1 + K_b \frac{V_{ICW}}{V_{ECW}}) \tag{2.16}$$

Another equation for determining the intracellular fluid volume was reported by Matthie [Mat05] as:

$$V_{ICW} = V_{ECW} \left[\left[\frac{\rho_{TBW}(R_e + R_i)}{\rho_{ECW} R_i} \right]^{\frac{2}{3}} - 1 \right] \tag{2.17}$$

The total body water volume can easily be calculated at this point by:

$$V_{TBW} = V_{ICW} + V_{ECW} \tag{2.18}$$

2.2 The BIS Testing Procedure

2.2.1 General Approaches

The actual BIS procedure requires measurements taken under controlled conditions. Several factors may affect the measurement of impedance, from technical ones like exact placement of the electrodes or necessary wiring to dependencies on body parameters like:

- Hydration. Patients which had ingested a high quantity of fluids may become over-hydrated. This may increase the conductivity, resulting in a low and inaccurate percent of relative body fat.
- Distribution of water (after a patient has been lying down for more than a few minutes, his fluids tend to 'settle'. This settling of body fluids may result in unpredictable changes in impedance, and false body composition results).
- Orientation of the tissues.

In order to control these and other factors (e.g. room temperature), measurements must be done by technical personnel [MOD07], and under laboratory conditions.

In the procedure, a current of 500 $\mu A_{peak-to-peak}$ (700 μA_{rms}) is generated according to standard EN60601 (figure 2.7), at frequencies from 5 kHz to 1 MHz. In the working frequency range the injected current must be bellow a value from 500 $\mu A_{peak-to-peak}$ to 10 $mA_{peak-to-peak}$, in order to ensure that the induced potential on the heart is significantly below the levels expected to induce fibrillation. With the tetra polar configuration, two electrodes inject the current I(t), while the measuring two electrodes sense the corresponding voltage V(t).

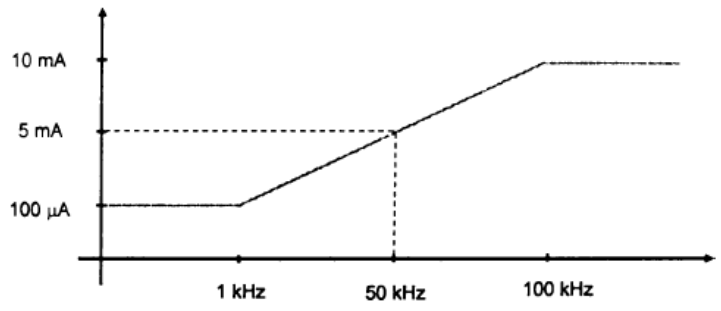

Figure 2.7: Permissible current through the body extracted from Standard EN60601. Frequency versus current injected

Measurements are taken in a lying position, with the electrodes placed on wrist and ankle as shown in figure 2.1. The distance and placement of the electrodes affects the measurement, e.g. the placement of the electrodes close to the joints will lead to an error, due to the high impedance at this part of the body. In addition, higher accuracy is obtained if the electrodes

are placed on the body with the greatest allowable distance, since the supplied current will take the longest possible path through the body.

Most of the actual BIS procedures use a tetra polar configuration (i.e. four electrodes are used), overcoming the influence of the skin-impedance in the measurement, which appears in a bipolar (using two electrodes) configuration.

2.2.2 Bipolar Configuration

In figure 2.8 a two-electrode measurement and its equivalent electrical circuit is depicted. In bipolar configuration, when a known current flows through an unknown load resistance, this unknown resistance is calculated by measuring the voltage that appears across it, divided by the injected current [HF09]. When a 2-electrode setup is used, the sensed voltage is measured not only across the unknown resistance, but also the resistance of the wires and contacts. In terms of bioimpedance measurement, not only the impedance of the body (Z_{body}) is measured but additionally the impedance of body, skin, wires and electrode impedances. In the following the combination of the skin, leads and electrode impedance is defined as $Z_{electrode-skin}$.

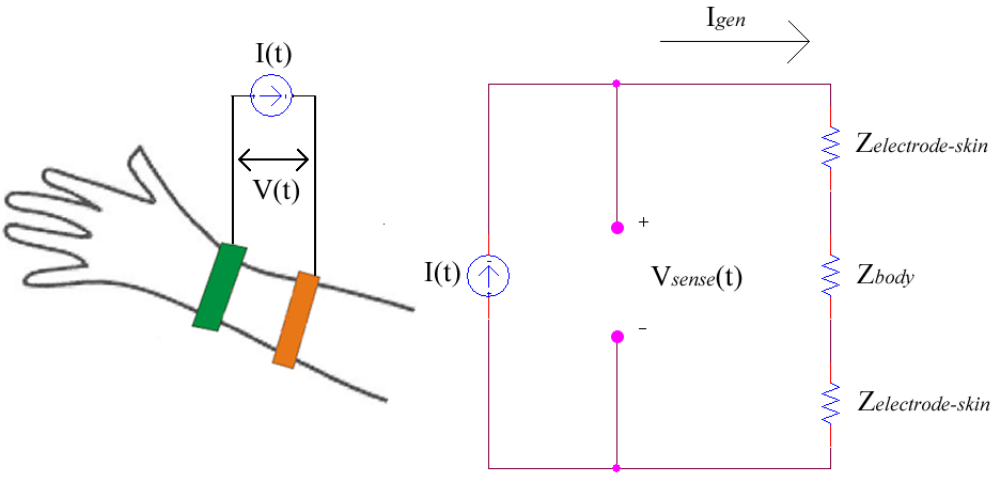

Figure 2.8: Bipolar Configuration

The electrical circuit, shown in figure 2.8 right, describes the two-electrode measurement. Equation 2.19 defines the measured impedance:

$$Z_{total-measured} = \frac{V_{sense}}{I_{gen}} = \frac{I_{gen}(2 \times Z_{electrode-skin} + Z_{body})}{I_{gen}} \tag{2.19}$$

The additional impedance, $Z_{electrode-skin}$, will introduce errors in the measurement. For this reason, a two-electrode measurement is not a suitable method.

2.2.3 Tetra Polar Configuration

A solution to the mentioned problem is a four-electrode configuration. As shown in figure 2.9, a second set of electrodes is used. In this configuration, the part that provides the voltage measurement presents a high input impedance, hence negligible current flows into the probes ($Z_{electrode-skin_3}$ and $Z_{electrode-skin_4}$), and only the voltage drop across the load resistance is measured. As a result, the impedance measurement is more accurate.

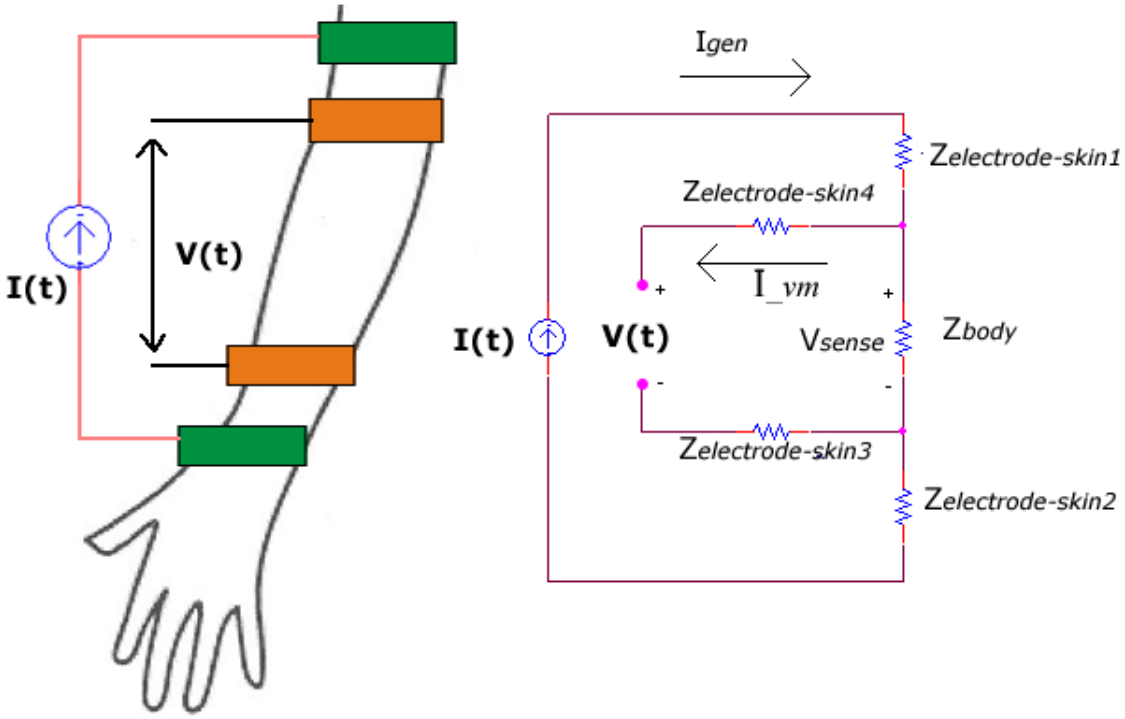

Figure 2.9: Tetra Polar Configuration.

The equivalent electrical circuit, shown in figure 2.9 right, describes a four-electrode configuration, from which equation 2.20 can be deduced to calculate the impedance.

$$Z_{total} = \frac{V_{(t)}}{I_{gen}} = \frac{(I_{gen} - I_{vm})Z_{body} + I_{vm}(Z_{electrode-skin_3} + Z_{electrode-skin_4})}{I_{gen}} \tag{2.20}$$

Due to the high impedance presented by the measurement part of the circuit, the amount of current flows through the measuring electrodes can be approximated to zero($I_{vm} = 0$).

Finally, one obtains that the measured impedance corresponds to Z_{body} is 2.21:

$$Z_{body} = \frac{V_{sense}}{I_{gen}} = \frac{I_{gen}Z_{body}}{I_{gen}} \tag{2.21}$$

2.3 Electrodes in BIS Measurements

BIS measurements can be divided into two types based on the manner in which electric current is applied to the tissue and potential differences are measured: one uses a galvanic contact approach and the second uses a capacitive-coupling approach. The term 'galvanic contact' implies that the electrodes are in contact with the skin and there is a direct transfer of electric current between the current electrodes and the tissue. On the other hand, in a capacitive-coupling measurement a metal-conducting isolated plate is placed in contact with the body's surface. This plate and the body's surface form a capacitor and the electric signal can be derived over it. The developed system is based on the use of capacitive electrodes.

2.3.1 Galvanic-Contact Electrodes (Conductive Electrodes)

Nowadays, commercially available electrodes consist of aluminium or silver and are covered with hydrogel, which serves as an adhesive between the electrodes and the skin and as an electrolytic medium. To maintain correct contact with the skin, an electrolytic paste or the conductive adhesive is usually required; this establishes a low-resistive contact with the subject [DP72].

The gel/adhesive is physiologically inert over short periods. However, when used over long periods, it presents limitations. Thus, when the electrolyte dries, the skin-electrode resistance increases [Whe62]. Another disadvantage of the conductive electrode can be found in its electrical behaviour; shifts in electrode potential appear at the electrode-skin coupling as DC drift, particularly if the subject moves [GH74]. In addition, long-term measurements using this method could cause irritation, discomfort, skin allergy and inflammation [Whe62]; also, bacterial and fungal growth can take place under electrodes worn for extended periods [MDK67]; these are disadvantages for the daily use, because practical interfaces must be as non-invasive and nonintrusive as possible to gain acceptance from users [MED07].

A simplified equivalent circuit for an aluminium standard electrode, using passive components, can be found in figure 2.10. In this model, $Z_{skin-elektrode-Total}$ is composed of three impedances in a serial configuration ($Z_{skin-electrode-Total} = Z_{skin} + Z_{contact} + Z_{electrode}$). The values for Z_{skin}, between 56 Ω and 1916 Ω, are determined from [RCR+98]. The value of the contact impedance, $Z_{contact}$, corresponds to the resistive behaviour of the hydro gel and the wires.

2.3.2 Capacitively-coupled electrodes

A possible solution to the disadvantages that standard electrodes present, is the use of capacitive electrodes. Due to the lack of hydro gel, capacitive electrodes have a different behaviour concerning the skin contact. An insulated capacitively coupled electrode has two primary advantages over a galvanic-contact electrode: it can be used without paste on the unprepared skin and it is immune to voltage drifts that could appear because of the electrode-skin resistance [DP72]. On the other hand, it is more sensitive to movements of a patient.

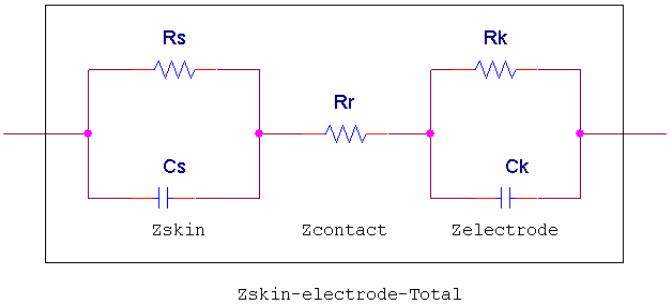

Figure 2.10: Equivalent Circuit Standard Aluminium Electrode. ([Hof08])

The biggest complication in the fabrication of capacitively-coupled electrodes is to obtain a high-quality dielectric layer on the surface of the conducting plate. This plate forms a capacitor with the body's surface through which the electrical signal is transmitted. The characteristics of an electrode depend on the properties of the dielectric, the resistance of the clothes, the noise levels, the range of frequencies transmitted, etc [GY84]. A literature review indicates that the dielectric layer should meet some requirements like it must be nontoxic and chemically stable with respect to the skin; it must have good adhesion and mechanical strength; it must have the highest possible dielectric constant and the least thickness, among others. Not all known dielectrics meet these conditions and can be used to fabricate capacitive electrodes.

A simplified electrical circuit of the skin-electrode impedance for a Capacitive Electrode can be seen in figure 2.11 In this model, $Z_{skin-electrode-Total}$ is composed of three impedances in a serial configuration ($Z_{skin-electrode-Total} = Z_{skin} + Z_{contact} + Z_{electrode}$). The electrical behaviour of the electrode is mainly capacitive, so $Z_{electrode}$ can be simplified by a single capacitance, C_k. $Z_{contact}$ in this case just includes the resistance of the wire ($Z_{contact} = R_{wire} = R_r$), since no hydro gel is used.

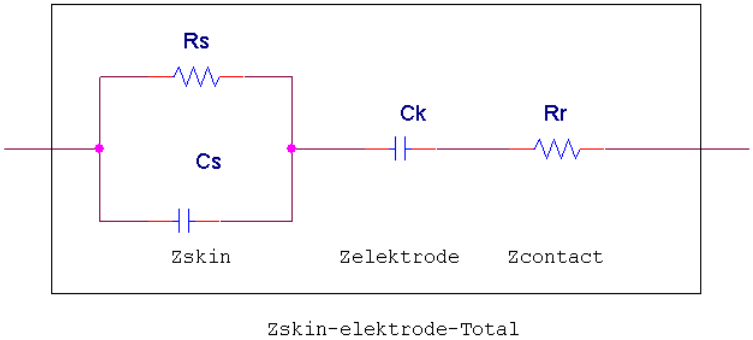

Figure 2.11: Equivalent Circuit Capacitive Electrode ([Hof08])

3 Analysis of the Actual Technology

The aim of this chapter is to show the limitations of the actual commercial technology to perform BIS measurements using capacitive electrodes, as reported in [Hof08], and to propose a possible solution to be implemented. In his work, Hoffmann [Hof08] carried out a four point measurement using four self-designed capacitve electrodes and the commercialised BIS device Hydra 4200, from Xitron Technologies. Hoffmann's tests were carried out in two clear stages. In a first stage, measurements were taken as above mentioned and using the combination of self-designed capacitive electrodes and standard aluminium electrodes connected to a volunteer's forearm (figure 3.1 right). In a second stage, measurements were performed using a dummy circuit (figure 3.1 left) simulating the body, capacitive electrodes were simulated by using variable capacitors in order to observe how the BIS measurement behaves with different capacitive electrode values.

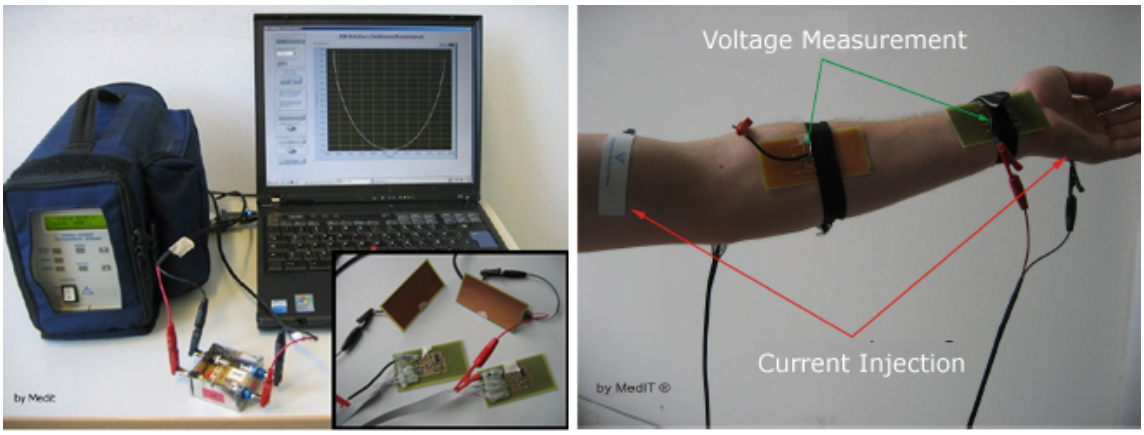

Figure 3.1: Hoffman Measurements, from [Hof08]

The following sections will explain the different parts involved in Hoffmann's [Hof08] tests, starting with the designed capacitive electrodes.

3.1 Designed Capacitive Electrodes for BIS Measurements

In Hoffmann's test active and passive capacitive electrodes were used. In the first case (active electrodes), an active element (Operational Amplifier) is involved, whereas on the second case (passive electrodes) no active element is involved. Figure 3.2 shows the electrode configuration used in the bioelectrical impedance test, where the current is injected through the passive and the voltage is sensed by the active electrodes.

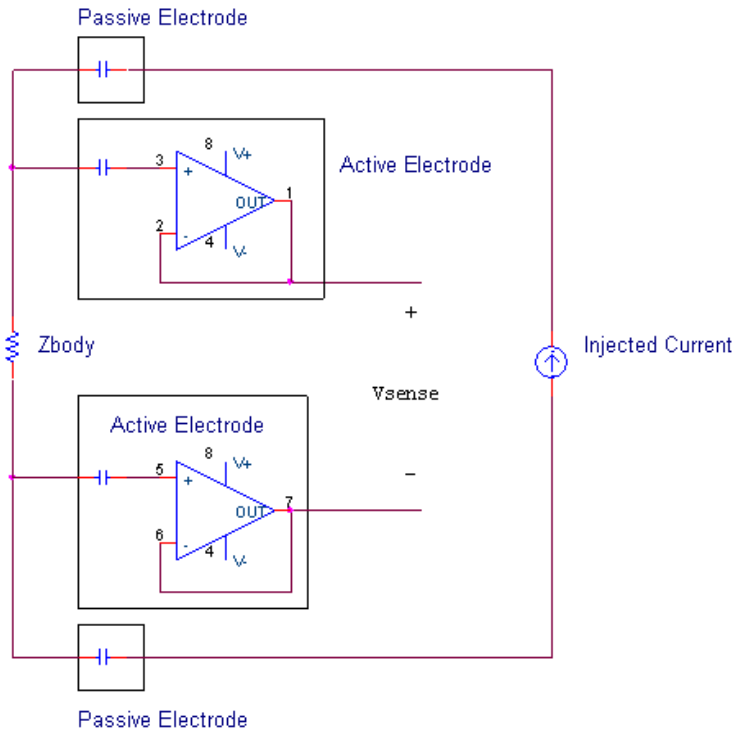

Figure 3.2: BIS Test with Active and Pasive Electrodes.

3.1.1 Electrode Design

The electrodes were fabricated as a double layer (two sides) printed circuit board. For the passive capacitive electrodes, the capacitor plate is directly connected to the cables of the BIS-device while for the active electrodes, one side serves as an electrode plate, the other side is for the circuit and the connection of the cables to the device. The capacitor plate is electrically connected to the circuit through a hole. Figure 3.3 shows both electrode designs.

On the active electrodes, two different types of operational amplifiers were tested for the electrical part (voltage follower): The OPA124 Precision Amplifiers, from Texas Instrument and the TL074 Low-Noise amplifier, from ST Microelectronics. The capacitor plate of the active electrodes is connected (through a hole in the plate) with the input of a voltage follower. The voltage follower is used to obtain high input impedance on the voltage path, so obtaining a low leakage current going through the voltage path and thus reducing the influence on the measurement.

Due to design specifications the active electrodes can only be used for measurements, whereas the passive electrodes can be used for voltage measurements and current injection.

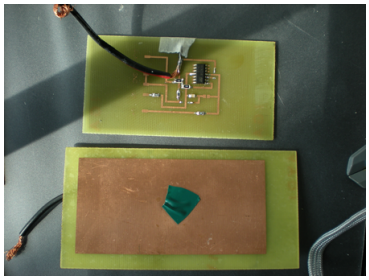

Figure 3.3: Built active capacitve electrodes

3.1.2 Dielectric Layer

The electrode surface is made of copper which is covered with a very thin layer of the 'synthetic resin'(protective paint), Kontakt Chemie Plastik 70 (CRS Industries GmbH). The thickness (d) of this layer is about 20 μm and has a relative dielectric constant (ϵ) of 2.3. The equivalent resistance of this thin isolating layer is calculated in equation 3.1 with the size of the plate A of 32 cm^2 and the specific resistance (ρ) of the synthetic resin' which is found at the product specifications.

$$R_{Dielec} = \frac{\rho d}{A} = 1.25 \times 10^{12} \Omega \tag{3.1}$$

The plate area was chosen to be $A = 32\ cm^2$, with a width of 4 cm and a length of 8 cm. It is desired that the size of the electrode is as big as possible in order to have a high capacity; however, taking into account the limited size (width and length) of a standard human arm, and avoiding the electrodes to overlap. By designing the electrodes one needs a compromise between these two factors.

Since A, d and ϵ are known one can estimate the capacity of the electrode-skin-transition (with the synthetic resin as a dielectric) with equation 3.2.

$$C_{Elec} = \epsilon_0 \epsilon_r \frac{A}{d} \tag{3.2}$$

The resulting value is 3.2 nF, although smaller values are expected due to building irregularities. As an example, depositioning the dielectric in the metal surface implies a complex method and normally irregularities appear in the surface, changing the parameters on the above-explained equations.

The size of the electrodes and the used dielectric are the same for the passive and active electrodes. Thus, the estimated value for the capacitance of the passive electrodes is also 3.2 nF.

3.2 Commercial Device Xitron Hydra 4200

The Hydra 4200 is a 3rd generation, single-channel, tetra polar BIS device for estimating ICW and ECW, TBW, FFM and fat mass (FM), in healthy individuals. Its accuracy compared to the dilution methods has been reported numerous times in scientific journals. Some specifications extracted from the Hydra brochure are:

- Frequency range: 5 to 1000 kHz
- Number of frequencies: 50
- Impedance range: 100 to 1000 Ω
- Phase resolution: 0.01°

3.3 The Dummy Circuit 'Johannes'

The dummy 'Johannes' is an electrical circuit that simulates a body segment and serves as a test circuit for BIS measurements. The circuit diagram is shown in figure 3.4. The internal structure is based on the Cole-Cole model (R_e, R_i, C_m). C_s and R_s describe the electrical behaviour of the electrode-skin interface. The values for the passive parts used in the model can be found at table 3.3.

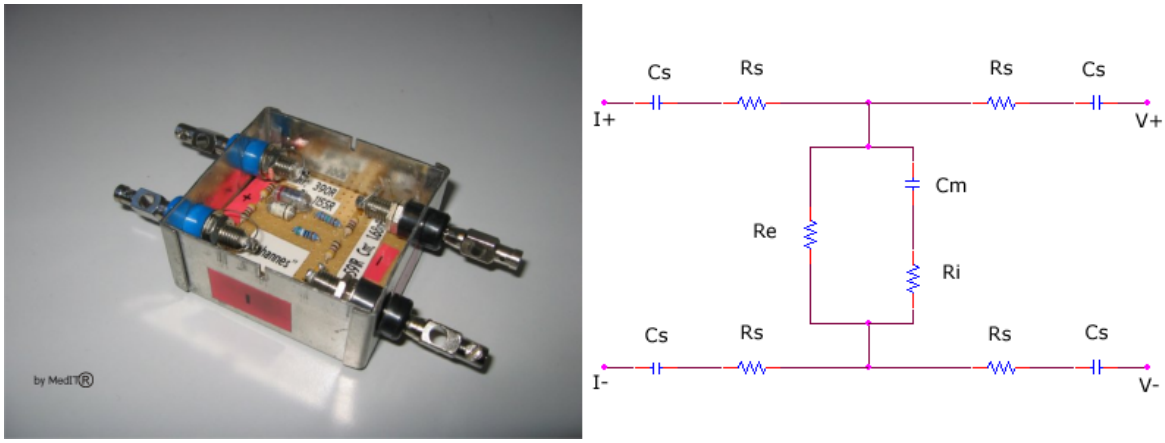

Figure 3.4: Left, dummy model Johannes. Right. Electric model.[Hof08]

Re	Ri	Cm	Rs	Cs
592 ohm	1155 ohm	1.68 nF	49.9 ohm	100 nF

Table 3.1: Dummy Model Johannes, values of the electrical equivalent circuit.

3.4 Analysis of Previous Results

In this section the tests performed in [Hof08] are analysed. Firstly, results concerning the combination of capacitive and conductive electrodes in a four-point measurement, connected to a volunteer's forearm, using the commercial device Xitron Hydra 4200 are examined. It has been noted from table 3.4 that a purely capacitive four-point measurement is not possible to be performed (see combinations No.9 and 15), since the Xitron device showed the message 'Current too low' and no results were obtained. Furthermore, it is also not possible to use two capacitive electrodes to inject the current into the body (see combinations No.7 and 8). In these cases, the Xitron also shows the error message 'Current too low'.

Nr.	Current (+)	Current (-)	Voltage (+)	Voltage (-)	BIS-Meas.
1	Cond.	Cond.	Cond.	Cond.	Meas. poss.
2	Cond.	Cond.	Cond.	**Capa.(1)**	Meas. poss.
3	Cond.	Cond.	**Capa.(1)**	**Capa.(1)**	Meas. poss.
4	Cond.	**Capa.(1)**	Cond.	Cond.	Meas. poss.
5	Cond.	**Capa.(1)**	Cond.	**Capa.(1)**	Meas. poss.
6	Cond.	**Capa.(1)**	**Capa.(1)**	**Capa.(1)**	Meas. poss.
7	**Capa.(1)**	**Capa.(1)**	Cond.	Cond.	Current too low
8	**Capa.(1)**	**Capa.(1)**	Cond.	**Capa.(1)**	Current too low
9	**Capa.(1)**	**Capa.(1)**	**Capa.(1)**	**Capa.(1)**	Current too low
10	Cond.	Cond.	Cond.	**Capa.(2)**	Current too high
11	Cond.	Cond.	**Capa.(2)**	**Capa.(2)**	Meas. poss.
12	Cond.	**Capa.(1)**	Cond.	**Capa.(2)**	Current too high
13	Cond.	**Capa.(1)**	**Capa.(2)**	**Capa.(2)**	Meas. poss.
14	**Capa.(1)**	**Capa.(1)**	Cond.	**Capa.(2)**	Current too low
15	**Capa.(1)**	**Capa.(1)**	**Capa.(2)**	**Capa.(2)**	Current too low

Table 3.2: Combination of Electrodes in Hoffmann Test. Combination of the electrodes for the BIS measurement: Cond. = conductive Electrode; Capa.(1) = passive, capacitive Electrode; Capa.(2) = active, capacitive Electrode. [Hof08]

Secondly, two measurements are analysed. The first one (figure 3.5 right) shows a BIS measurement with different values of capacitance instead of the designed capacitive electrodes in combination with the dummy model 'Johannes', in order to know the minimum capacitance value tolerated by the Xitron. The second one (figure 3.5 left) shows a BIS measurement with different values of measuring electrodes capacitances using the Xitron Hydra in combination with the dummy model 'Johannes', this test shows the influence of the measuring electrodes.

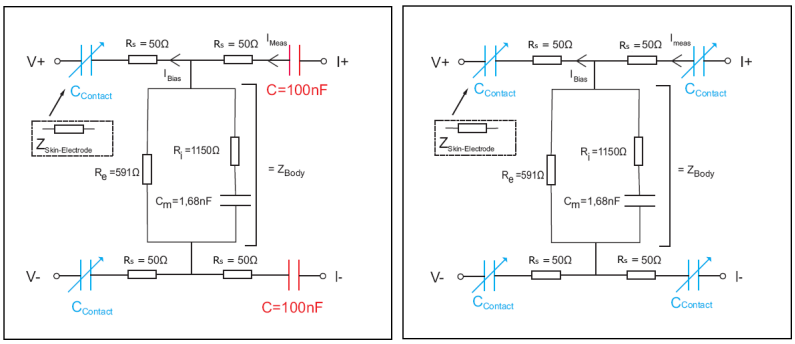

Figure 3.5: Electrode configuration for the testing of the commercial device Xitron Hydra 4200

Figure 3.6 shows the impedance plot corresponding to the first test. One can see that for capacitance values below 3.75 nF measurements are not viable ('Current too low'). It is important to emphasize that the designed capacitive electrodes have a theoretical capacitance value of 3.2 nF, hence results from table 3.4 (see No. 7) and figure 3.6 share equal conclusions. Measurements in the Xitron [Xit01] are performed using a variable current between 50 μA_{rms}(at low frequencies) and 700 μA_{rms}(at high frequencies), one can deduce that the message ('Current too low') is produced by the inability of the current source to generate the minimum current 50 μA_{rms}. One can observe two big influences in the measured impedance: first, an atenuation in the resisitive part probably produced by a voltage divider created by the combination of the impedance of the measuring electrodes and the input impedance of the differential amplifier. Second, an added impedance in the reactive part of the impedance in the low frequency range. Probably this is due to a leakage current that adds the impedance of the measuring electrodes into the impedance of the body dummy model measured.

Figure 3.7 shows the impedance plot corresponding to the second test. From the results one can observe that measurements with small values of capacitive electrodes (10 pF) can be carried out, thus one can deduce that the message ('Current too low') is produced probably by the influence of the injecting electrodes or the combination of injecting and measuring electrodes. This supposition is corroborated taking a look to combinations No.7 and 8 in table 3.4. Figure 3.7 shows the same behaviour in resistance and reactance as the one mentioned in the previous analysis.

As it has been observed the current injecting electrodes could have a big influence in the measurements, since Hoffmann [Hof08] did not reported the influence, this topic will be analysed in the validation of the designed and developed system.

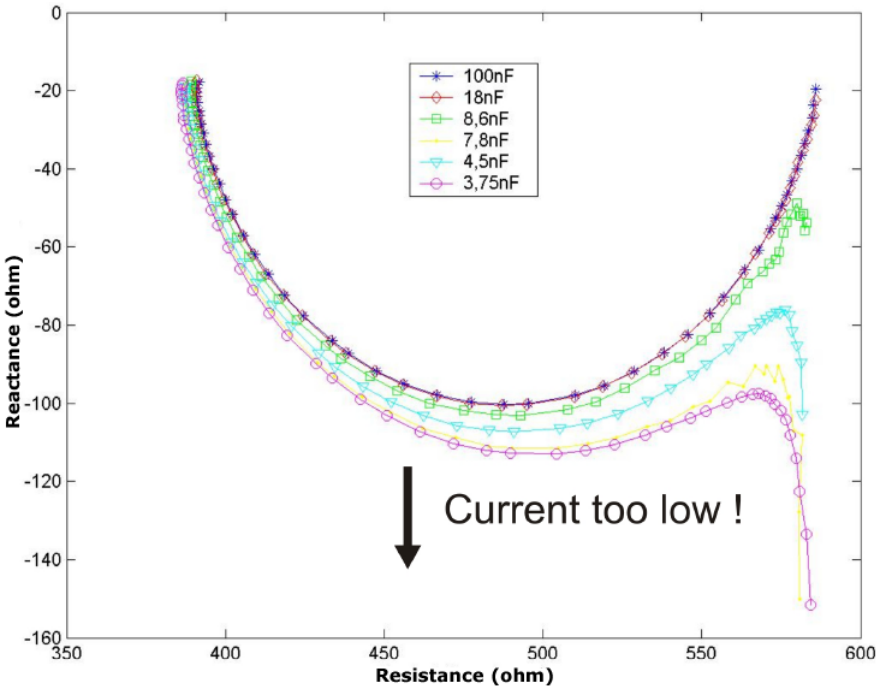

Figure 3.6: Hoffman BIS Test, with different values of injecting and measuring capacitive electrodes (all four electrodes having the same value)

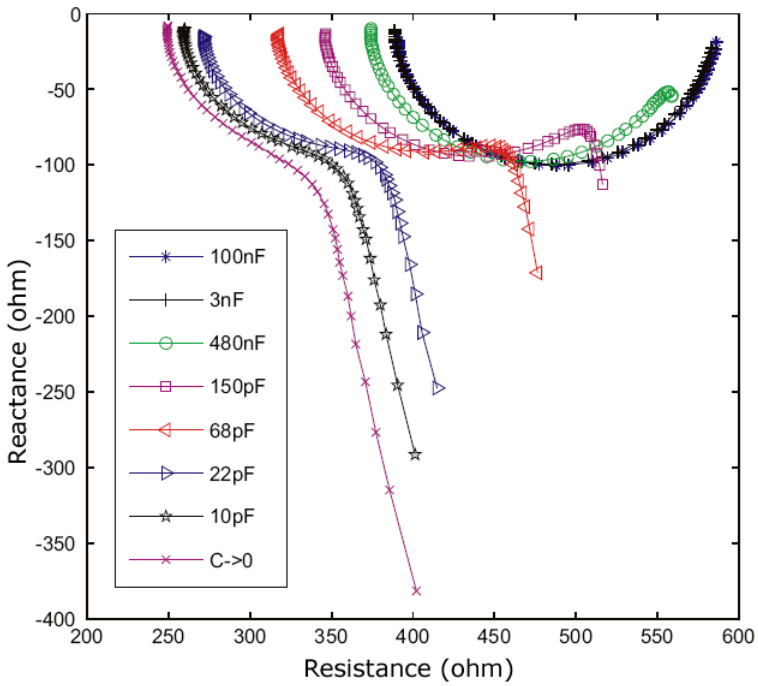

Figure 3.7: Hoffman BIS Test, with different values of measuring capacitive electrodes (both electrodes having the same value)

3.5 Proposal for a Solution

In order to explain the capacitance value limitation, a deeper study was applied to the capacitive electrodes. The study (figure 3.8) was carried out with the aid of the E4980A precision LCR meter (Agilent Technologies) and the use of agar (an unbranched polysaccharide used to make salt bridges for use in electrochemistry) in a four-point measurement, in order to determine the impedance value of the system formed by the four electrodes over the desired frequency range. Depending on the load under measurement the E4980A uses a current from $\approx 0A_{rms}$ to $\approx 10mA_{rms}$ in the frequency range from 20 Hz to $\leq 1MHz$. Since the agar presents a very small resistive behaviour, the results mainly present the impedance value of the four electrodes. It should be noted that the impedance presented by the electrodes, affects the measurements and is an additive load that the current source has to overcome in order to inject the current into the tissue. In order to obtain a better understanding, the impedance results were processed and can be seen in figures 3.9 and 3.10.

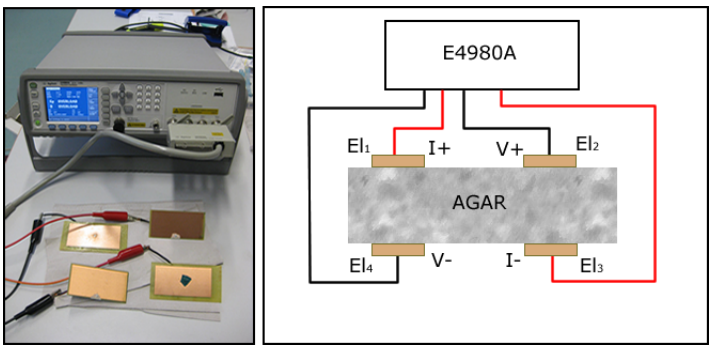

Figure 3.8: Impedance test performed to the capacitive electrodes

Figure 3.9 show the reactance presented by the system formed by the four electrodes. The value of reactance vary from -16350Ω at 5 kHz to -139Ω at 1 MHz. Form figure 3.10 one can observe that at 5kHz the resistance presented by the electrodes is 4300Ω. Thus, at low frequencies the system formed by the four electrodes is presenting a very high impedance values mainly influence by the reactive part of the impedance. This behaviour was expected since the electrodes are capacitive. Because measurements in the Xitron [Xit01] are performed using a variable current between 50 μA_{rms}(at low frequencies) and 700 μA_{rms}(at high frequencies), on can deduce that at low frequencies the current is too low (50 μA_{rms}) and the the current source is unable to overcome the high impedance presented by the electrodes. Thus the Xitron shows the message 'current to low'. From the results one can conclude that in order to control the current injected into the system and overcome the high impedance presented by the capacitive electrodes, it is important to analyse how the current behaves in a capacitor.

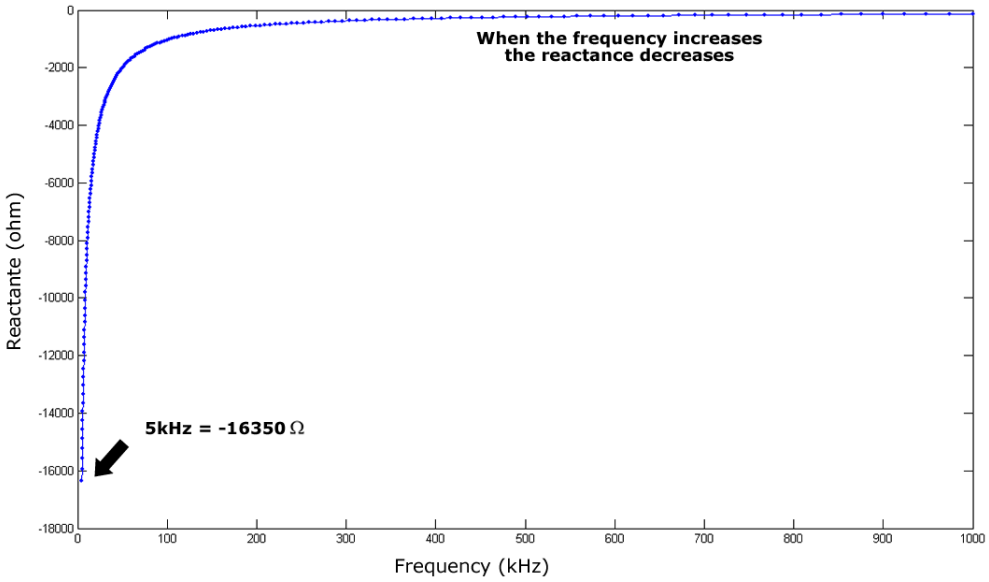

Figure 3.9: Reactance presented by the system formed by the four electrodes over the frequency 5kHz to 1MHz.

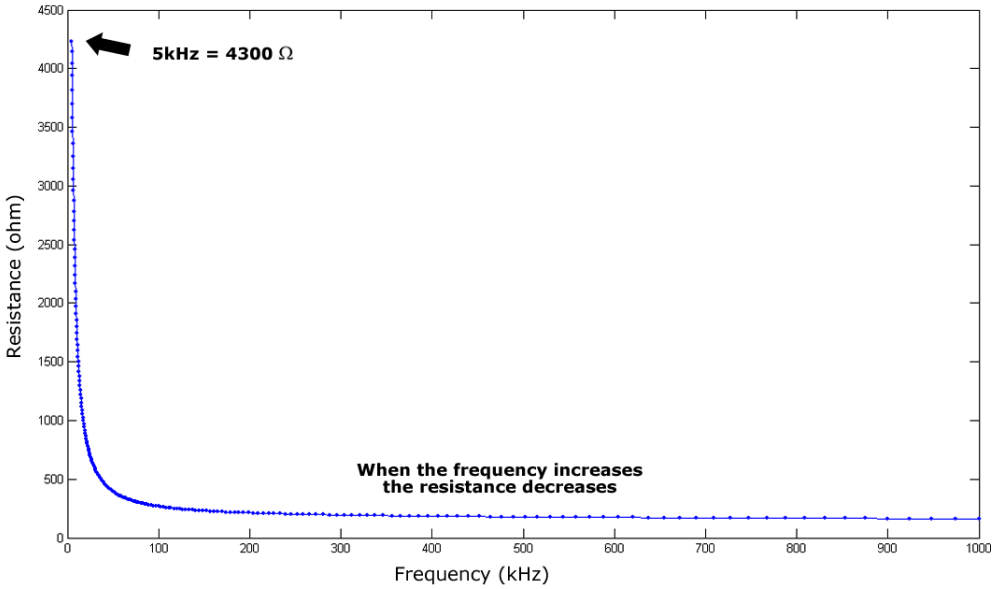

Figure 3.10: Resistance presented by the system formed by the four electrodes over the frequency 5kHz to 1MHz.

3.5.1 Theoretical Background of the Capacitor and Proposed Solution

Taking a glance at the theoretical behaviour of the capacitor for alternating current, some solutions to the limitations in the actual technology presented in [Hof08] can be deduced. A current $i(t)$ through a component in an electric circuit is defined as the rate of change of the charge $q(t)$ that has passed through it. Physical charges cannot pass through the dielectric layer of a capacitor, but rather build up in equal and opposite quantities on the electrodes: as each electron accumulates on the negative plate, one leaves the positive 'plate'.

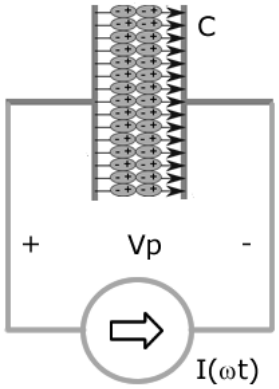

Figure 3.11: [CAP09]

Thus, the accumulated charge on the electrodes is equal to the integral of the current.

$$v(t) = \frac{q(t)}{C} = \frac{1}{C}\int i(\tau)d\tau + v(t_0) \tag{3.3}$$

The derivative form can be found as:

$$i(t) = C\frac{\partial v}{\partial t} \tag{3.4}$$

$$v(t) = V_p sin(\omega t) \tag{3.5}$$

Combining 3.4 and 3.5 we obtain 3.6.

$$i(t) = C\omega V_p cos(\omega t) \tag{3.6}$$

with:

C: constant capacitance value
ω: frequency
V_p: Voltage applied to the terminals

A capacitor is an element, which stores energy and has a limitation to sudden changes in the current, in charge and discharge. Another detail is the relation between the capacitance, the frequency, the applied voltage and the current (equation 3.6). When a voltage change occurs in the capacitor, the bigger the capacitance, the bigger the resulting current at a fixed frequency. Likewise, at a fixed voltage the bigger the frequency in the capacitor, the bigger the current.

Proposed Solution As mentioned a current of 50 μA_{rms} is very low, when the BIS device is used in combination with capacive electrodes. Thus to perform a measurement at low frequencies a higher value of current is needed. Standard EN60601 (figure 2.7) defines that at 5 kHz the injected current must have a value below 500 $\mu A_{peak-to-peak}$ to ensure that the induced potential on the heart is significantly below the levels expected to induce fibrillation. In order to obtain the desired value of current, some possibilities could be taken:

1. Increasing the area of the electrodes by consequently increasing the value of capacitance, but reaching some physical impossibilities because of the body proportions.
2. Limiting the frequency range to higher values. (The main idea was to maintain this range)
3. The voltage applied to the terminals could be varied and set to a desired value. This could be done redesigning the current source and increasing its voltage supply. Consequently permitting a wider voltage output, doing so increasing the voltage at the terminals of the capacitor.

Because the redesign of the current source does not imply a limitation in the electrodes and the range of measurement, this was the selected option. In order to determine the most appropiate voltage supply for the current source some simulations (see section 5.6) were carried out. The simulation are performed using the circuit simulation tool OrCAD PSpice 9.2. On them the selected current source is tested using different capacitance values as loads, and various voltage supplies.

4 Developed BIS system

In this chapter, the developed BIS system is explained. During the research and building process, various hardware designs were taken into account. First, the design specified in [Gar07] has been taken as a guide. However, due to technological limitations, it has been decided that commercialized hardware products should be applied (AFG3000 and NI USB-6251).

4.1 Characteristics of the System

The block diagram of the designed BIS system is shown in figure 4.1:

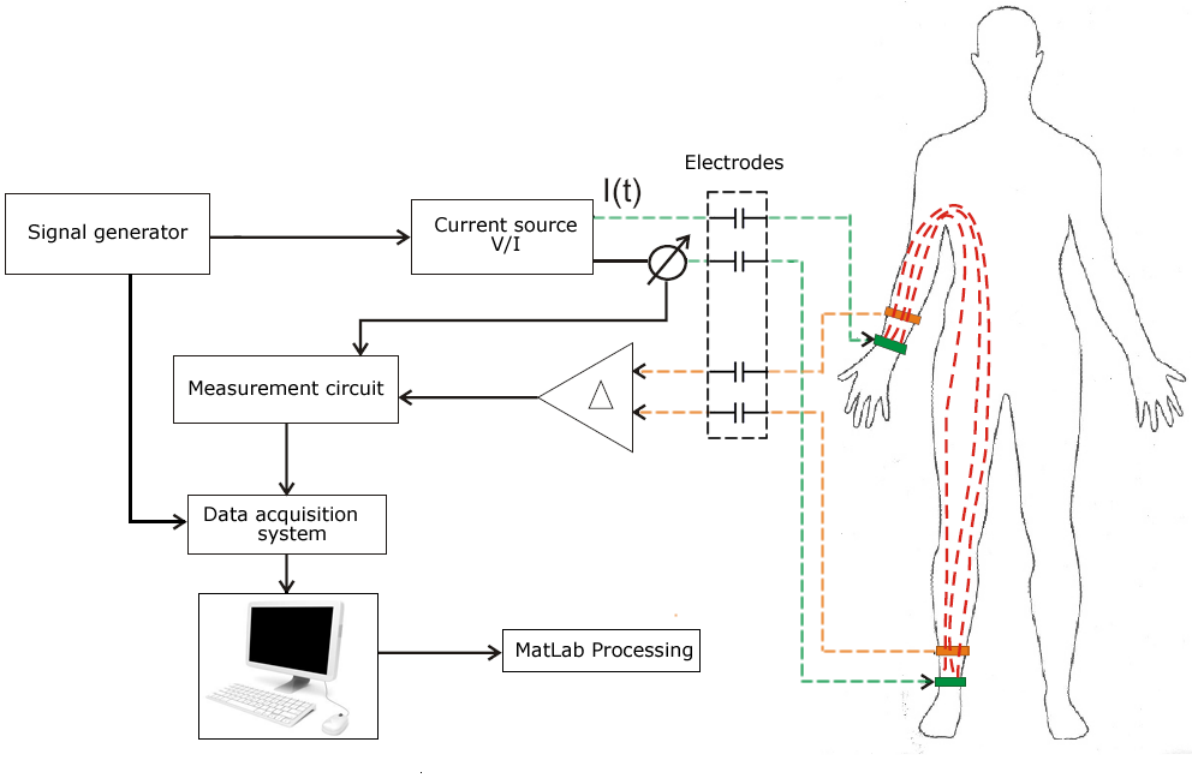

Figure 4.1: Block diagram of the designed device.

The performance of the BIS system is explained in a few steps:

1. The signal generator AFG3000, Tektronix, Inc., provides two orthogonal signals, which are used to feed the current source and secondly are sampled in order to be used in the demodulation process.

2. A current of 700 μA_{rms}, in the range of 5 to 43 kHz, is generated by the current source and injected into the electrical dummy, which simulates the human body, through capacitive electrodes.

3. The current and voltage are measured by a custom designed circuit and subsequently acquired by the Data Acquisition System NI USB-6251, National Instruments.

4. The data processing, including the demodulation and the plotting of the results, is performed with Matlab (Matlab processing block). In this block it is obtained the real and imaginary parts of the impedance Z and the cole-cole electrical parameters.

4.2 Main Elements

As explained in the previous section, the measurement process implies different processes in hardware and software design. The theoretical and working backgrounds of the parts used in the process are described in the following paragraphs. In figure 4.2 can be seen each part of the built system.

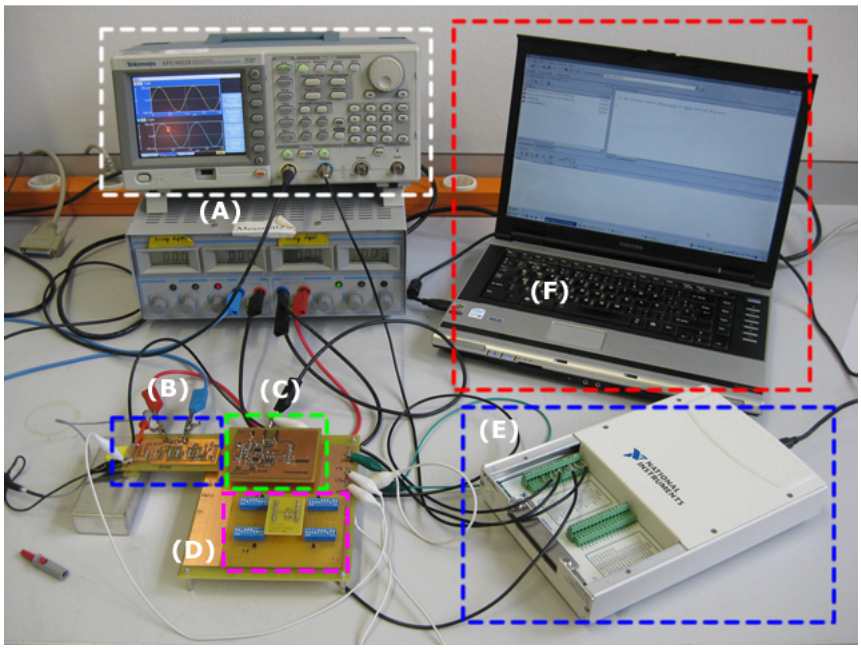

Figure 4.2: Parts involved in the developed BIS system

4.2.1 Signal Generator

For the signal generation (figure 4.2 (A)) the signal generator AFG3000, from Tektronix Inc. (figure 4.3), was selected. As mentioned, it is intended to provide the voltage for the demodulation process and for the voltage to current conversion in the current source, where the aim is to obtain a constant current of 500 μA_{p-p}. In relation to our system the main characteristics of the AFG3000 are, two output channels both used to feed the current source and in the demodulation process. Frequeny in the range of 5 kHz to 1 MHz, and phase in the range of 0° to +90.00°, to stablish both sine and cosine signals for the

demodulation. Signal amplitude in the range of 1.25 V_{p-p}, high accuracy $\pm(1\%$ of setting $+$ 1 mV). Adaptable output impedance in order to adapt correctly with the input impedance of the current source.

Figure 4.3: AFG3000, Tektronix Inc.

4.2.2 Current Source

The current generation block (figure 4.2 (B)) is one of the most important parts developed in this project. This section shows, in short, the main features that a current source for BIS measurments has to accomplish since a deeper study into this topic can be found in chapter 5. In order to develop a general current source for a BIS system, some demands have to be achieved:

- High output impedance. $Z_{out} > 1000 \times Z_{body}$ over the whole frequency range
- To overcome the resistance constituted by the capacitive electrode and the skin. In order for the current to flow into the tissues
- Constant amplitude
- Stability at different loads at the defined range [BFA99]
- Frequency stability
- Security against electric shock
- Symmetry [BH96]
- Accomplish the stadard EN60601 figure 2.7)

The research has lead to the study of a few current sources, e.g. Howland Topologies, EIT's, Max435, Tietze and Current mirror Topologies. The selection of the current source was based on the best performance in current magnitude, phase delay and output impedance on the defined frequency working range. The results of the sutdy can be found in chapter 5.

4.2.3 The electrical dummy

Due to the lack of electrical security implementation in the system, the tests were done using electrical equivalents of the body (figure 4.4), and the use of an electrical dummy (figure 4.2 (C)). In the same case, to test the accuracy of the commercial Xytron Hydra 4200 the body models were used. In figure 4.4 left, R_e, R_i and C_m represent the parameters of the Cole Cole Model for a 70 Kg, 175 cm person. The second body model correspond to a woman thorax, and the values of the Cole Cole model are $R_e = 60ohm$, $R_i = 80ohm$ and $C_m = 12.2nF$.

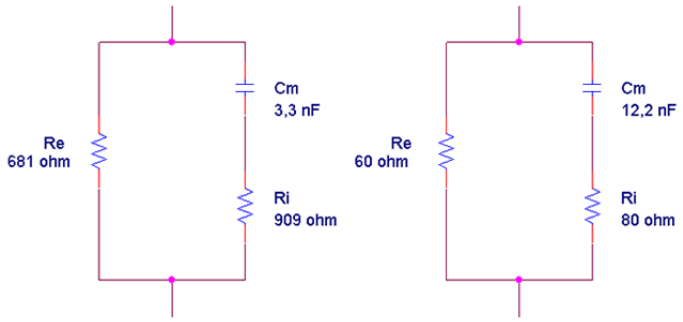

Figure 4.4: Electrical body models. Left: Whole body model. Right: Woman thorax model.

The electrical dummy simulates the values of the skin impedance (R_{skin}) and electrode capacitance (C_{elec}). The built dummy can be modified to test different value combinations. By means of some switches it is possible to modify R_{skin} and C_{elec} for the four arms of the circuit, current injection and voltage measurement. A schematic of a symmetrical arm of this dummy is shown in figure 4.5:

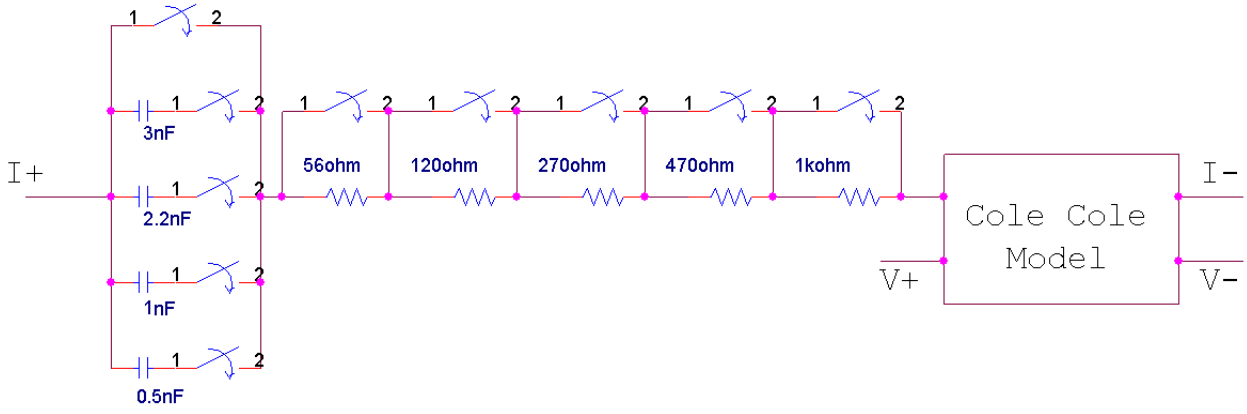

Figure 4.5: Schematic of the switch.

The whole circuit diagram can be seen in figure 4.6 right. R_1, R_2, R_3 and R_4 represent the resistive behaviour of the skin (R_{skin}) where the electrodes are placed. The values for R_{skin} (from 56 Ω to 1916 Ω) are determined from [RCR+98]. C_1, C_2, C_3 and C_4 represent the

theoretical values for the selected capacitive electrode area to test. The selected capacitive values to test were:

- 3.5 nF: Corresponds to an electrode area of 35 cm^2
- 3 nF: Corresponds to an electrode area of 30 cm^2
- 2.2 nF: Corresponds to an electrode area of 22 cm^2
- 1 nF: Corresponds to an electrode area of 10 cm^2

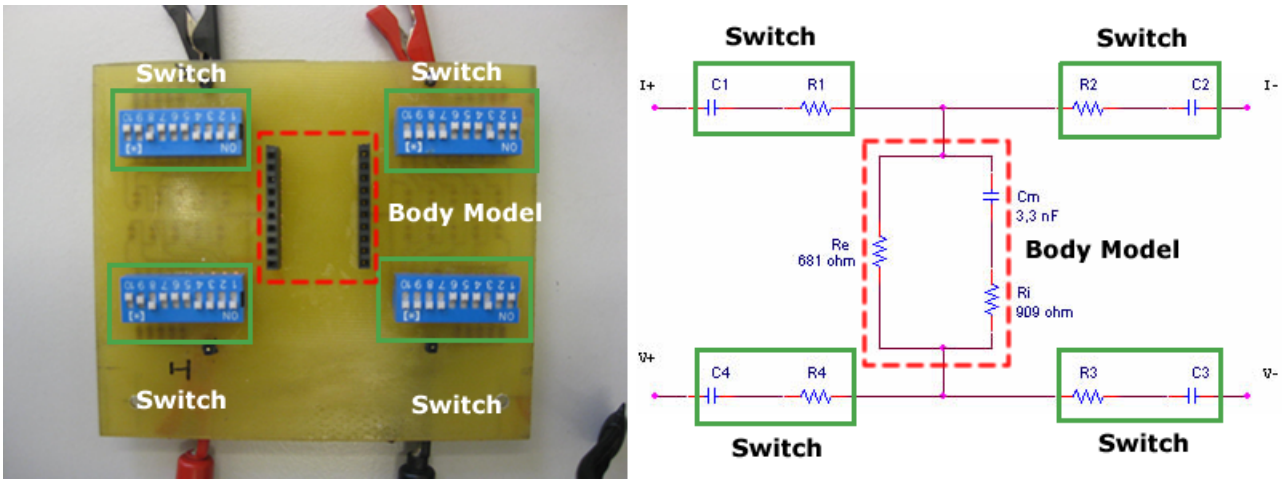

Figure 4.6: Circuit diagram of the dummy model

4.2.4 Current and Voltage Measurement

The current and voltage measurement module (figure 4.2 (D)) has been extracted from previous BIS systems developed in the MedIT group (see [MB06], [MBZ+] or [Gar07]). The circuit is divided into two branches: current and voltage measurement, each one divided into two stages, measurement and amplification. Figure 4.7 shows the basic block system for the measurement process. In the current branch, each measured milliampere will be converted into 1.7 V. Similarly in the voltage branch, each measured Volt will be converted to 1.7 Volts.

Measurement (Differential Amplifiers) In the first stage, both the voltage and the current are measured using differential amplifiers. In the case of current measurements (figure 4.8), the current source of the system is connected directly to the measurement module (I_+ from the current source). Before injecting the current into the body, the voltage drop over a high accurate 100 Ω resistor (R_1) is measured. Subsequently the current will flow through the body (Z_{body}) via the electrodes (I_+ to electrode). The measured voltage will be amplified in a next stage in order to increase the accuracy in the subsequent sampling stage (A-D

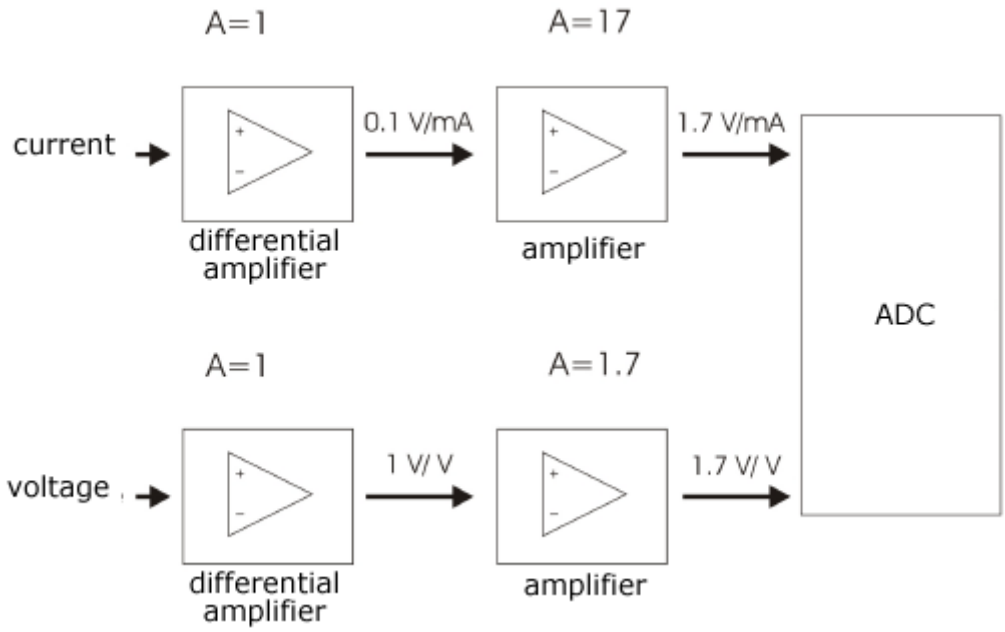

Figure 4.7: Current and voltage measurement block.

converter). Since the current source is symmetrical, two paths are needed for the current, I_+ and I_-, but only one is measured since by design they have the same magnitude.

Two resistors(R_1, R_2) are used in the circuit due to the following functions:

1. To measure the current before it is injected into the body (R_1)
2. To preserve the symmetry of the circuit (R_2)

The measurement of the current is necessary to keep the safety standard (IEC 60601-1) as well as to accurately calculate the body impedance. In the branch of the voltage measurement, the use of a resistance is not necessary, as the difference of voltage generated between the respective electrodes (wrist to ankle) is directly measured by means of a differential amplifier.

The Basic Differential Amplifier

The basic configuration of a differential amplifier it is shown in figure 4.9:

The voltage output can be expressed by equation 4.1.

$$V_{out} = E_1 \frac{-R_2}{R_1} + E_2(1 + \frac{R_2}{R_1})(\frac{R_4}{R_3 + R_4}) \tag{4.1}$$

Where E_1 and E_2 are the two input voltage to measure.

However, instead of equation 4.1 a linear equation 4.2 will facilitate to show the relation between in- and output.

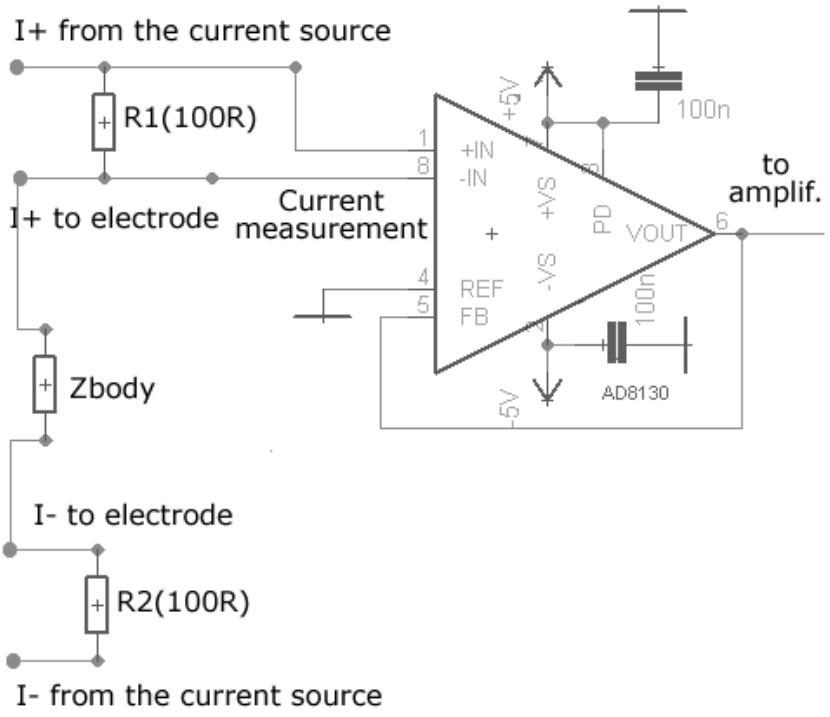

Figure 4.8: Differential amplifier for the current measurement

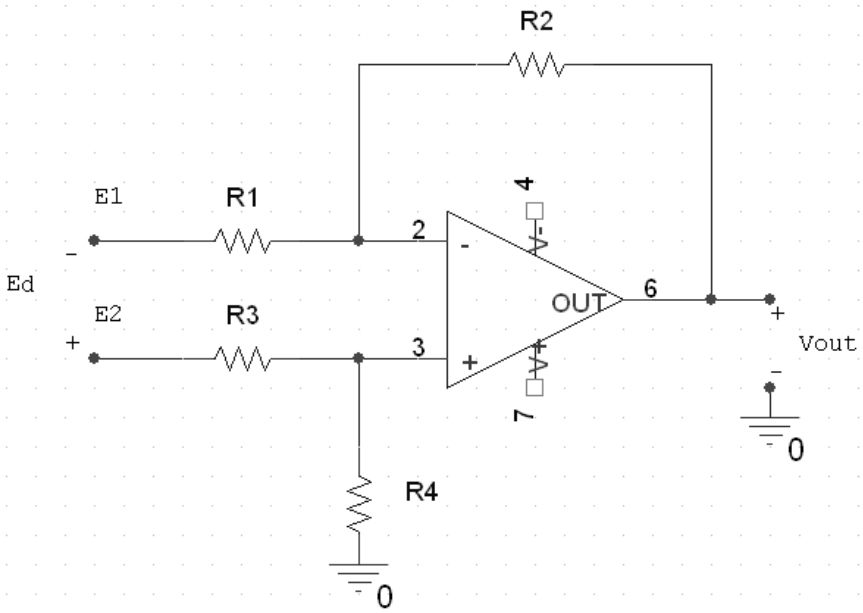

Figure 4.9: Basic Differential Amplifier

$$V_{out} = k(E_2 - E_1) \tag{4.2}$$

Where k is a constant that defines the desired gain (G), in our case 1.

Ideally, balanced inputs are expected at the differential amplifier. However, undesired signals can appear added to the main signal, which are called „common mode voltage“ (E_{CM}). E_{CM} is the unwanted part of the voltage between the inputs of the differential amplifier and ground, which is added to the voltage of the original signal.

The E_{CM} and E_d (differential voltage) can be expressed by equations 4.3 and 4.4 respectively.

$$E_{CM} = \frac{(E_2 + E_1)}{2} \tag{4.3}$$

$$E_d = E_2 - E_1 \tag{4.4}$$

Combining the previous equations, the output voltage is (equation 4.5):

$$V_o = E_{CM}\frac{R_4R_1 - R_2R_3}{R_1(R_3 + R_4)} + E_d\frac{1}{2}[\frac{R_2}{R_1} + (1 + \frac{R_2}{R_1})\frac{R_4}{R_3 + R_4}] \tag{4.5}$$

Differential amplifiers with high Common Mode Rejection Ratio (CMRR) are used in order to reject E_{CM}. This ratio is defined as:

$$CMRR = \frac{|E_d|}{|E_{CM}|} = \frac{1}{2}[\frac{R_1R_4 + R_2R_3 + 2R_2R_4}{(R_1R_4 - R_2R_3)}] \tag{4.6}$$

For an infinite or very high CMRR, the relationship between resistors showed in equation 4.7, has to be accomplished.

$$R_1R_4 - R_2R_3 = 0 \tag{4.7}$$

On the other hand, if an amplification is desired, expressions 4.8 and 4.9 will define the output voltage.

$$\frac{R_4}{R_3} = \frac{R_2}{R_1} = k \tag{4.8}$$

$$V_o = kE_d = k(E_2 - E_1) \tag{4.9}$$

The selected amplifier for this work is the AD8130 from Analog Devices. The most important features of this component are described in the following lines. The low DC offset and low noise features shows the small influence of the device in the measurement. The very high input impedances (6 Mohm for differential mode, 4 Mohm for common mode) allows the independence from the previous stage. Completely balanced inputs, as mentioned ideally

balanced inputs are expected at the differential amplifier. High Common Mode Rejection Ratio (CMRR: 94 dB (from 1 Hz to MHz)) in order to reject the undesired E_{CM}. Finally the amplifier does not need external components for Gain = 1, this feature adds simplicity to the design.

Amplification In the second stage the measured voltage and current are amplified by a defined amplification factor. The schematic for the voltage amplification in the current branch is shown in figure 4.10.

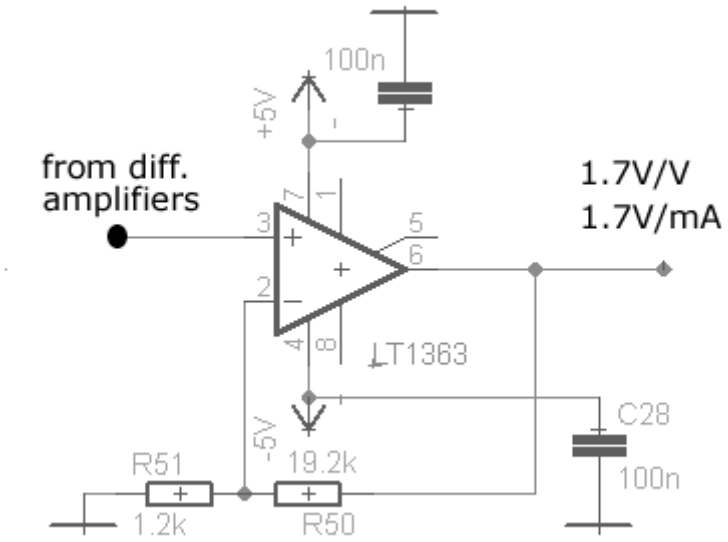

Figure 4.10: Amplification Circuit.

In the current branch, the final voltage gain is 1.7 Volts for each 1 mA. Due to the current specifications, the maximal allowed current value is 500 μA, so the measured voltage would be of 850 mV, although some inaccuracies are expected. In the voltage branch, the final voltage gain is 1.7 Volts for each Volt measured. For this purpose the LT1363 from Linear Technologies has been chosen. Some of the characteristics of the LT1363 are low introduction of noise into the system b lower input bias current, lower input offset voltage. Working range higher than 1 MHz (70MHz Gain Bandwidth and 1000V/ms Slew Rate).

4.2.5 Analog to Digital Conversion

For the analog-to-digital conversion (figure 4.2 (E)) the data adquisition system USB-6251 from National Instruments, was chosen. The USB-6251 is a USB data acquisition module optimized for accuracy at sampling rates till 1 MS/s. It is designed specifically for mobile or space-constrained applications (26.67 cm x 17.09 cm x 5 cm). Direct screw-terminal connectivity simplifies signal connections.

It should be mentioned that common BIS measurements are taken from 5 to 1000 kHz, whereas the used analog to digital converter (ADC) was limited to a multichannel sampling frequency of 1 MS/s. Because four channels of the analog-to-digital converter were used in the measurements at the same time, the sampling frequency of each channel was reduced to 250 kS/s. This hardware limitation causes 'inter-channel delay' explained in the sampling paragraph 4.2.5 this section.

[Smi90] has shown that sampling four points per cycle makes it possible to obtain acceptable impedance results. This sampling frequency leads to a four point per signal cycle demodulation, fig. 4.11, and the possibility to use signals with a maximum frequency of 62.5 kHz. However, the test done to our system (section 6) showed that at least 10 points were necessary to obtain realiable results.

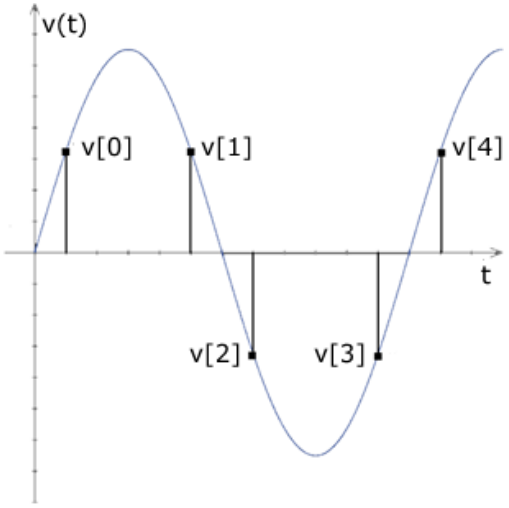

Figure 4.11: Four points per cycle sampling.

In this stage, the data is sampled by the analog to digital converter using four inputs; two of these inputs belong to the voltage and current measurement, and the remaining two belong to the orthogonal signals used in the demodulation process. The most important features of this device are the ones related to the analog inputs. The USB-6251 contains 16 single ended input channels, in the working voltage range of -1 to 1 V, with a maximum multichannel sampling Rate is 1 MS/s. However the simultaneous sampling is not possible (see section 4.2.5), being the multichannel settling time of 1 μs. The resolution (16 bits) permits a correct digital sampling of the input signal, see section 4.2.5.

Theoretical Background of A-D Conversion The mode of operation of an analog to digital converter can be explained in three basic blocks: sampling, quantization and binary encoding. The A-D Conversion blocks are shown in figure 4.12.

Sampling N samples of the analog signal, $V_x(t)$, are taken at sampling period T. The sampling period is affected by the number of channels, the 'Inter-channel Delay' and the

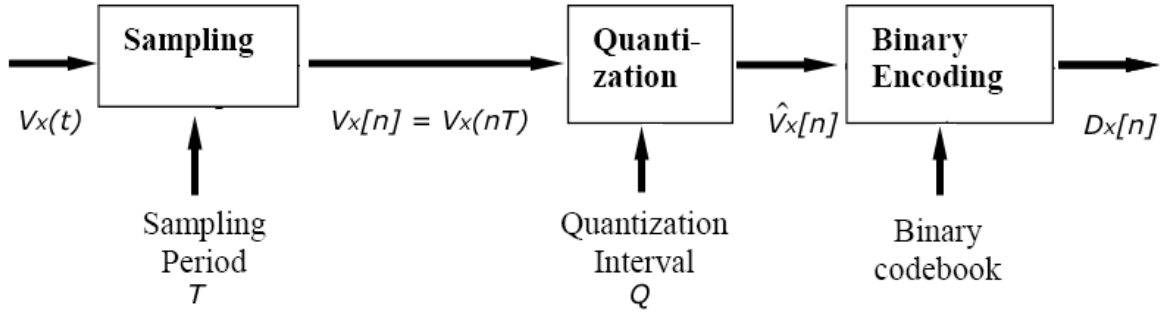

Figure 4.12: Basic blocs of A-D Conversion.

'Scan Interval' (see figure 4.13).

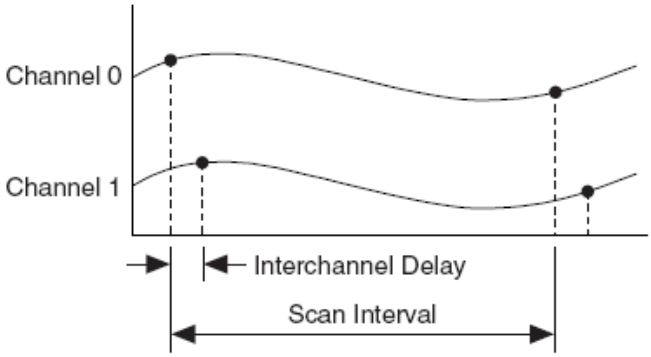

Figure 4.13: Inter-Channel Delay and Scan Interval.

The inter-channel delay is the time that the Data Acquisition System needs to change between two channels in order to allow a multichannel sampling (theoretically $1\mu s$ for the USB-6251), while the scan interval is the time between adjacent samples at the same channel (in a four channel measurement 4 μs). This last parameter is important, because the scan interval limits the maximum sampling frequency. In order to compare the phase shift between sampled signals, it is important to take into account the inter-channel delay since this effect introduces a time delay in the sensing process.

Quantization Quantization (figure 4.14) describes the process of approximating the set of values of the continuous input signal (V_x) to a finite discrete set of values. These finite sets of values are defined by the quantization interval (equation 4.10), which is limited by the minimum voltage difference the ADC converter can detect. This conversion involves a comparator action where the value of the analog input voltage (V_x), is compared with a reference voltage (V_{ref}).

$$Quantization\ interval = Q = \frac{V_{s+} - V_{s-}}{2^n} = 1\ LSB \tag{4.10}$$

Where V_{s+} and V_{s-} are the voltage supply of the „voltage comparator“.

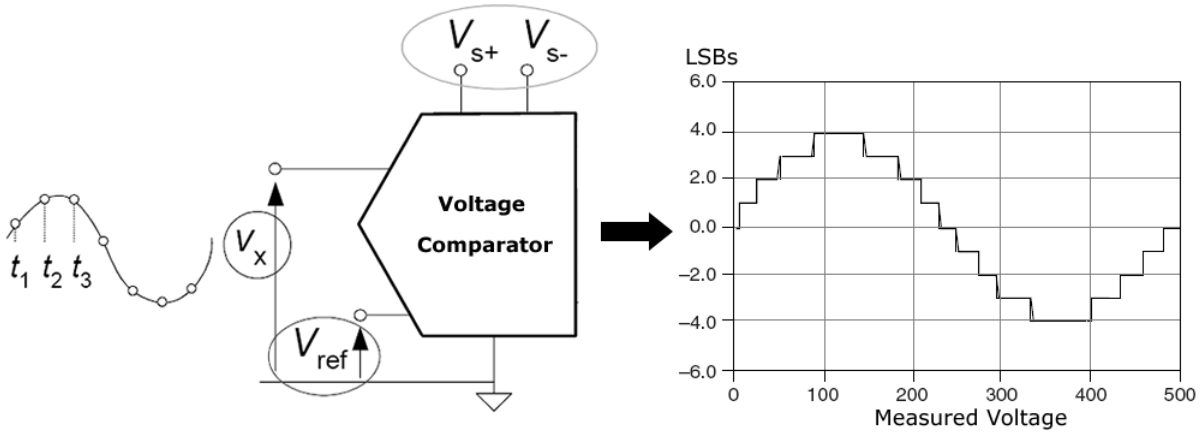

Figure 4.14: Quantization.

In the case of the NI USB-6251, with a resolution of 16 bits the A-D conversion parameters are:

- No. of quantization levels $= 2^{16}$ bits $=$ 65536 levels
- Selected Voltage range $=$ from -1 to 1 V
- Quantization interval (Sensitivity) $=$ 12.8 μV / level

The quantization interval is an important parameter, since it defines the smallest voltage change that can be detected. As an example, in figure 4.15 the electrical equivalent circuit used to simulate the human body can be seen. The electrical parameters of this body model are R_e=681 Ω, R_i=909 Ω and C_m=3.3 nF.

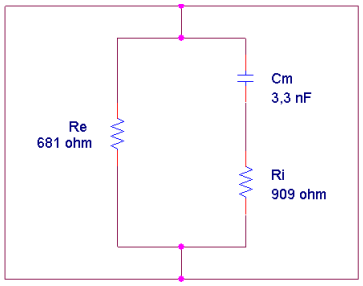

Figure 4.15: 'Whole Body' Electrical Model.

In appendix A.6 the results of a BIS analysis of the body model using the Xytron Hydra 4200 device can be found. From the obtained results, it can be deduced that the minimum impedance difference that can be found over the whole frequency range, appears between 5 kHz and 6 kHz:

- 5kHz: 667.27 ohm
- 6kHz: 665.04 ohm

The difference between the measured impedances is 2.23 ohm. With a current of 500 μA and an amplification factor (due to measurement circuit) of 1.7 V/V, we obtain a voltage of 1.8955 mV. Thus, the minimum difference the ADC has to be able to discern is 1.855 mV. Concerning to previous calculations it can be observed that the USB-6251 offers an interval of 12.8 $\mu V/level$, so it accomplishes the required specification.

Binary Encoding Binary encondig is the final stage of the analog to digital conversion, in this step the measured and quantized voltage (V_x) is finally converted to a digital (binary) value. One of the possible techniques is shown in figure 4.16, where each value of the quantized voltage is codified in a 3 bit code number. In the example the quantified voltage 0 V, is converted to the code number 000. In our case the USB-6251 uses 16 bits for the encoding.

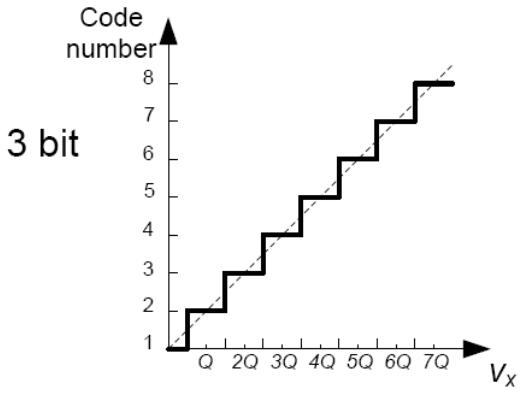

Figure 4.16: Binary Encoding

4.2.6 Digital Demodulation and Data Processing

The stage is performed by software (figure 4.2 (F)). The sampled data is operated in order to obtain the desired values of impedance. Both of the components of Z (resistance and reactance) are obtained by demodulating the differences in the measured voltage and current. Digital demodulation is very similar to analog demodulation. The main difference is that in the case of digital demodulation, the acquired signal is sampled and demodulation is performed over a number of complete cycles of the signal period.

The sampled current and voltage are demodulated in order to obtain their amplitude and phase. In most of the systems described in the literature, demodulation is achieved using some of the following systems:

- Double balanced modulator ([IEE63])

- I-Q demodulator ([Kir99])
- Peak and Phase detector ([SDSH04])
- Amplitude demodulation ([Sis07])
- Lock-in amplifiers ([ins00])
- Phase Locked Loop demodulation ([Pin])
- Quadrature amplitude demodulation ([HR07])

One possible method to measure the amplitude and phase of a signal is to use a peak detector for the amplitude and a phase detector, based on zero crossings, for the phase. Nevertheless, this is not a good approach in the case of bioimpedance measurements where the amplitude of the injected current is very low (500 $\mu A_{peak-to-peak}$), and the environment is quite noisy. Inadequate sampling of data can result in inaccurate values for the locations and amplitudes of peaks, and the non-detection of valid peaks. In addition, the appearance of high-frequency noise could result in the detection of a large number of peaks, but only a few of these will actually be of interest. It is advisable to use some kind of demodulation to reject the noise or the interferences outside the frequency range of interest.

Likewise, some other characteristics for bioelectrical impedance spectroscopy measurements have to be taken into consideration. The changes of bioimpedance in the body are very slow and this implies that there is no need for a high-speed demodulation process; hence, the test could take place in the order of minutes. In turn, measurements are taken over a wide frequency range, typically 5 to 1000 kHz, where each of the injected signals is centred in a known frequency and has a spectral width of some hertz. Due to such requirements, a synchronous demodulation (quadrature amplitude demodulation) method (figure 4.17) has been used in this thesis.

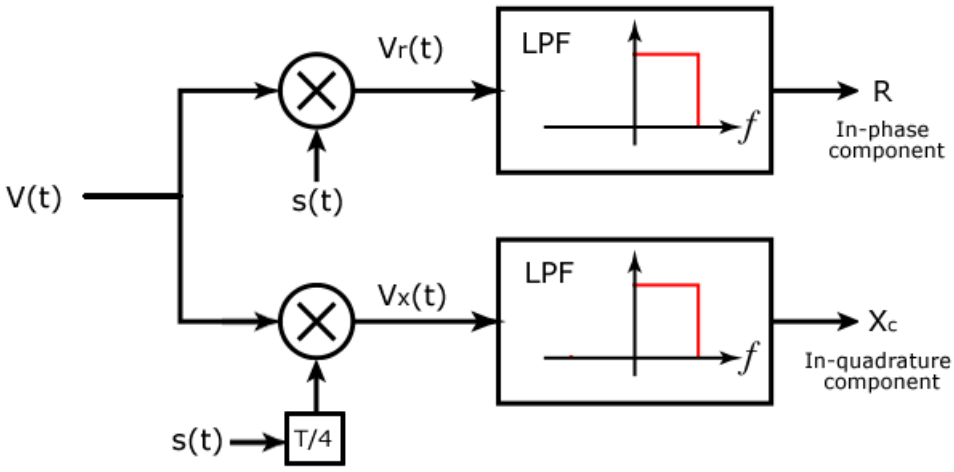

Figure 4.17: Quadrature amplitude demodulation block diagram.

Demodulation is done in order to obtain the real (R) and the imaginary (X_c) part of the body impedance ($R + jX_c$). In the demodulation process, the measured voltage is multiplied by a

cosine and a sine, and subsequently by a low-pass filter in order to extract the components in phase (R) and in quadrature (X_c). The in-phase component belongs to the real part of the measured voltage, while the in-quadrature component to the imaginary part. The demodulation result depends on the reference signal amplitude, the amplitude of the acquired signal and the phase difference between these two signals.

In this case the demodulation process has been performed implementing the I-Q demodulation in figure 4.17, using Matlab. The mathematical formulation of the demodulation scheme and its performance is briefly introduced:

Considering that equation 4.11 represents the reference signal, and the impedance at frequency f_0 is constant and described by equation 4.12, we get:

$$s(t) = cos(2\pi f_o t) \tag{4.11}$$

$$Z = |Z|\, cos(\Theta) + j\,|Z|\, sin(\Theta) = R + jX_c \tag{4.12}$$

$$i(t) = Is(t) \tag{4.13}$$

If the impedance is measured by the injection of the current defined by equation 4.13, and $V_z = I\,|Z|$, then the measured voltage remains as in 4.14.

$$v(t) = Zi(t) = V_z cos(2\pi f_0 t + \Theta) \tag{4.14}$$

The signal after the product, at the upper branch in figure 4.17, is the multiplication of two cosines and if the equation 4.15 is applied, we obtain equation 4.16.

$$v_r(t) = V_z cos(2\pi f_0 t + \Theta) cos(2\pi f_0 t) \tag{4.15}$$

$$v_r(t) = V_z[cos(2\pi f_0 t) cos(2\pi f_0 t) cos(\Theta) + sin(2\pi f_0 t) cos(2\pi f_0 t) sin(\Theta)] \tag{4.16}$$

$$v_r(t) = V_z[\frac{cos(2\pi 2 f_0 t) cos(\Theta)}{2} + \frac{cos(\Theta)}{2} + \frac{sin(2\pi f_0 t) sin(\Theta)}{2}] \tag{4.17}$$

The Low Pass Filter is designed to reject frequency dependent components. The component of the equation that carries the important information is the DC component. Hence, at the output of the upper branch we obtain equation 4.18.

$$R_V = \frac{V_z cos(\Theta)}{2} \tag{4.18}$$

Equation 4.19 is equivalent to the real part (R) of the measure voltage.

$$R_V = V_z cos(\Theta) \tag{4.19}$$

In the same way, for the lower branch, the multiplication leads to equation 4.20, and as a result at the output of the LPF we obtain equation 4.21. Hence, at the output of the lower branch we obtain 4.21.

$$v_x(t) = V_z cos(2\pi f_0 t + \Theta)(-sin(2\pi f_0 t)) \tag{4.20}$$

$$X_V = -\frac{V_z sin(\Theta)}{2} \tag{4.21}$$

Equation 4.22 is equivalent to the imaginary part of the measured voltage.

$$X_V = V_z sin(\Theta) \tag{4.22}$$

The real and imaginary components of the measured voltage can finally be expressed as (equation 4.23):

$$V = R_V + jX_V = \frac{V_z cos(\Theta)}{2} + j\frac{V_z sin(\Theta)}{2} \tag{4.23}$$

If the same demodulation process is applied to the current injected into the body, then the current in terms of real and imaginary part can be expressed as equation 4.24.

$$I = R_I + jX_I \tag{4.24}$$

And finally the desired impedance is defined as equation 4.25.

$$Z = \frac{R_V + jX_V}{R_I + jX_I} \tag{4.25}$$

Thus, quadrature amplitude demodulation can be applied to obtain the resistance and the reactance of the impedance, by demodulating the injected current and the measured voltage drop over the body.

5 Current Source for BIS Measurements

5.1 Introduction

This chapter describes the research and analysis of current sources for our developed BIS measurement system. This chapter is divided into five sections. In the first section the requirements inherent to current sources in BIS measurements are explained. In the second section a research of the available technologies was carried out. In addition, a selection of the most suitable current sources for our system was performed. In the third and fourth section, the characteristics and procedures to simulate (OrCAD) a comparison of selected current sources are presented. The last section summarizes the results of the simulations and the conclusions.

5.2 Requirements for Current Sources in BIS Measurements

Listing general specifications for current sources includes many aspects. Considerations include voltage and phase stability, drive current capability and sensitivity with respect to the various circuit components. Thus for BIS measurements the aim is to design a current source according to the previously mentioned parameters that maintains its performance across a frequency band. Based on the considerations mentioned above, the following criteria should be accomplished:

- The current amplitude should be as large as possible without compromising safety. According to the standard EN 60601 and the working frequency range between 5 kHz and 1 MHz, the current should be between 500 $\mu A_{peak-to-peak}$ and 10 $mA_{peak-to-peak}$ (figure 2.7). This ensures that the induced potential on the heart is significantly below the levels expected to induce fibrillation.

- High internal output resistance, $Z_{out} > 1000 \times Z_{body}$, over the whole working frequency range. A high output impedance is important to ensure that the current is independent from the load (formed by the skin, the capacitive electrode and the body) and stable in the magnitude. The higher the output resistance, the higher the load can be driven ([BFLA04] and [BFA99]).

- The relationship between the control voltage and the output current (transconductance) should be linear.

- The electrical components of the current source should introduce a minimal common-mode voltage into the measuring circuit.

- Security against electric shock. High current values may cause tissue damage or fibrillation. Standard EN60601 (figure 2.7) defines the maximum permissible current for measurements in humans.

- The application of an alternating current thorugh the body (high frequencies) on living tissue results in electromagnetic stray fields which reduce the amount of current actually injected into the tissue under study. This radiation effect can be reduced by use of a symmetrically configurated current source [GFRH98]).

5.3 Research of the Available Technologies

In order to select the most suitable current source, an analysis of the state of the art was carried out. A general literature research on BIS and Electrical impedance tomography (EIT) systems was made, since EIT and BIS current sources have to accomplish the same requirements. The technical features of the current sources, most suitable for our design, were deduced from these papers. Subsequently a more specific literature research was made about the selected current sources.

General Literature Research: In the first step five documents were examined exhaustively. The first ones ([Jun05] and [Fou08]) were research documents from the MedIT group, where some current sources used in developed systems from MedIT were evaluated:

- Howland, symmetrical howland current pump
- EIT, power source with transformer
- IC Max435, symmetrical wideband transconductance amplifier from Maxim
- Tietze topology

In [BFBW00], [CRB+96] and [BRR94], the following current sources were implemented and examined concerning their performance under EIT measurements:

- EIT
- Howland
- Current mirror topologies
- Current conveyors

First Selection Process In the selection process the main goal was to find a design that combines the following characteristics:

- Good performance over the whole frequency range, i.e.:
  - High output impedance
  - Constant current magnitude
  - Phase stability

- Electrical design adequate to the rest of the characteristics of the circuit, like number of electrodes, size, selected voltage supply, etc.

According to the literature found, the Tietze and Howland topologies present the best performance over the whole frequency range [Jun05] [Fou08]. Therefore these topologies for current sources were chosen to be deeper examined.

Tietze and Howland Current Sources: While the electrical design of the Tietze topology is fixed, Howland topologies allow several kinds of design such as:

- Bridge configurations ([Pol99] and [SEO06]), use of a second electrode in the current injection as a feedback path to perform control task.
- Single configurations use a single current injection path without feedback.
  - ISSA or Improved Howland Current Pump, positive feedback configuration ([BFBW00],[KUE06],[BH96],[RSNI03],[JTJ94] and [SG92]).
  - ICSA or Improved Howland Current Pump with voltage follower, positive feedback configuration (own design)
  - ISSB or Improved Howland Current Pump, negative feedback configuration ([JEO03] and [Pea08])
  - ICSB or Improved Howland Current Pump with voltage follower, negative feedback configuration([TSU04]))

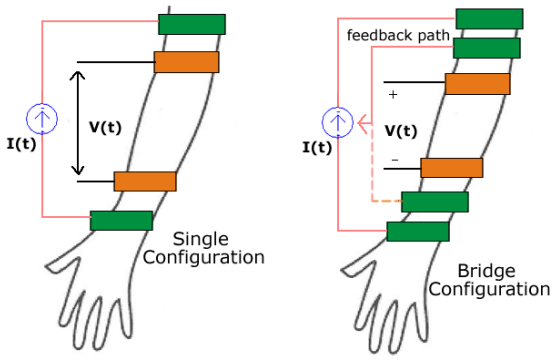

Figure 5.1: Single and bridge configurations.

Two different howland circuits in bridge configurations have been reported in [Pol99] and [SEO06]. While a high accuracy concerning constant current module and phase are obtained, a multitude of electrical components is necessary, even another pair of electrodes is required for the current injection in order to establish a control feedback path. Thus, four electrodes are used just for current injection in this topology. The use of additional electrodes leads to a more uncomfortable and complex system, specially with capacitive electrodes more errors may occur. It should be mentioned that the number of electrodes -in the same way as the size- is an important factor, since adequate skin contact is difficult using more electrodes.

In single configurations, two big groups can be found, **ISS** and **ICS**. ISS, or Improved Howland Current Pump, is a operational amplifier configuration for Howland current sources. While ICS, Improved Howland Current Pump with Voltage Follower, defines a configuration with two operational amplifiers, where one is configured as a voltage follower at the output, leading to a higher output impedance. Examples for ICS configurations can be found in [TSU04]. Similarly examples for ISS configurations can be found in [BFBW00]

One of the most determining factors in order to select the most appropiate current source was the number of electrodes. For this reason the current sources in single configurations were selected for simulation. In the following section one can find the five selected current sources.

5.4 Selected current sources

As mentioned in the previous section, five current sources were selected for the analysis. This section shows an overview of the electric configuration for each current source while in next sections they will be deeper analysed. It should be mentioned that for each current source, were carried out some aditional simulations in order to discover the resistor configuration that behaves best for the parameters explained in section 5.5. The results of the simulations can be found in the correspondig appendixes of each current source.

5.4.1 ISSA. Improved Howland Current Pump.

The ISSA (appendix A.1) ([BFBW00],[KUE06],[BH96],[RSNI03],[JTJ94]and [SG92]), uses a single operational amplifier with both negative and positive feedback (figure 5.2). Advantages of this topology over other designs include its small number of passive components, the need of only a single active device and the ability to adjust the output resistance, using a potentiometer instead of resistor R_3. The selected resistor configuration is $R_1 = R_2 = R_3 = 5\ k\Omega, R_{4a} = 2.5\ k\Omega, R_{4b} = 2.5 k\Omega and C_p = 10pF$.

The transconductance of the source is given by equation 5.1:

$$I_{gen} = -V_{sg}\frac{R_2}{R_1 R_{4b}} + V_{out}\frac{R_2 R_3 - R_1 R_{4b} - R_1 R_{4a}}{R_1 R_{4b}(R_3 + R_{4a})} \tag{5.1}$$

and the output resistance by equation 5.2:

$$R_{out} = \frac{R_1 R_{4b}(R_3 + R_{4a})}{R_2 R_3 - R_1(R_{4a} + R_{4b})} \tag{5.2}$$

The presence of both positive and negative feedback allows the simple adjustment of the output resistance. These two feedback paths may cause the enhanced Howland circuit to oscillate when driving large capacitive loads at high frequencies. To stabilize the circuit, a 10 pF capacitor (C_p) may be added in parallel with the negative feedback element.

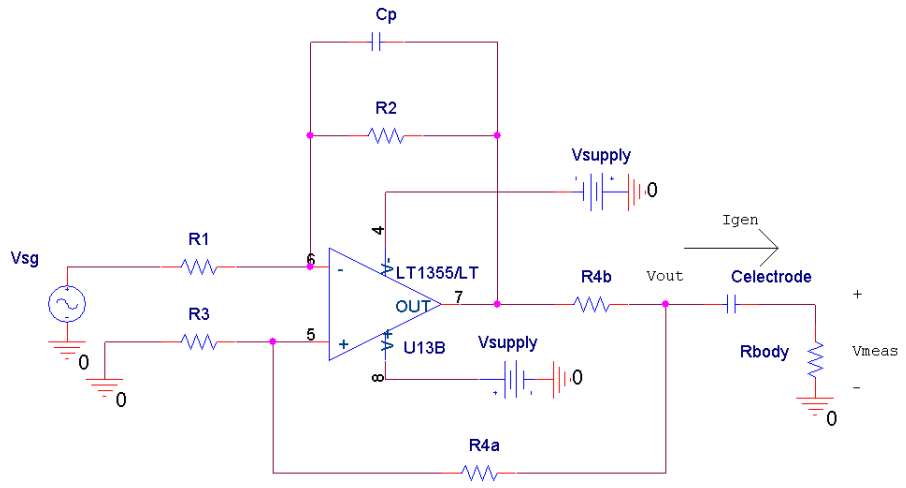

Figure 5.2: Circuit of the Improved Howland Current Source A

5.4.2 ICSA. Improved Howland Current Pump.

The Improved Howland Current Source A with Voltage Follower (appendix A.2), uses two operational amplifiers and a voltage follower in the negative feedback (figure 5.3). The aim of the voltage follower is a reduction of the current needed in the negative feedback branch. The advantage of this topology over other designs is an increment of the output resistance. The selected resistor configuration is $R_1 = R_2 = R_3 = 5\ k\Omega, R_{4a} = 2.5\ k\Omega, R_{4b} = 2.5 k\Omega and C_p = 10pF$.

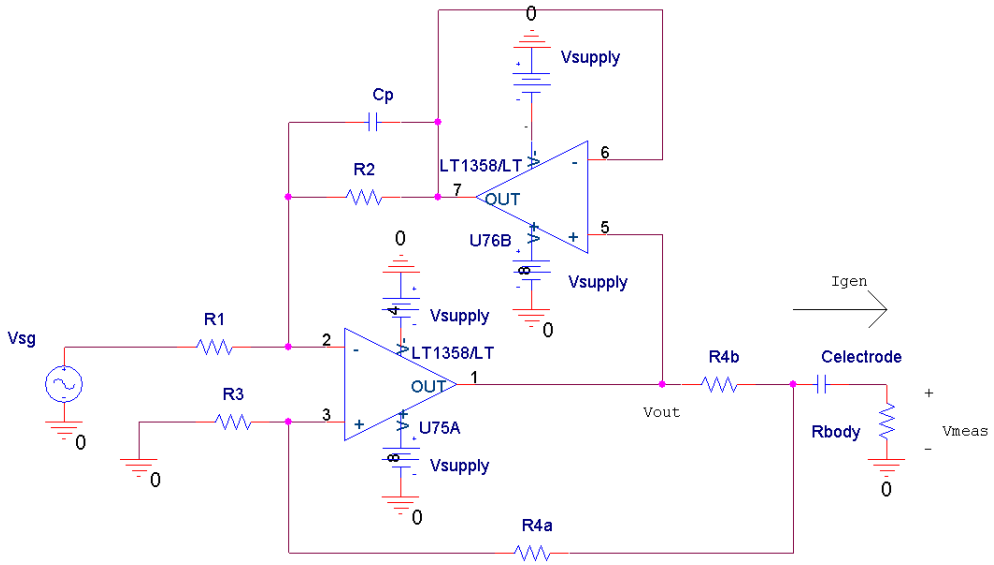

Figure 5.3: Improved Howland Current Source A with Voltage Follower.

The transconductance of the source is equal to the ISSA. The output impedance of the current source, in this case is affected by the input impedance of the voltage follower due to the circuit design, leading to a higher output impedance.

5.4.3 ISSB. Improved Howland Current Pump.

As the source ISSA, the ISSB (figure 5.4) uses a single operational amplifier with both negative and positive feedback. Although both configurations, A and B, are similar they show a different behaviour. Simulation for this current source can be found in appendix A.3. Te corresponding configuration is $R_1 = R_{4a} = R_3 = 2.5\ k\Omega, R_2 = 1\Omega, R_{4b} = 2.5k\Omega and C_p = 10pF$.

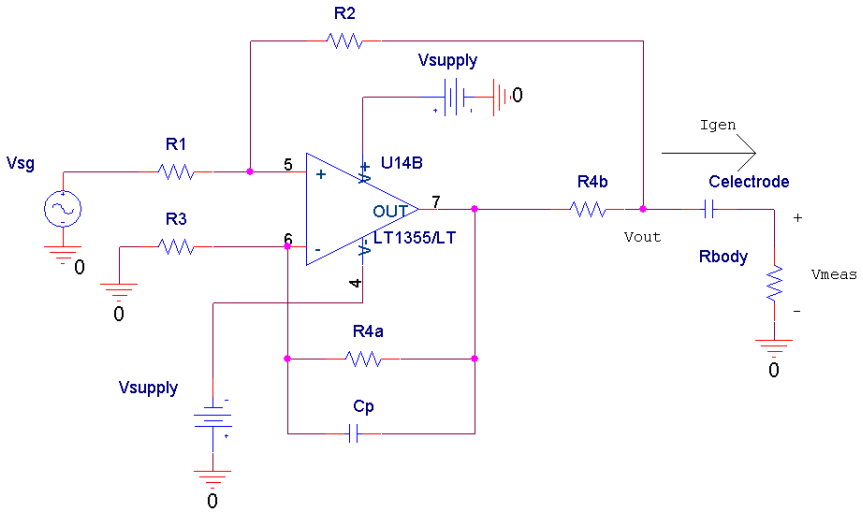

Figure 5.4: Improved Howland Current Source B

The transconductance of the ISSB is the function 5.3:

$$I_{gen} = V_{sg}\frac{R_2R_{4a} + R_3R_{4b} + R_3R_2}{R_3R_{4b}(R_2 + R_1)} + V_{out}\frac{R_1R_{4a} - R_3R_{4b} - R_3R_2}{R_3R_{4b}(R_1 + R_2)} \tag{5.3}$$

5.4.4 ICSB. Improved Howland Current Pump.

ICSB uses two operational amplifiers with the voltage follower in the positive feedback. As in the case of Howland Current A with voltage follower, the voltage follower is added to reduce the current needed in the positive feedback tool, also is noticed an increment of the output resistance. The simulation for this current source can be found in appendix A.4. The used configuration is $R_1 = R_2 = R_3 = R_{4a} = 2k\Omega, R_{4b} = 2.5k\Omega and C_p = 10pF$.

The transconductance of the source is given by the equation 5.4:

$$I_{gen} = \frac{Vsg}{R4b} \times \frac{R2(R3 + R4a)}{R3(R1 + R2)} + V_{out} \times \frac{R_{4a}R_1 - R_2R_3}{R_3R_{4b}(R_1 + R_2)} \tag{5.4}$$

As in the case of Howland Current A with voltage follower, the positioning of the voltage follower in one of the feedback paths increases the output impedance of the circuit, with regard to the same configuration but with one amplifier.

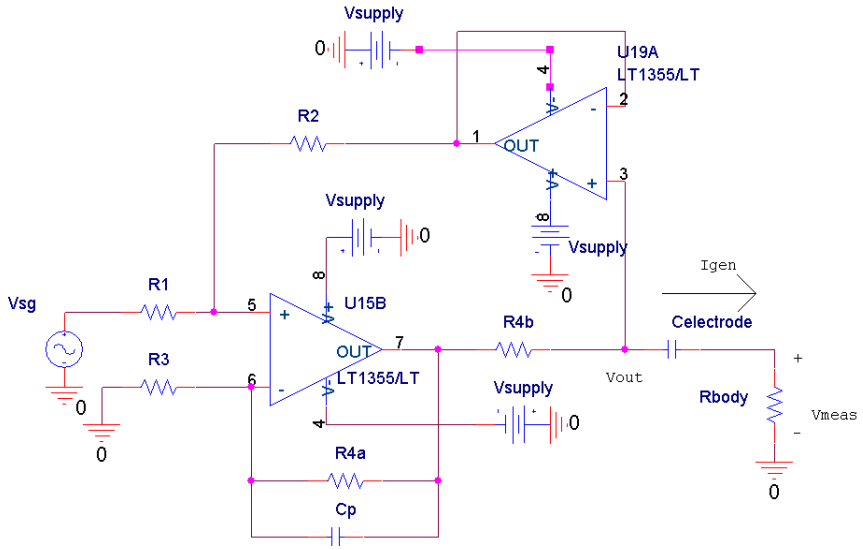

Figure 5.5: Improved Howland Current Pump Configuration B with Voltage Follower.

5.4.5 Tietze Topology

The last of the current sources studied is the Tietze topology [Tie02]. This current source uses two operational amplifiers in cascade configuration figure 5.6. A deeper study can be found in appendix A.5. The selected configuration is $R_2 = 27\ k\Omega$, $R_3 = 25.5\ k\Omega and R_{4b} = 2.5 k\Omega$.

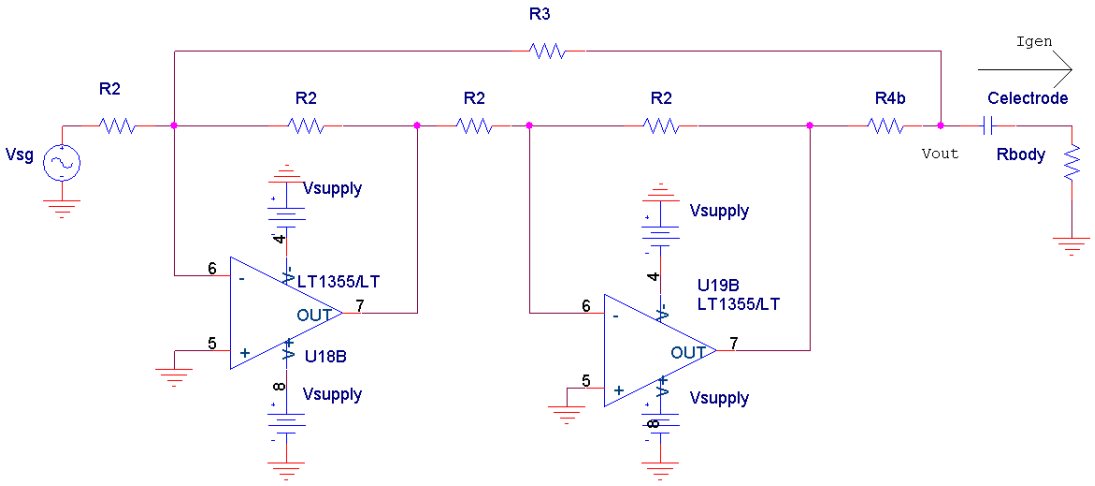

Figure 5.6: Tietze Current Source

The transconductance of the source is given bt the equation 5.5:

$$I_{gen} = \frac{V_{sg}}{R_{4b}} + V_{out}\frac{R_2 - R_3 - R_{4b}}{R_{4b}R_3} \tag{5.5}$$

5.5 Parameters to Analyse and Procedure of Validation

In order compare the selected current sources three intrinsic parameters, over the range of operation for a BIS measurement (from 5 to 1000 kHz), were analysed:

Current Magnitude: The current amplitude should be as large as possible, in order to flow through the injecting electrodes and the body, and to accomplish the standard EN 60601. Simulations were performed using the maximum current permited (700 μA_{rms}).

Phase Delay: To maintain a constant phase signal is important for the selected demodulation technique (section 4.2.6).

Output Impedance: A high output impedance is important to ensure that the current is independent from the load.

Simulations for the complete current sources were performed using OrCad Capture CIS 15.7 and PSpice. The procedure of validation has been divided into two steps. First, for each current source different resistor configurations were tested in order to find the configuration that behaves better concerning the parameters of analysis. This was done due to the fact that in the examined research papers a resistor configuration that accomplished our design specifications was not found. Simulations were performed using a capacitive load of 3.2 nF, the same capacitive theoretical value as the designed capacitive electrodes (section 3.1.1) and two different resistive loads, 500 Ω a value in the range of the whole body model and 1 kΩ in order to observe the behaviour with different load values. After that, the simulations using the best configurations were compared. Two parameters concerning all the current sources under test should be mentioned:

- A current of 700 μA_{rms}, in the range of 5 kHz to 1 MHz, is used.
- A voltage supply of $\pm 15V$ has been used.

5.6 Current Source Voltage Supply

As it was mentioned in the section 3.5.1 the voltage at the terminals of the capacitive electrodes is directly related to the voltage supply of the current source. Since increasing the voltage supply increases the voltage output, hence the voltage at the terminals of the electrode. In order to discover the most appropiate voltage supply, that means the one that permits a constant 700 μA_{rms} over the frequency range from 5kHz to 1MHz, some simulations using the circuit simulation tool OrCAD PSpice 9.2 were performed. The simulations were carried out with two of the selected current sources (ISSA and Tietze), on them a capacitance value of 3.2nF (the same capacitive electrode value as the one reported in section 3.1.1) was used as a load, and various voltage suppplies were tested.

Simulations showed that a voltage supply of $\pm 15V$ was enough to supply a constant 700 μA_{rms}. Since the maximum permitted voltage supply for the used amplifiers (LT1355, Linear Technology) is $\pm 16V$, hence $\pm 15V$ was selected.

5.7 Results

5.7.1 Output Impedance

Concerning the output impedance, the ICSA (green plot) and ISSA (pink plot) current sources were expected to show the higher value due to the transconductance function. In the same way, a high value is expected for current source ICSB (red plot), since the use of the voltage follower increases the output impedance of the circuit. As one can see, the simulations (figures 5.8 and 5.7) confirm these expectations. In figure 5.8 ICSA and ISSA showed the highest values of impedance, in fact the ICSA showed a high difference with a value of 50 MΩ at 5 kHz. Similarly in figure 5.7, ICSA and ISSA showed the highest values of 14.6 kΩ and 9.59 kΩ respectively.

In figure 5.8 although the simulation unit is Voltage instead of Ω, a quick conversion could be applied by dividing the voltage value by 1 Ampere.

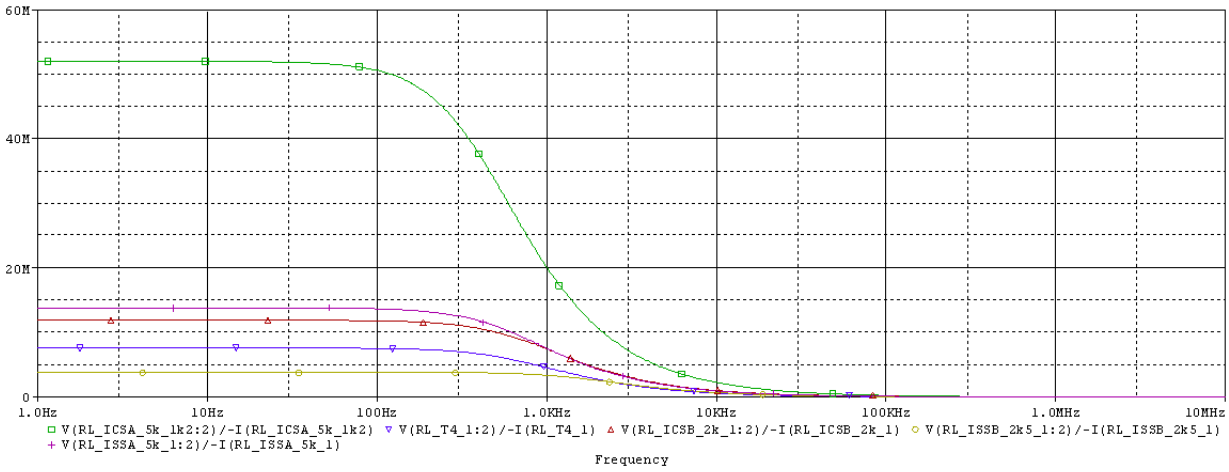

Figure 5.7: Simulated output impedance in the range from 0 to 10 MHz.

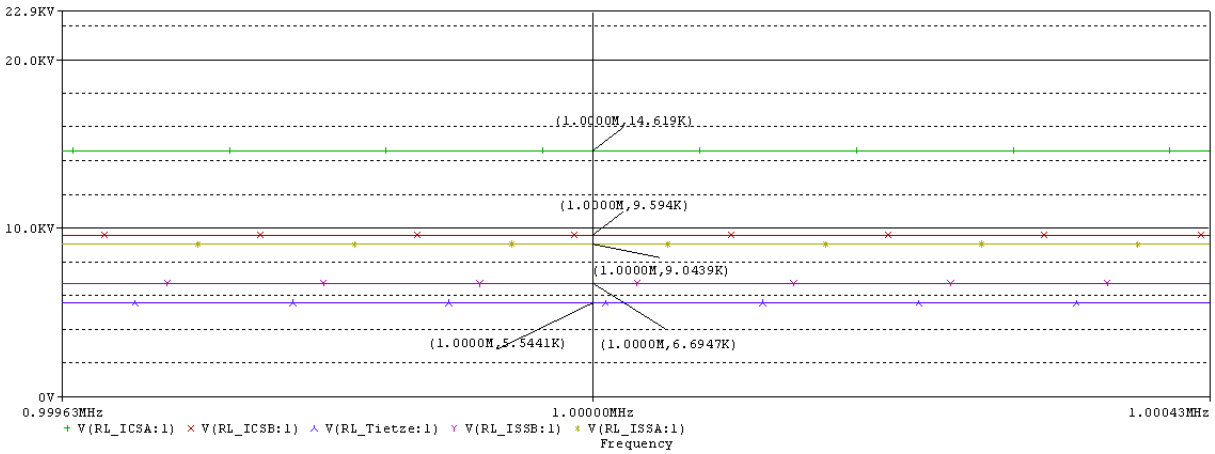

Figure 5.8: Simulated output impedance at 1 MHz.

5.7.2 Current Magnitude

Concerning the current magnitude only simulations at 5 kHz and 1 MHz have been plotted, since in the mid range the values smooth change from the value at 5kHz to the value at 1MHz, without big alterations. From simulations at 5 kHz (figure 5.9) and at 1 MHz (figure 5.10), it can be observed that the current source ICSA (red line) showed the best performance in current magnitude stability: an almost constant value in the whole range, 498 μA at 5 kHz and 497 μA at 1 MHz. On the contrary ICSB (purple line) showed a small error at low frequencies but at high frequencies the performance is highly degraded. One should pay attention to Tietze topology (abbreviation: RL_{T4}); although it has not the best performance the error in magnitude is almost constant for low and high frequencies. It is interesting to emphasize that in the same way [Jun05] reported that Tietze topolgy performs better than ISSA.

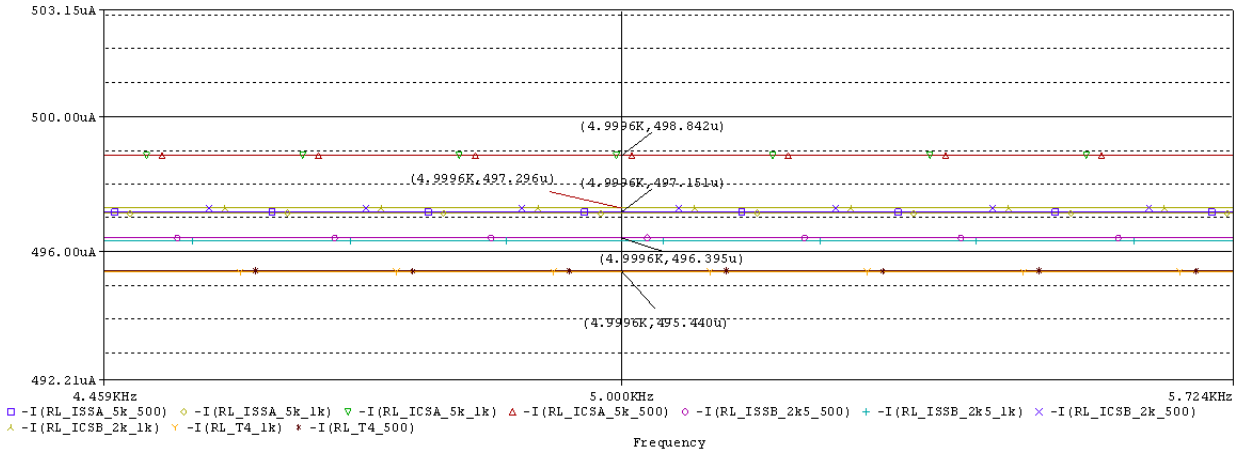

Figure 5.9: Simulated current cagnitude stability at 5 kHz

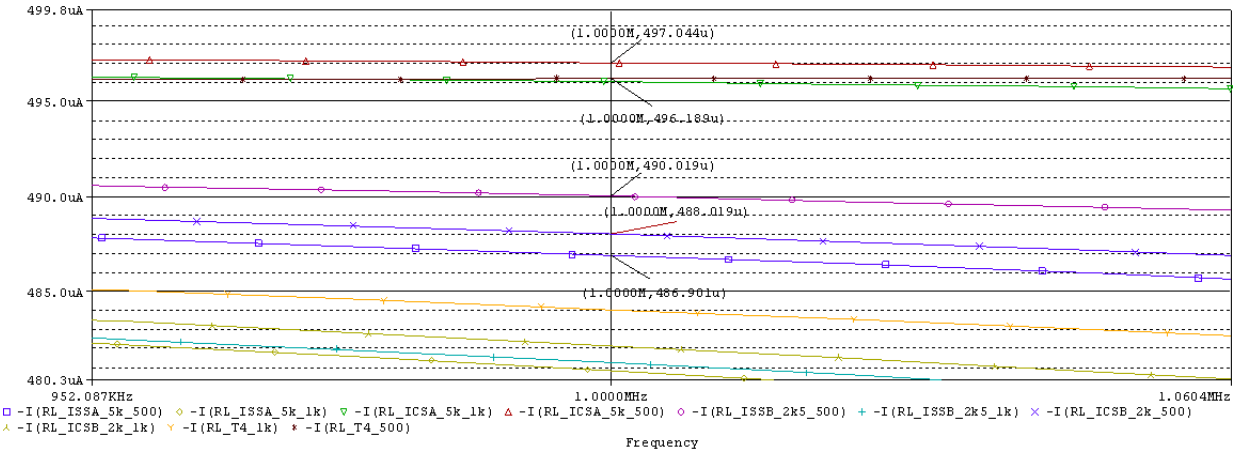

Figure 5.10: Simulated current cagnitude stability at 1 MHz.

5.7.3 Phase Delay

With regard to the phase delay, only simulations at 1 MHz (figure 5.12) are of interest for the analysis, since the phase delay at low frequencies (figure 5.11) is in the order of mili degrees, which will have almost no effect in the performance of the current source. It can be observed that at 1 MHz the ISSB (red plot) and ICSA (green plot) showed the best performance with a phase delay of -4° and -12.1° respectively. In the same way [Jun05] reported a high phase delay for Tietze topologies at high frequencies $\approx -25°$, in our simulations -24.5°.

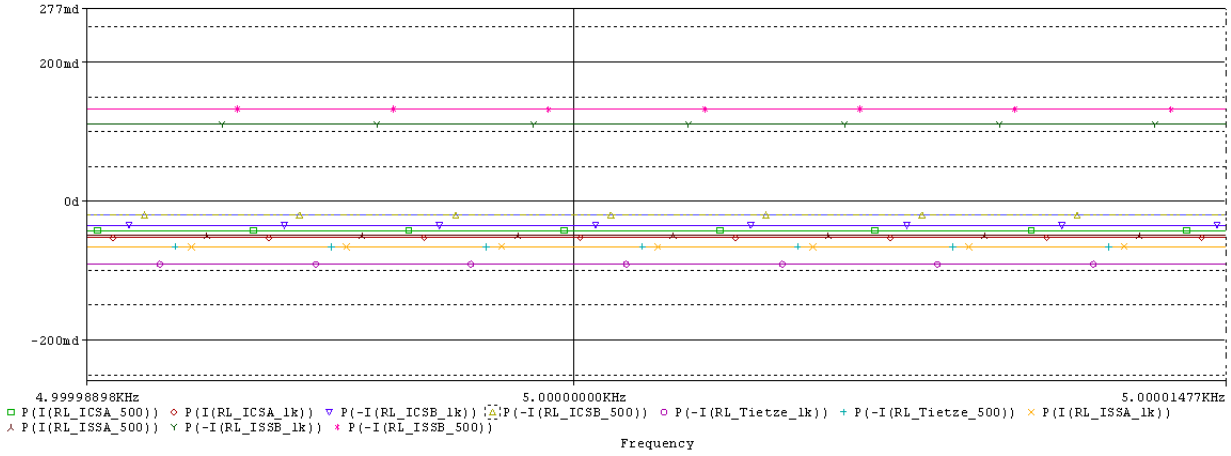

Figure 5.11: Phase delay behaviour at 5 kHz

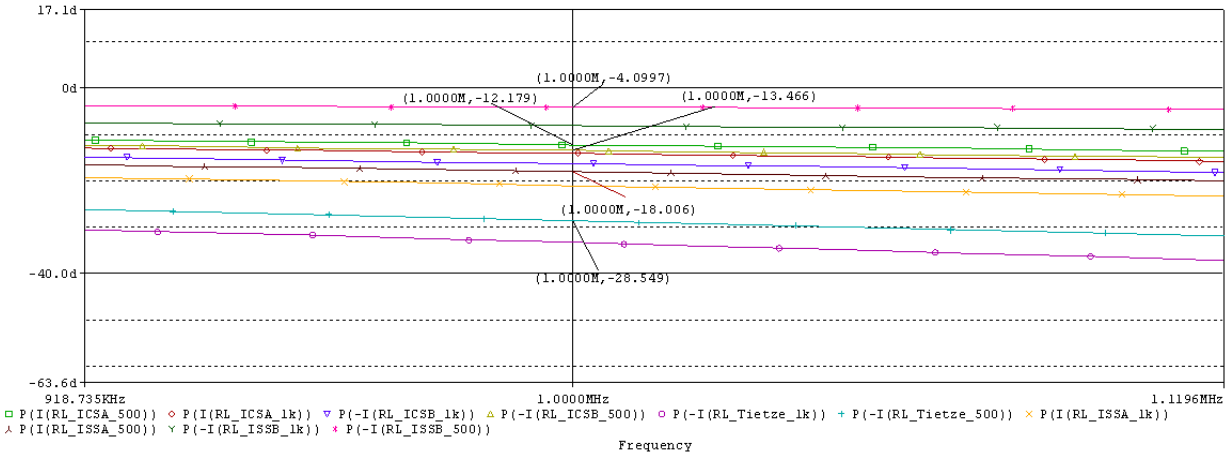

Figure 5.12: Phase delay behaviour at 1 MHz

5.8 Analysis of the Results and Conclusions

The most important data for the analysis has been extracted from previous simulations and compiled in Table 5.1. From these results, some conclusions can drawn:

While at low frequencies it is easy to find a current source that accomplishes the specification $Z_{out} > 1000 \times Z_{body}$, at high frequencies the output impedance gets quickly degraded. To achieve high accuracy at higher frequencies an auxiliary circuit is required. A Howland topology in parallel with a generalized impedance converter (GIC), will almost allow an independent adjustment of output resistance and output capacitance at high frequencies.

The current source with the best behaviour in most of the introduced and simulated parameters (current magnitude and output impedance) has been the ICSA. ISSB topolgy showed the best performance in phase delay $-4°$, however the output impedance is ten times smaller than ISSA. Tietze topology showed a constant good behaviour in current magnitude, the phase delay has more weight in our decision, since in the demodulation process the value of the phase of each signal is highly important. In addition, the output impedance is half the value of the ISSA.

The performance of variations on the basic Howland circuit have been reported by several researchers, especially to obtain balanced dual sources. A critical feature of a symmetric source design is that the current imbalance is kept low, that means in both sources the current magnitude and frequency have to be the same. To reduce imbalance, component values must be well matched between the two sources. Even 0.1% component tolerance was inadequate and additional trimming is required.

The current magnitude error is expressed in % and is calculated as mean relative error (equation 5.6) from the expected value of $500\mu A$.

$$mean\,relative\,error(\%) = 100 \times \frac{500\mu A - Result}{500\mu A} \tag{5.6}$$

Current Source Type	Current Magnitude error (at 5 kHz)	Current Magnitude error (at 1 MHz)	Phase Delay (at 1 MHz)	Output Impedance at low freq.	Output Impedance 1MHz
ISSA	0.57%	2.6%	-18°	13 Mohm	9 kohm
ICSA	0.4%	0.57%	-12.1°	50 Mohm	14.6 kohm
ISSB	0.72%	1.99%	-4°	5 Mohm	6.7 kohm
ICSB	0.54%	2.39%	-13.5°	12Mohm	9.6 kohm
Tietze	0.9%	0.76%	-28.5°	7 Mohm	5.5 kohm

Table 5.1: Table of results extracted from the simulations

6 System Validation and Results

This chapter describes the validation of the developed bioimpedance spectroscopy system (figure 6.1). The validation was carried out in two steps. In a first step, in order to show the limitations of the actual commercially availible devices, impedance measurements were performed in a four-point setup, using the BIS device Xitron Hydra 4200 and the designed dummy (figure 6.3). In these measurements, combinations of different values for the electrode capacitances have been tested. In a second step, impedance measurements were performed with our system using the same configurations as in the first stage. In both steps capacitive electrodes were simulated by using capacitors, where the value is selected by using switches which allow changing the capacitance values. The system has been tested in the critical frequency range, namely in the lower frequency range (5 kHz - 43 kHz).

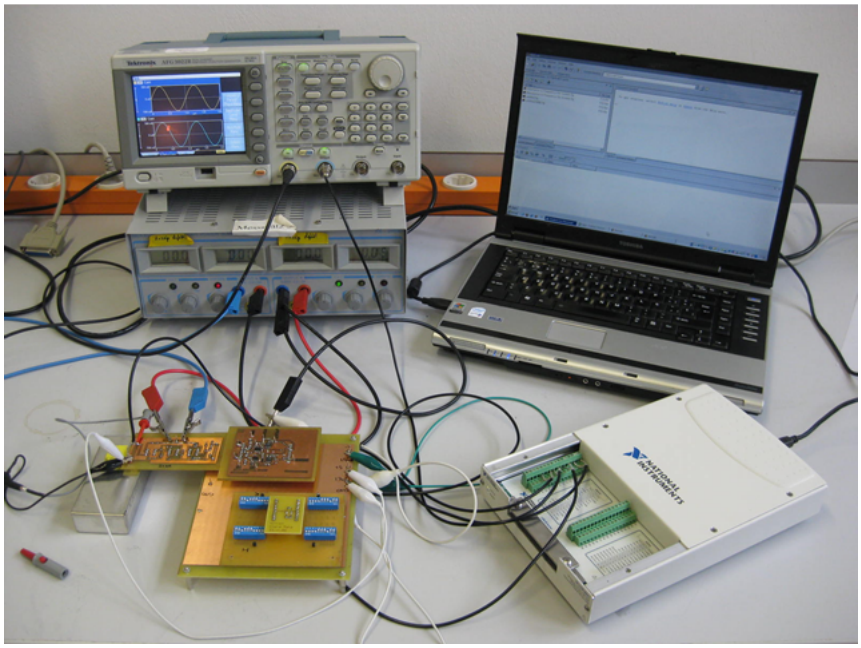

Figure 6.1: Parts involved in the developed BIS system

The first section shows the procedure of testing for the developed system. The second section covers an analysis of the Xitron Hydra using the capacitive electrodes. Next, the developed system is tested with the same electrode setups. The section summarizes the obtained results and the main errors observed in the system and in the measurements process.

6.1 Procedure of the validation

In this section the procedure to perform measurements with the developed system is described, and the parts involved in each step are shown:

1. The current source (A), measurement circuit (B) and dummy model (C) are placed on the background PCB (figure 6.1 bottom-left).

2. The body model is placed on the dummy.

3. The desired combination of resistances and capacitors values in the dummy model are selected using the switches.

4. The starting frequency, voltage amplitude and phase are selected on the AFG3000 (D) for each channel (figure 6.2 top-left).

5. Data acquisition and demodulation is performed using the data acquisition system (E) and a Matlab program (F) (figure 6.2 left).

6. The next frequency (range from 5 kHz to 43 kHz) is selected on the AFG3000 and step 4 is repeated.

7. Once all the values are obtained the impedance curve is plotted. It should be mentioned that an algorithm is used to complete the plot till 1 MHz and to calculate the electrical body model parameters R_e, R_i and C_m.

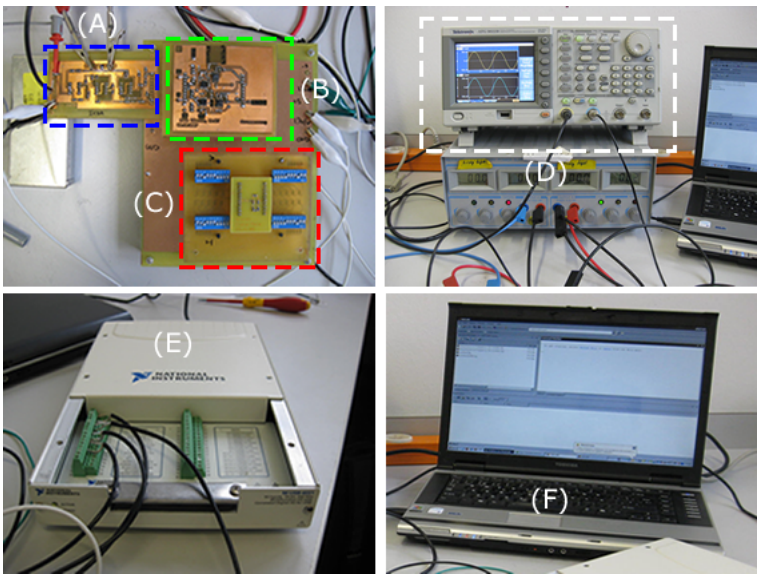

Figure 6.2: Parts of the designed bioimpedance measurement system

6.2 Performance and limitations of the Xitron Hydra

The commercial device Xitron Hydra 4200 (figure 6.3) has been tested in the frequency range from 5 kHz to 1 MHz, performing impedance measurements using the body models (section 4.2.3) and five electrode configurations. One configuration simulates the effect without capacitive electrodes (abbreviation: N.E.), the rest of the configurations used four capacitors with the same capacitive value (3.5nF, 3nF, 2.2nF and 1.5 nF). The measurements with abbreviation N.E. were carried out since, in order to detect the specific influence of the capacitive electrodes in the measurements, the influence of the built system has to be known. Results are plotted in comprehensive graphics (figures 6.4 and 6.5) and the cole-cole parameters are presented in tables 6.2 and 6.2.

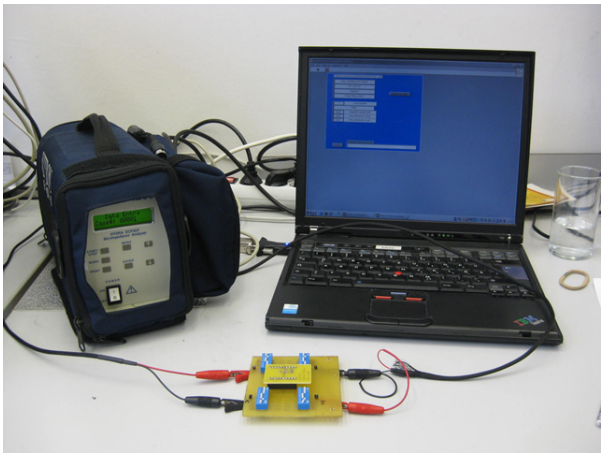

Figure 6.3: Dummy Model Test using BIS device Xitron Hydra 4200.

The following conclusions can be drawn from the results:

- A reliable test can be performed in combination without the effect of the capacitive electrodes (abbreviation N.E.).
- For the selected values of 3.5 nF and 3 nF the measurements are possible but with a high error in reactance for the lower frequency range (right side of figure 6.4 and 6.5).
- With capacitances of 2.2 nF the measurement is still possible, but with a very high error making the results useless (results are out of the plotting range).
- With values nelow 2.2 nF the Xitron showed the error message 'Current Too Low'.

One should pay attention to the results obtained by Hoffman, shown in figure 3.6, where the same conclusions are shared.

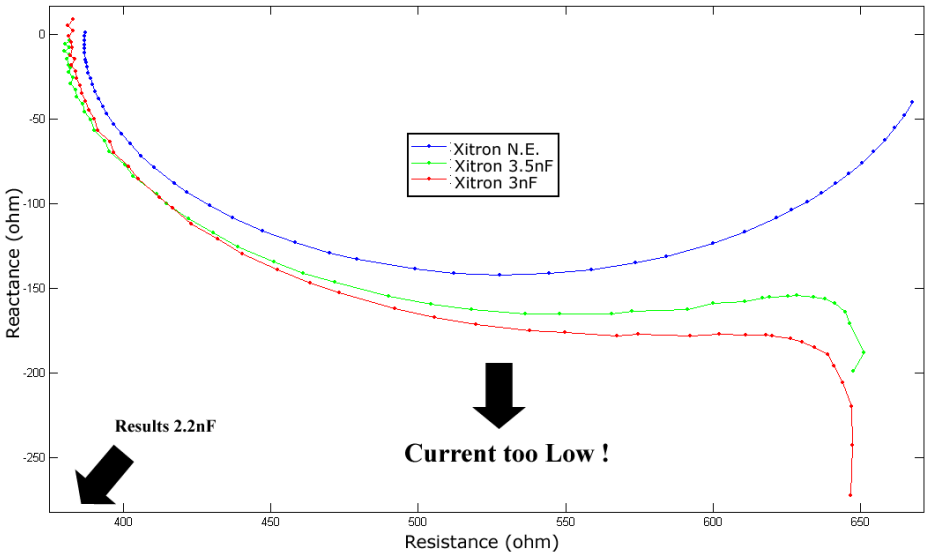

Figure 6.4: Resistance vs reactance plot for the whole body model with 56 Ω for R_{SKIN} and variations of values for C_{ELEC}

	Re (Ω)	Ri (Ω)	Cm (nF)
Original Value	$681 \pm 1\% error$	$909 \pm 1\% error$	$3.3 \pm 5\% error$
Xitron N.E.	675.7	904.5	3.26
Xitron 3.5nF	721.5	817.3	4.4
Xitron 3nF	762.7	791.8	5.4

Table 6.1: Xitron estimation of the cole-cole parameters for measurementes using the whole body dummy model.

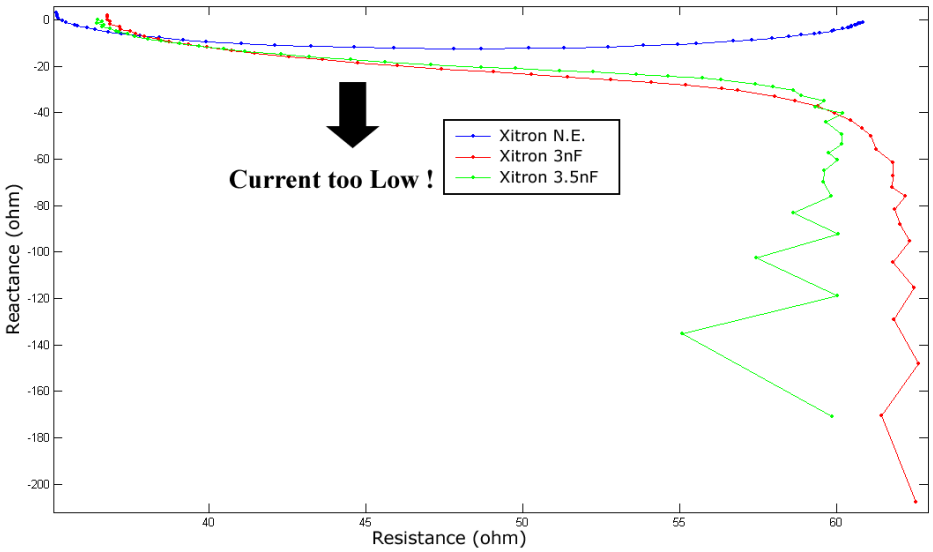

Figure 6.5: Resistance vs Reactance plot for the woman thorax dummy model with 56 Ω for R_{SKIN} and variations of values for C_{ELEC}

	Re (Ω)	Ri (Ω)	Cm (nF)
Original Value	$60 \pm 1\% error$	$80 \pm 1\% error$	$12.2 \pm 5\% error$
Xitron N.E.	60.7	86.9	11.8
Xitron 3.5nF	1336.30	49.61	172
Xitron 3nF	1643.44	49.89	140

Table 6.2: Xitron estimation of the cole-cole parameters for measurementes using the woman thorax dummy model

6.3 System calibration

This section is divided into two parts. In the first one, the influence of the system in the measurements is presented in comparison to the measurements obtained with the commercial device Xitron. Measurements without the effect of capacitive electrodes, are carried out using the developed system and both whole body and woman thorax dummy models. In the second part the main errors induced by the software and hardware are analysed and corrected.

6.3.1 Measurements

The impedance values obtained in the tests, in the frequency range from 5 kHz to 43 kHz, were processed with the Cole-Cole algorithm (section 6.3.2) in order to determine the electrical parameters. Next, from the electrical parameters, the impedance values in the frequency range from 43 kHz to 1 MHz were estimated. Finally the results were plotted from 5kHz to 1MHz.

Figure 6.6 show the measurements for the whole body dummy model and figure 6.7 for the woman thorax dummy model. The calculated Cole-Cole parameters are shown in tables 6.3.1 and 6.3.1. In the plotted results one can see two impedance plots, the one with abbreviation „Dan.“ correspond to the results of the developed system (plotted from the calculated cole-cole parameters).

	Re (Ω)	Ri (Ω)	Cm (nF)
Original Value	$681 \pm 1\%$	$909 \pm 1\%$	$3.3 \pm 5\%$
Xitron N.E.	675.7	904.5	3.26
Dan. N.E.	644.1	385.1	3.71

Table 6.3: Cole-Cole electrical parameters for a whole body dummy model measurement.

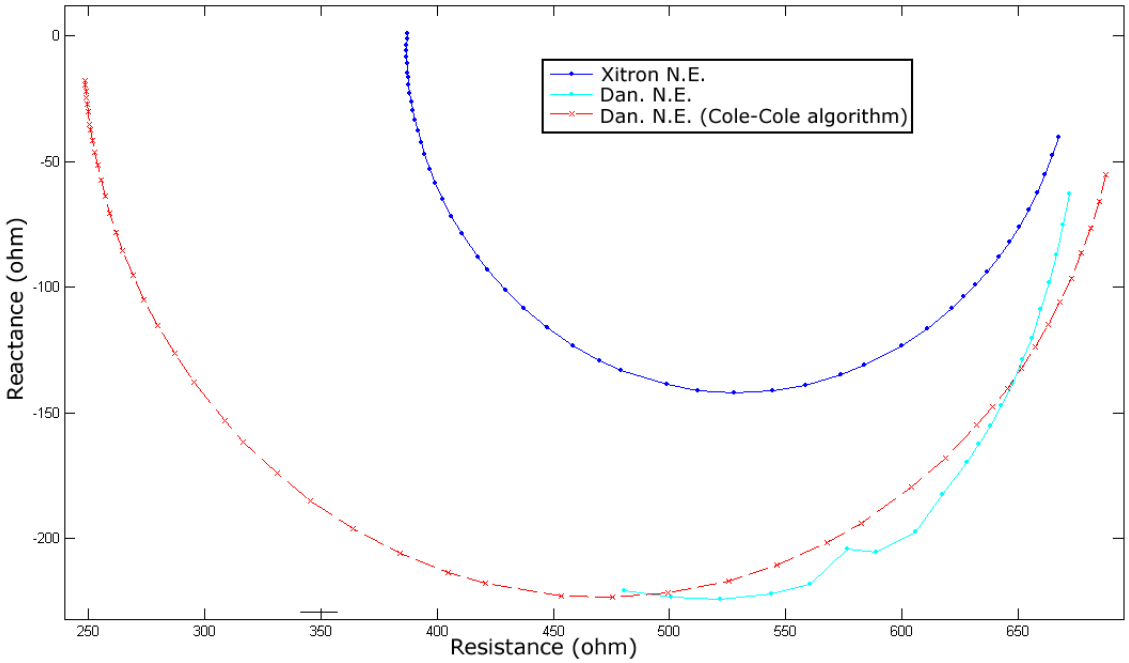

Figure 6.6: Resistance vs. reactance plot for the whole body dummy model with 56 Ω as R_{skin} and different values of C_{elec}.

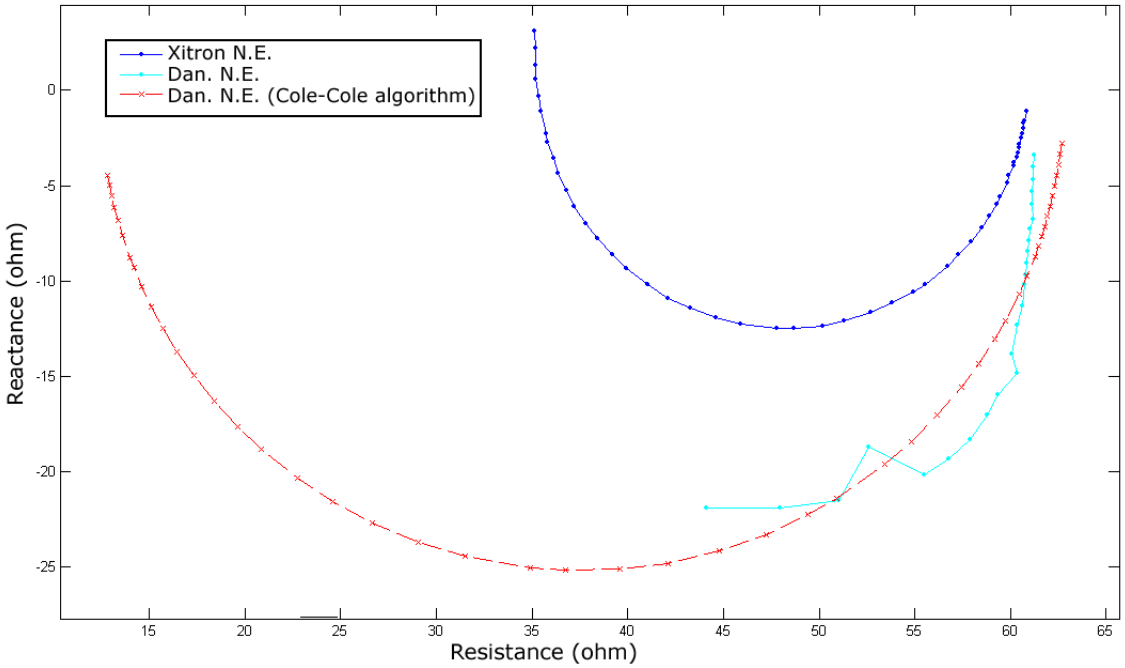

Figure 6.7: Resistance vs. reactance plot for the woman thorax dummy model with 56 Ω as R_{skin} and different values of C_{elec}.

	Re (Ω)	Ri (Ω)	Cm (nF)
Original Value	$60 \pm 1\%$	$80 \pm 1\%$	$12.2 \pm 5\%$
Xitron N.E.	60.7	86.9	11.8
Dan. N.E.	62.8	15.5	22.6

Table 6.4: Cole-Cole electrical parameters for a woman thorax dummy model measurement

The following observations were drawn from the measurements:

- The most obvious observation is the difference between the results obtained with the commercial device Xitron and the developed system. The measurements with the built system show an additional resistante and reactance added to the expected impedances.
- Measurements performed with both dummy models showed the additional impedance, then is expected that the errors were caused by the system.
- Big errors appear in the calculated R_i parameter. This error was expected since the built system just performs measurements in the low frequency range and the used Cole-Cole algorithm has to approximate the impedance values at high frequencies.

There are several factors in the system that could cause the deviations in the results. To implement a system whose properties are as close as possible to the optimum, requires a study of the errors of the system. Additionally a calibration may be use to correct them. Most of the significant errors concerning each part of the built system are explained in the following sections.

6.3.2 Software Errors. Estimation of the Cole-Cole Parameters

One good way to compare the measurements, of the BIS systems, is by means of the electrical cole-cole parameters R_e, R_i and C_m. These parameters define the values of the electrical body model. In order to calculate these parameters an algorithm is necessary. The algorithm implemented in our system uses the general equation 6.1 which defines the impedance of the electrical model (figure 4.6 right). By means of least square estimation the Cole-Cole parameters can be estimated from the measurements.

$$Z_{measured} = \frac{R_e * (R_i + \frac{1}{j*\omega*C_m})}{R_e + (R_i + \frac{1}{j*\omega*C_m})} \tag{6.1}$$

where ω=2πf and j=$\sqrt{-1}$.

In order to achieve a correct comparison, it is important to determine the difference between the equation used in our system and the one used in the commercial device Xitron Hydra. For this purpose an impedance measurement using the whole body electrical model and the Xitron was carried out. The results were processed independently by the Xitron, using the

software of the device „Hydra-Utilities“, and with the mentioned algorithm. The Cole-Cole parameters were estimated with each method and compared in table 6.3.2.

From the results shown in table 6.3.2, is possible to observe that the general equation does not approximate accurately the Cole-Cole parameters. This error has to be taken into account, since as one can see for example in the C_m parameter the error is bigger (11.6%) than the tolerance of the electrical component (5%). This is an error that can be easily corrected since just implies a mathematical rectification in the calculated parameters.

	Re (Ω)	**Ri (Ω)**	**Cm (nF)**
Original Value	$681 \pm 1\%$	$909 \pm 1\%$	$3.3 \pm 5\%$
Xitron	675.7	904.5	3.26
relative error ($\%$)	0.8	0.5	1.2
General equation	672.1	911.9	2.9
relative error ($\%$)	1.3	0.3	11.6

Table 6.5: Comparison of the estimation for the cole-cole parameters. Xitron Hydra vs general equation

6.3.3 Hardware Errors

This section is divided into two stages. In the first stage the main errors that can be found in the electronic part of our system are explained. In a second stage, the error in impedance phase and module, which is introduced by the system in our measurements, has been estimated and modelled. The following errors can be found:

A. Analog to Digital Converter (ADC)

- Sampling frequency: From the performed measurements has been observed that the number of points needed for a correct sampling of the analogue signal was at least 8 points. Thus the sampling frequency decreases to approximately 43 kHz per channel (Sampling frequency = 1.25 MHz / 4 channels / 8 points/channel).

- As it was mentioned in section 4.2.5, there exist an error in the sampling process due to the interchannel delay. It has been observed that this delay affects the phase of the signal in the demodulation process, introducing an error in the impedance calculation. It is logical to think that this error increases while the frequency of the sampling signal increases so reaching a limit in the frequency range.

- Stray capacitances could affect the inputs of the ADC, and thus the measurement. It has been demonstrated ([DP88] and [RMPAR88]), that these error sources are mainly involved in the measurement of the bioimpedance reactive component, and that the effect increases as the frequency increases.

B. leads

- Leads have resistance, inductance, core-shield and shield-shield capacitance. In [SB87], it has been found that, typical wire capacitance values gave rise to an input error even with bootstrapped cable screens.

C. Current Source

- Smaller values of capacitance for the injecting electrodes provoke the current source to require a higher power supply, in order to maintain the required current.

- Frequency behaviour: When the frequency increases, the current magnitude does not remain constant.

- Asymmetry: Although 1% resistors were used, the current magnitude and phase are not equal in both branches of the current source. This inaccuracy probably occurs due to the mismatch of the resistors and between amplifiers. A phase shift appears between the injected currents, probably caused by the mentioned mismatch in each arm and the high pass filters used. It should be mentioned that the symmetry of the current source is a required parameter [BH96].

- Output impedance: The current source has finite output impedance that decreases with increasing frequency. It was observed that the output impedance is a function of the load. This way, the current source and the differential amplifier are non-ideal and dependent on each other. An unwanted common-mode voltage develops from the interaction between the source and the rest of the circuit. The current source output impedance will divide the current output by an amount that depends on the ratio of the current source output impedance and the impedance of the injecting electrodes.

D. Amplifiers

- CMRR: every amplifier has a finite common-mode rejection ratio (CMRR) and input impedance.

- Amplifier noise. Spurious signals could be added to the main signals.

- The amplifcation of the measurement circuit (figure 6.1 (B)) was smaller than the desired value (1.7V/V). This value is an important factor in the demodulation process, so it affects the final value of impedance.

- Mismatches between amplifiers. Amplifiers could differ in behaviour.

E. Grounds

- Unequal grounds: Misconnection between grounds could result in not sharing the same potential, thus producing the reference voltage to be different in each stage of the circuit and introducing an error in the measurement.

6.3.4 Calibration Model

In order to determine the error introduced by the system, the performance under pure capacitive and pure resisitive loads have been studied. Measurements, without the effect of capacitive electrodes, haven been carried out in the frequency range from 5 kHz to 43 kHz using the developed system and the mentioned resistive and reactive loads. Figures 6.8 and 6.9 show the results for the pure resistive test under the frequency range 5 kHz to 43 kHz. The plots show the behaviour for four resistive loads determined by the resistive range from the used electrical body models. The values 671 Ω and 388 Ω correspond to the whole body dummy model, 68.8 and 38 Ω to the woman thorax dummy model. Under pure capacitive loads less concrete results were obtained, and have not been taken into account.

In figure 6.8 one can observe how the phase delay introduced by the system is constant for different loads and increases with the frequency, at $5kHz$ the phase delay is $-1.9°$ increasing to $-12.7°$ at $43kHz$. Similarly in figure 6.9 one can be observe how the error increases with the frequency and shows a quasi-similar behaviour for different loads. However the error decreases when the value of the load decreases, consequently less error is expected with the woman thorax dummy model.

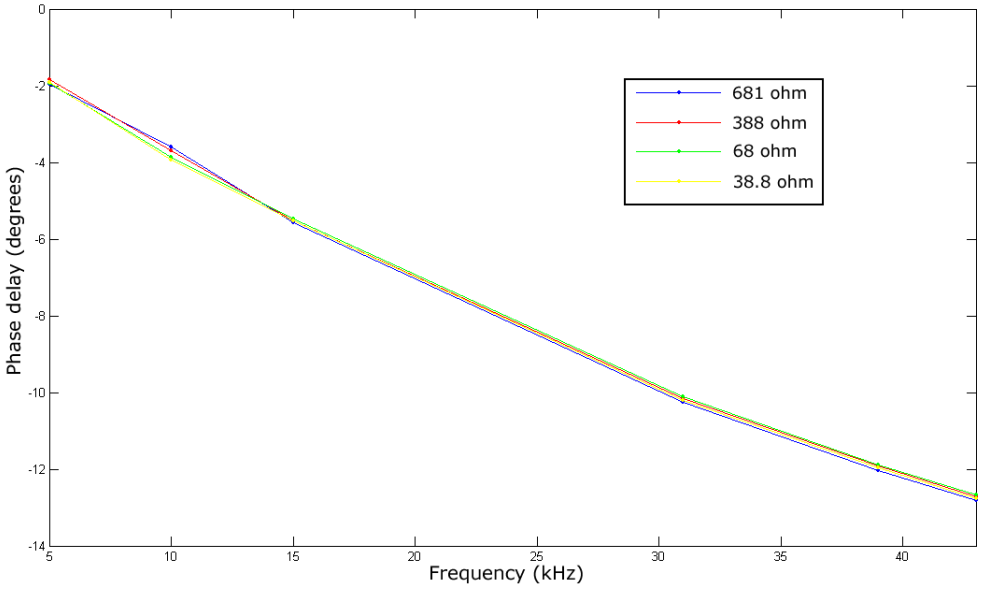

Figure 6.8: Error in the phase of the impedance introduced by the system.

$$mean\ relative\ error(\%) = 100 \times \frac{Load\ under\ measurement\ \Omega - Result\Omega}{Load\ under\ measurement\ \Omega} \tag{6.2}$$

Finally from the observed errors and the curve fitting tool from Matlab, two calibration models, one to correct the phase delay and one for the impedance module error, have been designed. It should be mentioned that better accuracy could be obtained in the calibration if individual calibration models are designed for the woman thorax and whole body model.

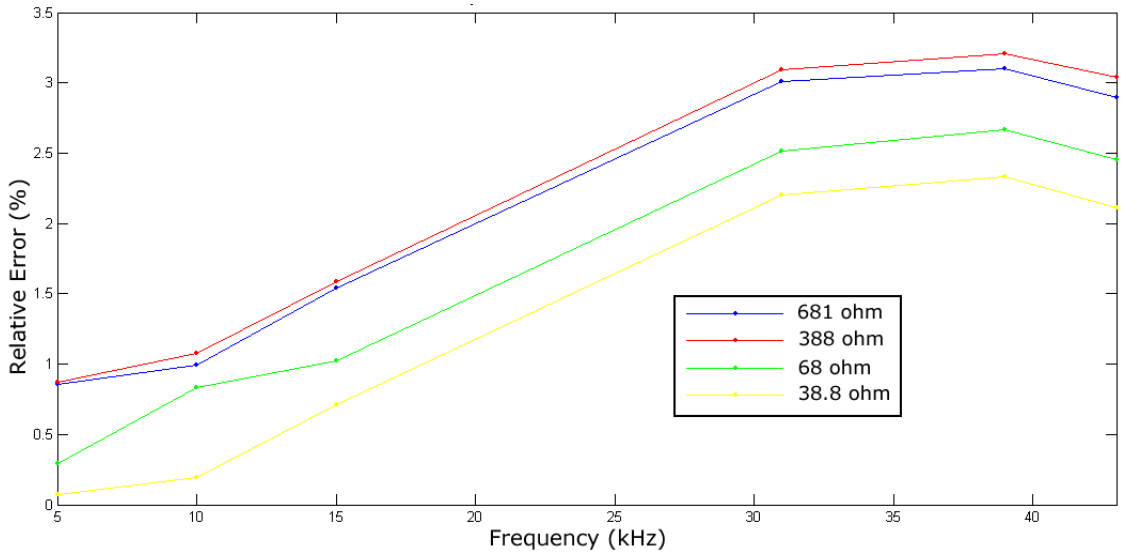

Figure 6.9: Error in the module of the impedance introduced by the system.

6.4 Results and Analysis of the Electrodes

This section is divided into two parts, the first one presents the results to measurements carried out with the developed system using the calibration model explained in section 6.3.4. The second one analyzes the influence of the electrodes in the measurements.

6.4.1 Results

The system was tested with the same electrode setups as the commercial device Xitron (see section 6.2) using both woman thorax and whole body dummy models. This section shows the results, of the built system and the Xitron, in the frequency range from 5kHz to 43kHz since is the working range of the developed system, although the Cole-Cole parameters for each measurement has been calculated with the algorithm explained in section 6.3.2.

Figures 6.10 and 6.11 show the results obtained. Tables 6.4.1 and 6.4.1 summarize the Cole-Cole parameters of each measurement.

From the results the following conclusions were extracted:

- The most obvious observation is that although with some errors, measurements with capacitive values of 3.5nF and 3nF can be carried out in the low frequency range.
- The measurement without the influence of capacitive electrodes showed small errors in comparison to the same configuration in the Xitron. Measurements start to differ at 20kHz.
- Both systems showed an influence in the reactive part at low frequencies, although the influences in the developed system are smaller. This is determined in the figure 6.10

as the bend in the plot at 7kHz. The smaller the value of electrode the higher the influence in reactance.

- The measurements with electrodes showed an attenuation in resistance and reactance. The smaller the value of electrode the higher the attenuation.
- Measurements with C_{elec} bellow 3nF gave totally erratic results. It was also observed that the current supplied with 3nF was smaller (150μA) in comparison to a measurement without electrodes (450μA).
- In relation to the Cole-Cole parameters small errors appear in the R_e parameter, although the difference is bigger for the R_i paremeter. This effect was expected since the system works in the low frequency range.
- The Cole-Cole parameter C_m showed bigger errors in the measurements with the woman thorax dummy model.

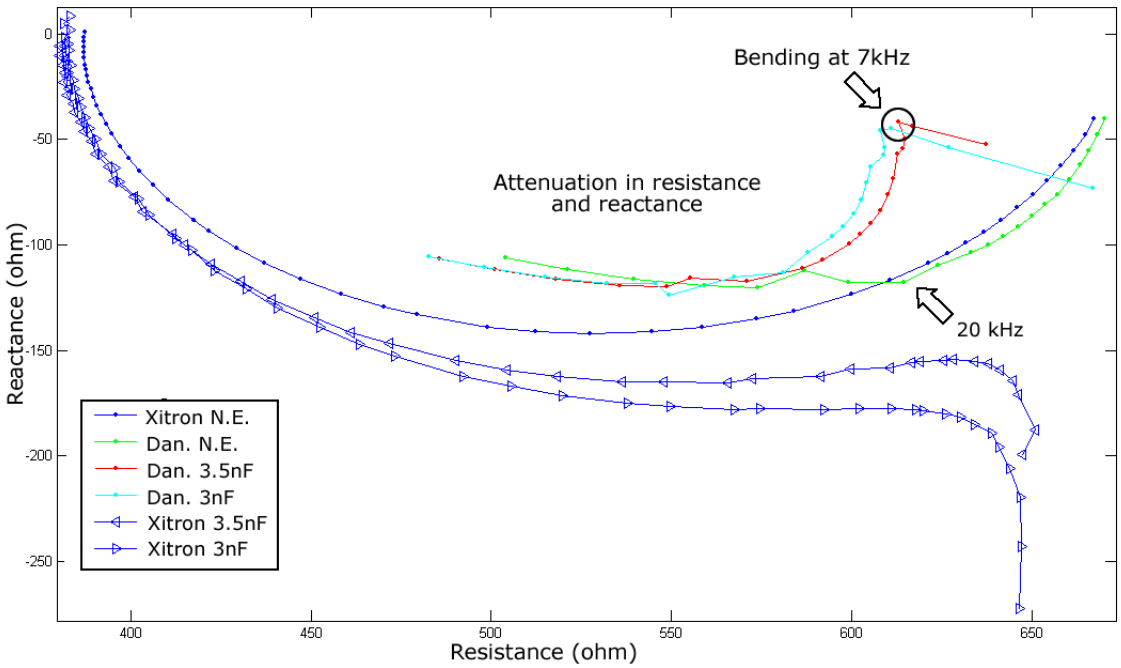

Figure 6.10: Calibrated resistance vs. reactance plot for the whole body dummy model with 56 Ω as R_{skin} and different values of C_{elec}.

	Re (Ω)	Ri (Ω)	Cm (nF)
Original Value	681 ± 1%	909 ± 1%	3.3 ± 5%
Xitron	686.18	876.19	2.99
Dan. N.E.	683.60	1249.47	2.80
Dan. 3.5nF	636.59	1049.09	2.72
Dan. 3nF	638.26	1135.48	2.84

Table 6.6: Cole-cole parameters for the whole body results

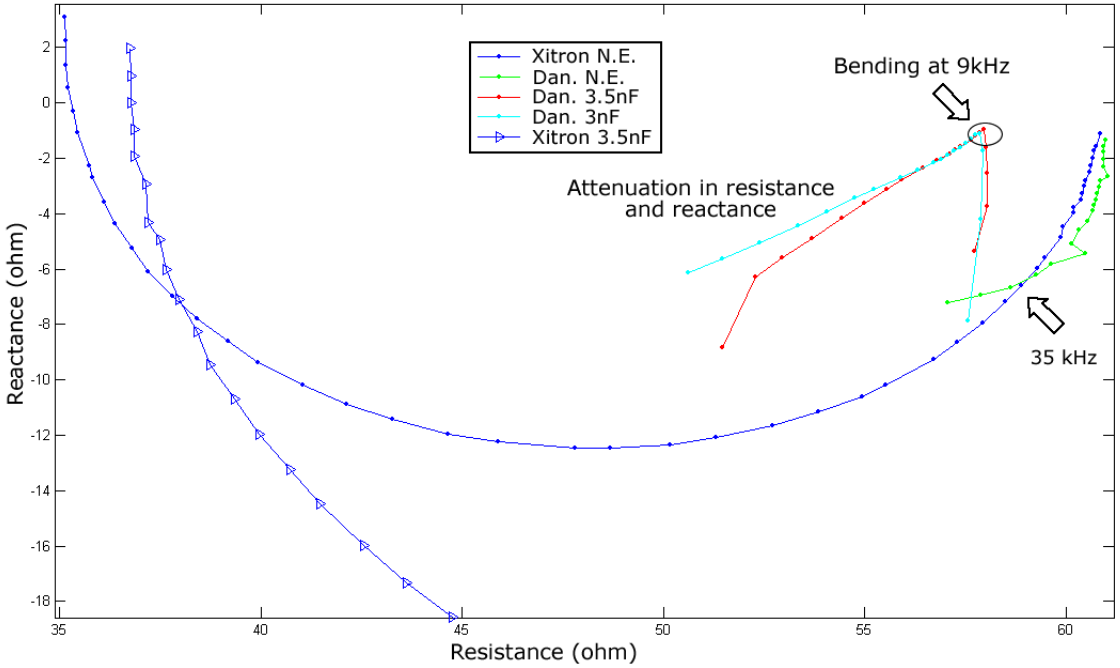

Figure 6.11: Calibrated resistance vs. reactance plot for the Woman thorax model with 56 Ω as R_{skin} and different values of C_{elec}.

	Re (Ω)	Ri (Ω)	Cm (nF)
Measured	60 ± 1%	80 ± 1%	12.2 ± 5%
Xitron N.E.	60.79	86.91	11.80
Dan. N.E.	61.37	141.88	9.80
Dan. 3.5nF	57.13	117.28	8.20
Dan. 3nF	57.23	228.15	1.03

Table 6.7: Cole-cole parameters for the woman thorax results.

6.4.2 Analysis of the Influence of the Electrodes

The analysis of the electrodes has been carried out in two steps. First the current injected by the current source has been analysed using different combinations of electrodes (figure 6.13). Secondly the effect of the injection electrodes has been tested as shown in figure 6.12 (A), using the lowest possible electrode value i.e. 3nF (figure 6.15). Finally, similarly to the second step the effect of the measuring electrodes has been tested as shown in figure 6.12 (B) using electrode values of 3.5nF and 3nF (figure 6.16).

It should be mentioned that for each measurement the Cole-Cole parameters were estimated, and from the parameters an impedance plot in the range of 5kHz to 1MHz was created. These impedance plots are additional information that helps to the analysis and can be seen in the corresponding figures.

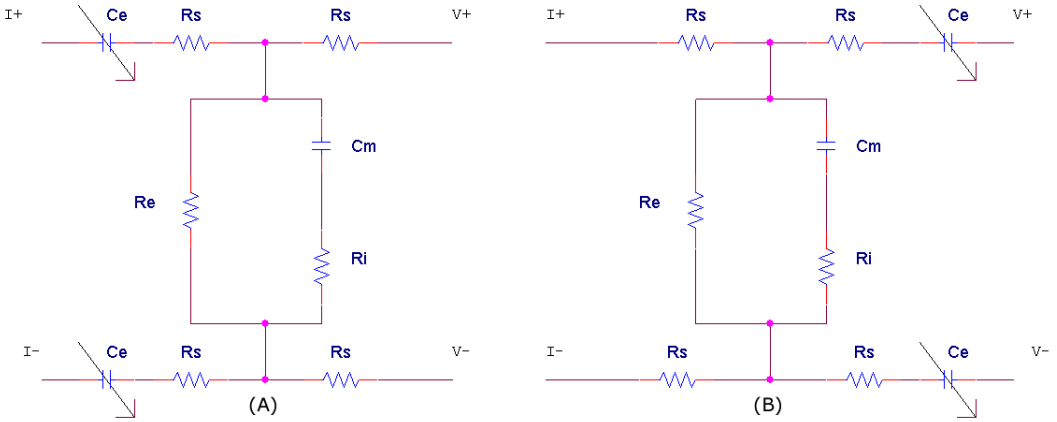

Figure 6.12: Combination of the electrodes for the analysis. Injecting electrodes (A). Measuring electrodes (B).

Current supply. In section 5.6 was determined that a voltage supply of $\pm 15V$ was enough to supply a constant 700 μA_{rms} using a capacitive value of 3.2nF as a load. As it was expected, figure 6.13 shows that in the measurement with electrode values of 2.2nF, the current supplied was quite small ($150\mu A$ peak-to-peak at 5 kHz). This is the cause of the inability of the system to carry out the measurement with this electrode value. On the contrary, one can observe that when the measurement with electrodes is possible the current supplied is high ($492\mu A$ peak-to-peak at 5 kHz) and increasing with the frequency. However the limit shown in standard EN60601 (figure 2.7) is never exceeded. Since the maximum current generated by the Xitron is $500\mu A$, this is probably the cause to not be able to carry out measurements with this electrode value.

A simple test using the designed current source, electrode capacitive values of 2.2nF, a resisitive load and different values of voltage supply was carried out. The test showed that when the voltage supply is not high enough to generate an adequate current, the measured voltage is attenuated and shows the typical charging/discharging shape (see figure 6.14)

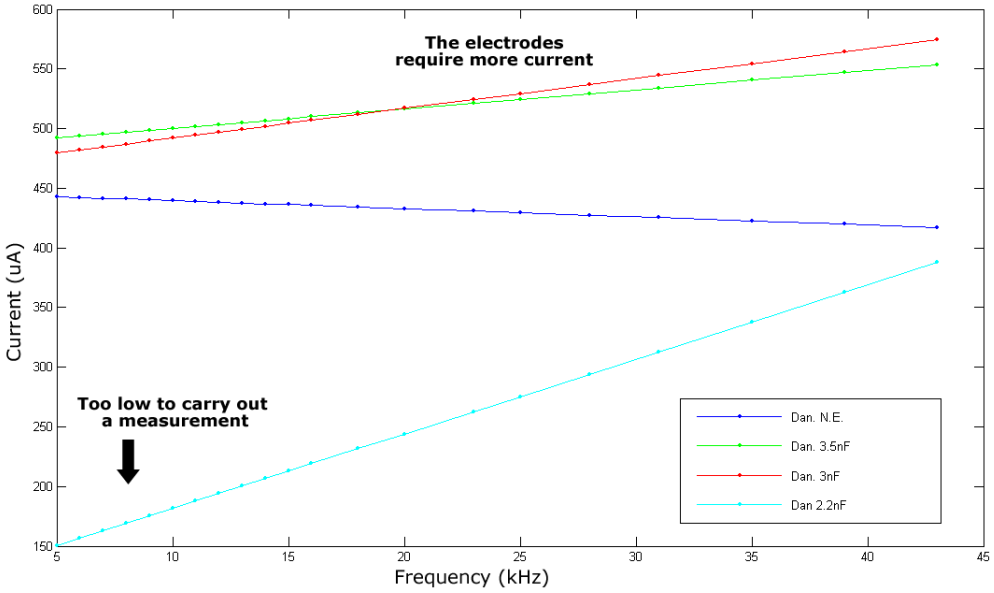

Figure 6.13: Current consumption deppending on the electrode value.

a capacitor instead of the expected sinusoidal shape. As it was expected either increasing the voltage supply or the frequency, the measured signal adquires the expected value and shape.

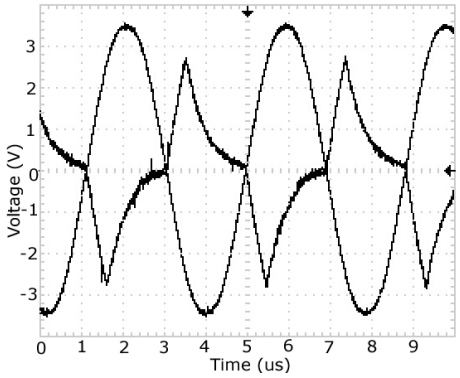

Figure 6.14: Effect of the electrodes in the current and measured voltage.

Measuring and injecting electrodes. If the results concerning to different electrode values, plotted in figure 6.10 for the whole body dummy model and figure 6.11 for the woman thorax model, are compared. It is observed that the measurments with the same electrode values showed a similar behaviour in both body models. With electrode values of 3.5nF the result is less attenuated than with electrodes of 3nF. A very big influence in the reactance appears at low frequencies, bigger in the measurement with electrode values of 3nF. In order to study these similitudes this section analyses the effect of the electrodes from measurements using the „whole body bodel“. Figures 6.15 and 6.16 showed the plotted results. Tables 6.4.2 and 6.4.2 summarize the Cole-Cole parameters.

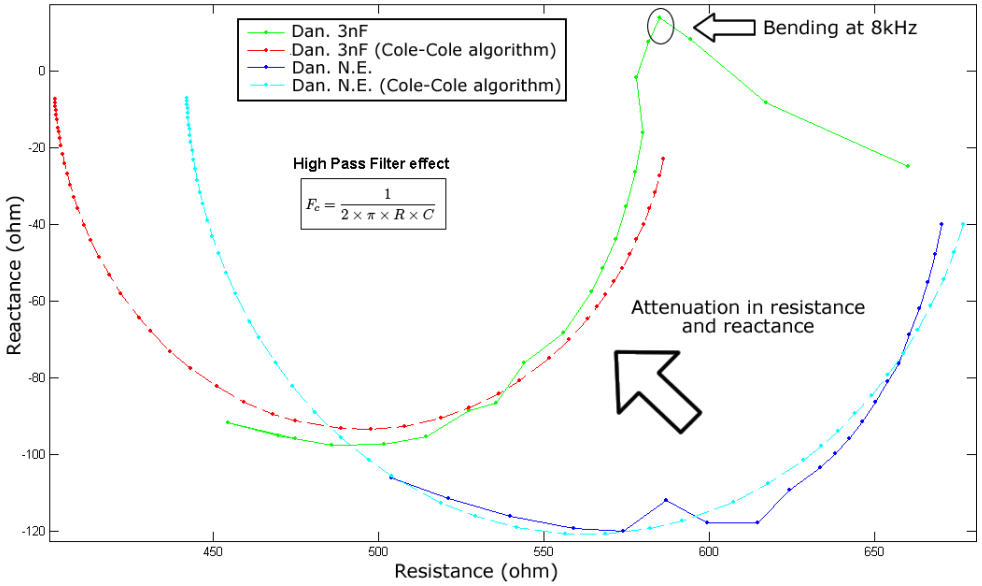

Figure 6.15: Influence of the injecting electrodes for the 'whole body model'

	Re (Ω)	Ri (Ω)	Cm (nF)
Original Value	681 ± 1%	909 ± 1%	3.3 ± 5%
Dan. N.E.	644.1	385.1	3.71
Dan. 3nF	602.2	284.9	3.43

Table 6.8: Cole-Cole parameters, influence of the injecting electrodes for the 'whole body model'.

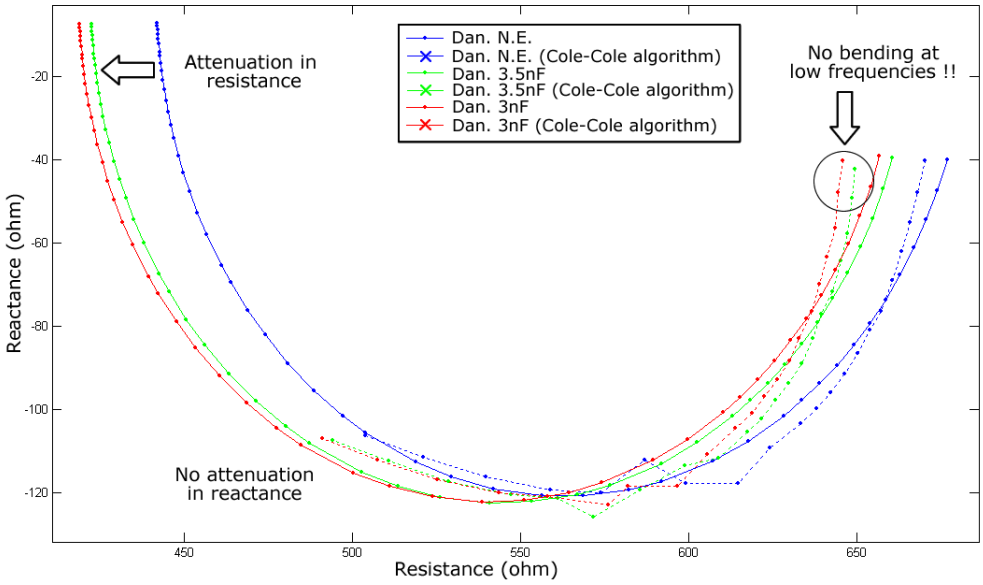

Figure 6.16: Influence of the measuring electrodes for the 'whole body model'.

	Re (Ω)	Ri (Ω)	Cm (nF)
Original Value	681 $\pm$ 1%	909 $\pm$ 1%	3.3 $\pm$ 5%
Dan. N.E.	644.1	385.1	3.71
Dan. 3nF	673.4	288.8	3.83
Dan. 2.2nF	669.7	282.7	3.86

Table 6.9: Cole-Cole parameters, influence of the measuring electrodes for the 'whole body model'.

From figure 6.15 one can observe that the injecting electrodes produced an attenuation in the measurement. One has to take into account that a high pass filter appears by the combination of the injecting electrodes and the body model, the cut-off frequencies using electrodes of 3nF (equation 6.3) are approximately $\approx 77.0kHz$ for the whole body model and $\approx 884.18kHz$ for the woman thorax model. This is the main cause for the higher attenuation in the woman thorax results (observed in figure 6.11). On the other hand the effect of the measuring electrodes was less significant (figure 6.16), in turn a voltage divider appears by the combination of the impedance of the measuring electrodes and the input impedances of the measuring amplifier.

$$F_c = \frac{1}{2 \times \pi \times R \times C} \tag{6.3}$$

It is very important to mention that although the behaviour of the electrodes shows a common pattern using different body models, the attenuation they provoke is different. Figure 6.17 shows the attenuation (in %) that the electrodes of 3nF provoke to a measurement using the whole body (green plot) and the woman thorax (blue plot) model. It is evident that exist a higher attenuation (0.5% to 0.775%) exists when measuring using the woman thorax model. One can observe that the attenuation depends on the value of the electrodes and the section of the body under measurement (whole body, thorax, etc).

In order to correct the observed attenuation one should keep in mind that BIS measurements are allways performed under specific and controlled conditions, where the value of the electrodes C_{elec}, the section of the body under measurement, the age and the gender of the patient are known. Consequently the attenuation of the electrodes can be modelled in advance and corrected in the measurements.

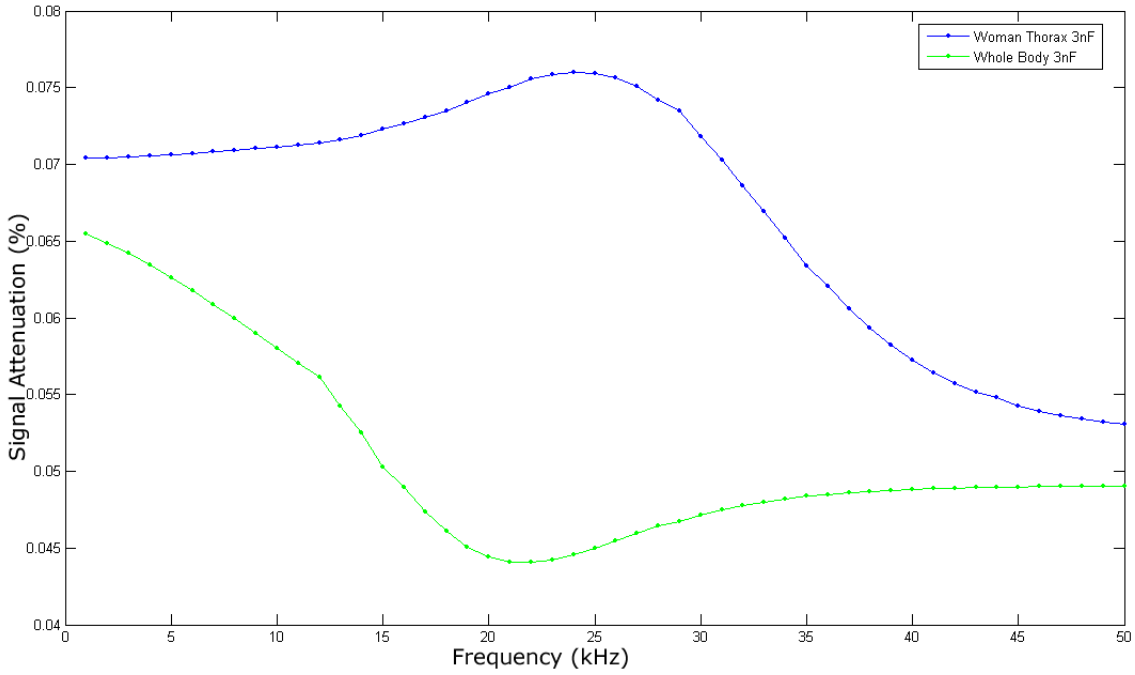

Figure 6.17: Difference in attenuation depending on the body model. Capacitive electrode value 3nF.

7 Conclusions

Within this project a BIS device able to perform measurements using capacitive electrodes has been developed. The device is able to work in the critical frequency range for capacitive measurements, namely from 5 kHz to 43 kHz. First results show the ability of the device to perform measurements with capacitive electrodes till a value of 3nF.

This represents an improvement in the technology, since an analysis of the actual commercialized device Xitron Hydra 4200 (section 6.2), has demonstrated its inability to perform impedance measurements using electrodes with this capacitance values. The reported limit of capacitance values is between 18nF and 8.6nF. The actual limitations were taken into consideration and the system was developed in consequence.

Additional test demonstrated the hypothesis (postulated in section 3.5.1) that an increase of the voltage supply of the current source, permits the current injection using capacitive electrodes with a value of less than 8.6nF. Consequently, the high impedance of the electrodes is overcome. Simulations in section 5.6 showed that a voltage supply of $\pm 15V$ was enough to generate a constant 700 μA_{rms} using electrode capacitance values of 3.2nF. Measurements with the built system confirm the simulations.

The implemented system presented however some limitations (see section 6.3.4). There are some factors that affect the measurement, factors such as the load dependency of the current source, the inexact amplification in the measurement circuit, the induced phase delay in the measured signals due to the interchannel delay of the analog to digital converter and, the most important for this thesis, the influence of the electrodes. Nevertheless, most of factors can be corrected using calibration models.

In regard to the influence of the electrodes in the measurement (section 6.4.2), the results indicated that the measured impedance is affected by the combination of the individual behaviours of the injecting and measuring electrodes. Concerning the measuring electrodes, a voltage divider appears by the combination of the electrodes' impedance and the input impedance of the measuring amplifier, although the latter influence was less significant. Regarding the injecting electrodes, they produced substantial attenuation in the measurement. A high pass filter appeared by the combination of the injecting electrodes and the body dummy model. The cut-off frequencies for the observed filter behaviour using electrodes of 3nF were approximately $\approx 77.0kHz$ for the whole body dummy model and $\approx 884.18kHz$ for the woman thorax dummy model. This is the main cause for the observed higher attenuation using the woman thorax model.

The attenuation produced by the injecting electrodes varies with the capacitance value of the electrodes and the section of the body under measurement (whole body, thorax, etc). It has been determined that if the measurements are performed under specific and controlled conditions, i.e., the value of the electrodes C_{elec}, the section of the body under measurement, the age and the gender of the patient are known, the influence of the electrodes can be modelled and extracted from the results.

The working frequency range of the system is limited to 5 kHz to 43 kHz, due to the selected analog to digital converter (USB-6251). From the performed measurements is deduced that the number of points needed for a correct sampling of the analogue signals was at least 8 points per cycle. The algorithm (section 6.3.2) used to calculate the Cole-Cole parameters can correctly approximate the R_e parameter since it is dependent on the low frequencies. However, some inaccuracies are presented in the R_i and C_m parameters since they are dependent on the high frequencies.

Concerning the selected current source (chapter 5), one can observe that in the simulations at low frequencies it was easy to find a current source that accomplished the specification of constant current magnitude (700 μA_{rms}). But, in practice (section 6.4.2), one can observe that the current depends on the load and the frequency. The test for current consumption showed that the smaller the electrode capacitance the higher is the current consumption. From these results, it was also discovered that the electrode capacitance value 3nF is the limit value for both the Xitron Hydra and the developed system.

In order to facilitate the treatment of the errors introduced by the hardware of the system, all have been grouped and modelled (section 6.3.4). From the results one can observe that the phase delay and the error in impedance module increased with the frequency and showed a quasi-similar behaviour for measurements under different loads. This pattern in the behaviour has facilitated the use of calibration models, and thus the correction of the mentioned problems.

Concerning the software of the system (section 6.3.2), an algorithm was used to calculate the Cole-Cole parameters of the body dummy model under measurement. From the results one can observe that the error introduced by the algorithm has to be taken into account, since in some cases the error was bigger than the tolerance of the electrical component under measurement. This is an error that can be easily corrected since it just implies a mathematical rectification in the calculated parameters.

8 Outlook

Although the possibility of using capacitive electrodes is demonstrated, one can see that several factors affect the measurement process. In order to obtain a deeper knowledge about the behaviour of capacitive electrodes in BIS measurements, one should overcome the errors introduced by the measuring system and focus on the electrode part. The effect of the injecting electrodes is an important topic in the system that requires a deeper research. As observed, the effect of these electrodes differs from the used body dummy model thus will be different from patient to patient, similarly the effect of the measuring electrodes and its voltage dividing behaviour. From the analysis of the electrodes was drawn the conclusion that the behaviour follows a pattern, thus if a study using different electrodes and different body models is carried out a solution could be found.

Concerning one of the big topics studied in this thesis, the current source, it was reported that the current magnitude directly depends on the load that the system must drive, in this case the electrodes and the body dummy model. This effect limits the current magnitude and therefore the driving capability at different frequencies. At this point some approaches could be taken. Firstly, if the application is not dependent on the number of electrodes, bridge configurations can be implemented. Second and more interesting, generalized impedance converters (GIC) or negative impedance converters (NIC) can be used. As some researchers have reported a Howland topology in parallel with a generalized impedance converter, will almost allow an independent adjustment of output resistance and output capacitance at different frequencies. This solution requires a digital auxiliary circuit that needs for an independent study to achieve the required precision.

The working frequency range of the developed system is so far limited to 43 kHz. This problem is basically due to the limited sampling frequency and the interchannel delay of the used analog to digital converter (USB-6251,) which induces a phase delay in the measured signals and consequently in the demodulation process. This can be solved by using an analog (by hardware) implementation of the demodulation process instead of the implemented by software. This solution will avoid the introduced phase delay in the measurements. In the same way this approach will increase the working frequency range and the accuracy in the calculation of the Cole-Cole parameters.

The inexact calculation of the Cole-Cole parameters R_e, R_i and C_m could be solved by increasing the frequency range for the measurements and the implementation of an extended Cole-Cole equation as the one used in the commercial device Xitron Hydra. Increasing the frequency range will increase the number of results and consequently the data from where the Cole-Cole parameters are estimated.

To conclude, if a compact system or portable system is desired, one should pay attention to new hardware solutions instead of the applied commercialized products (AFG300 and NI USB-6251). It is evident that the system can not perform BIS measurements with patients however the basis for further research in this field has been established.

A Appendix

A.1 ISSA. Improved Howland Current Pump.

The transconductance of the source is the function A.1:

$$I_{gen} = -V_{sg}\frac{R_2}{R_1 R_{4b}} + V_{out}\frac{R_2R_3 - R_1R_{4b} - R_1R_{4a}}{R_1R_{4b}(R_3 + R_{4a})} \tag{A.1}$$

if the condition $R_2R_3 = R_1(R_{4a} + R_{4b})$ is accomplished, the transconductance can be expressed as the function of three resistors, eq. A.2:

$$I_{gen} = -V_{sg}\frac{R_2}{(R_1R_{4b})} \tag{A.2}$$

and the Output resistance A.3:

$$R_{out} = \frac{R_1R_{4b}(R_3 + R_{4a})}{R_2R_3 - R_1(R_{4a} + R_{4b})} \tag{A.3}$$

Current Source Resistors Configuration Test The selected resistor configurations accomplish the design equation $R_2R_3 = R_1(R_{4a} + R_{4b})$. Table A.1 shows the resistor values selected for the test. From the simulations one can drawn that the best performance, in current magnitude and phase delay, is obtained with the configuration $ISSA_{5k}$, $(R_1 = R_2 = R_3 = 5\ k\Omega, R_{4a} = 2.5\ k\Omega, R_{4b} = 2.5k\Omega)$.

R1	R2	R3	R4a	R4b
2k5	2k5	2k5	1	2k5
5k	5k	5k	2k5	2k5
7k5	7k5	7k5	5k	2k5

Table A.1: Table of Resistor Values for ISSA

Simulations

In the simulations, it has been defined an abbreviation method in order to identify every parameter, which corresponds to the following format:

$RL -' namecurrentsource' -' ResistorConfiguration' -' ResistiveLoadValue'$

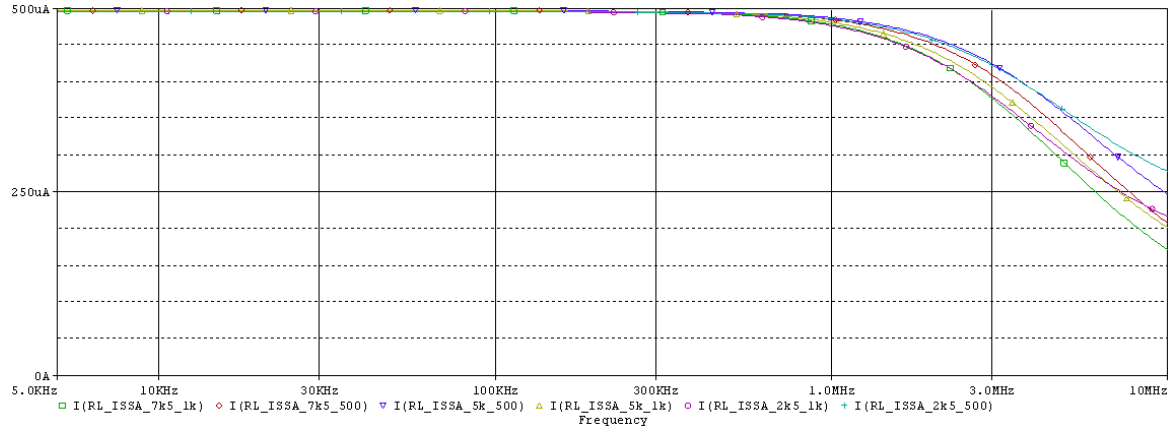

Figure A.1: Current Magnitude behaviour in the range of 5 to 1000 kHz.

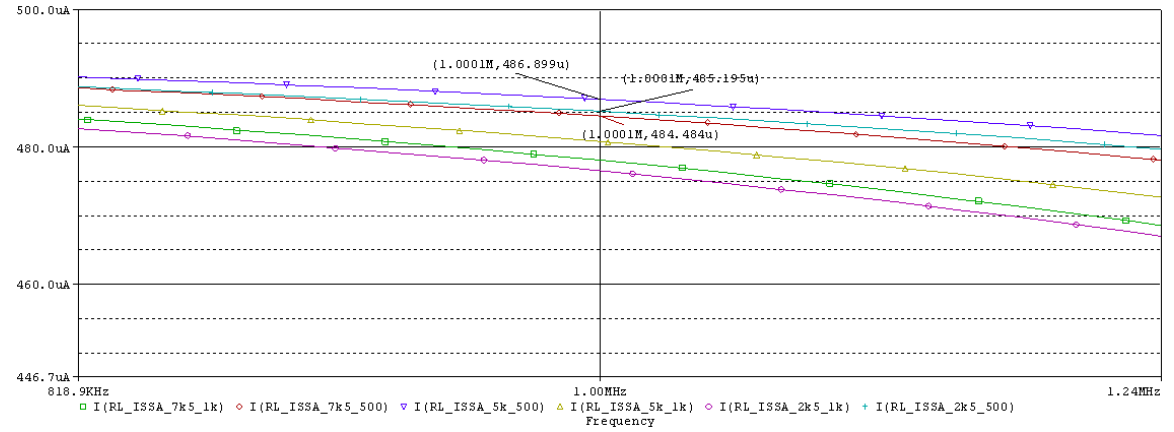

Figure A.2: Current Magnitude behaviour at 1 MHz.

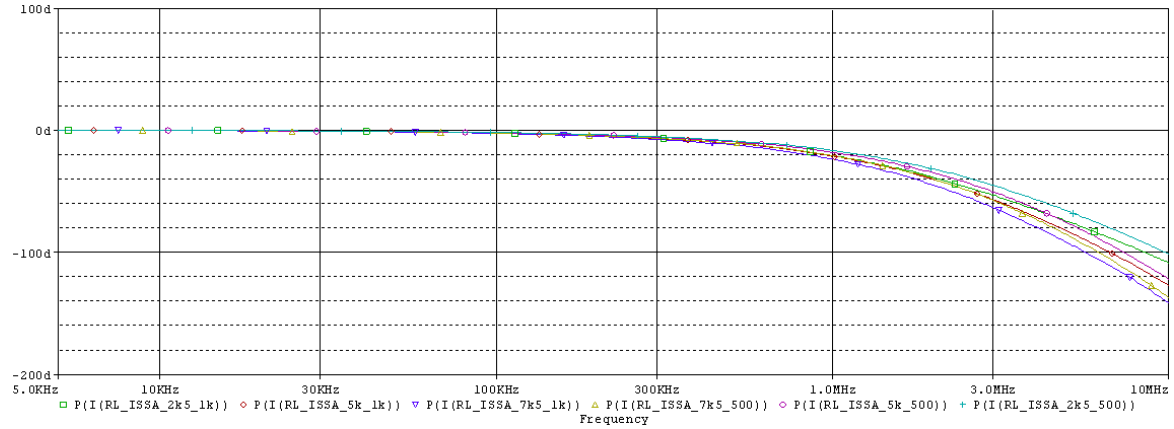

Figure A.3: Phase delay behaviour in the range of 5 to 1000 kHz.

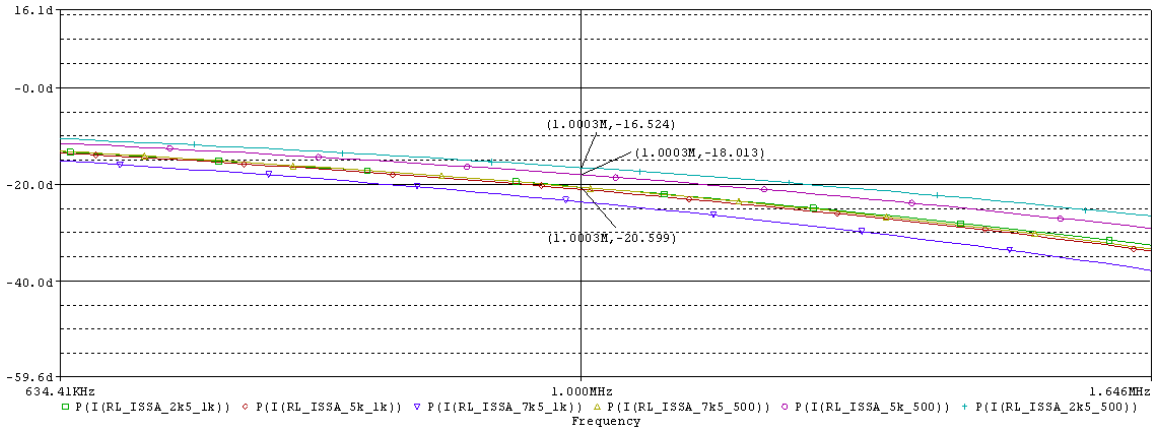

Figure A.4: Phase delay behaviour at 1 MHz.

A.2 ICSA. Improved Howland Current Pump.

The transconductance of the source is the function A.4:

$$Igen = -Vsg\frac{R_2}{R_1R_{4b}} + V_{out}\frac{R_2R_3 - R_1R_{4b} - R_1R_{4a}}{R_1R_{4b}(R_3 + R_{4a})} \tag{A.4}$$

If the condition $R_2R_3 = R_1(R_{4a} + R_{4b})$ is accomplished, the transconductance can be expressed as the function of A.5:

$$I_{gen} = -V_{sg}\frac{R_2}{R_1R_{4b}} \tag{A.5}$$

Current Source Resistors Configuration Test The selected resistor configurations accomplish the design equation $R_2R_3 = R_1(R_{4a}+R_{4b})$. Table A.2 shows the resistor values selected for the test. From the simulations one can drawn that the best performance is obtained with the configuration $ICSA_{5k}$ $(R_1 = R_2 = R_3 = 5\ k\Omega, R_{4a} = 2.5\ k\Omega, R_{4b} = 2.5k\Omega)$.

R1	R2	R3	R4a	R4b
2k5	2k5	2k5	1	2k5
5k	5k	5k	2k5	2k5
7k5	7k5	7k5	5k	2k5

Table A.2: Table of Resistor Values for ICSA

Abbreviations used in the following graphics correspond to the next format:

$RL -' namecurrentsource' -' ResistorConfiguration' -' ResistiveLoadValue'$

Simulations

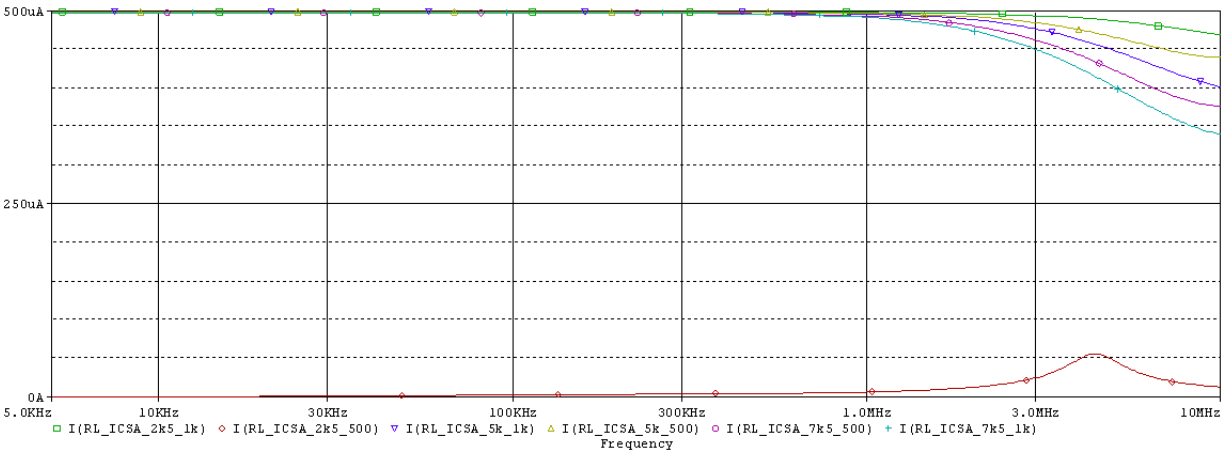

Figure A.5: Current Magnitude behaviour in the range of 5 to 10000 kHz.

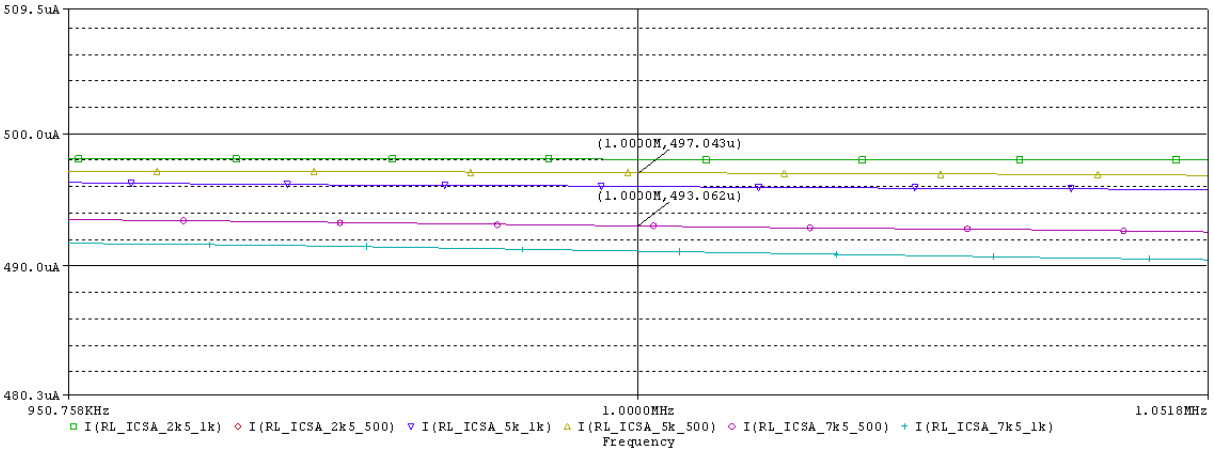

Figure A.6: Current Magnitude behaviour at 1 MHz.

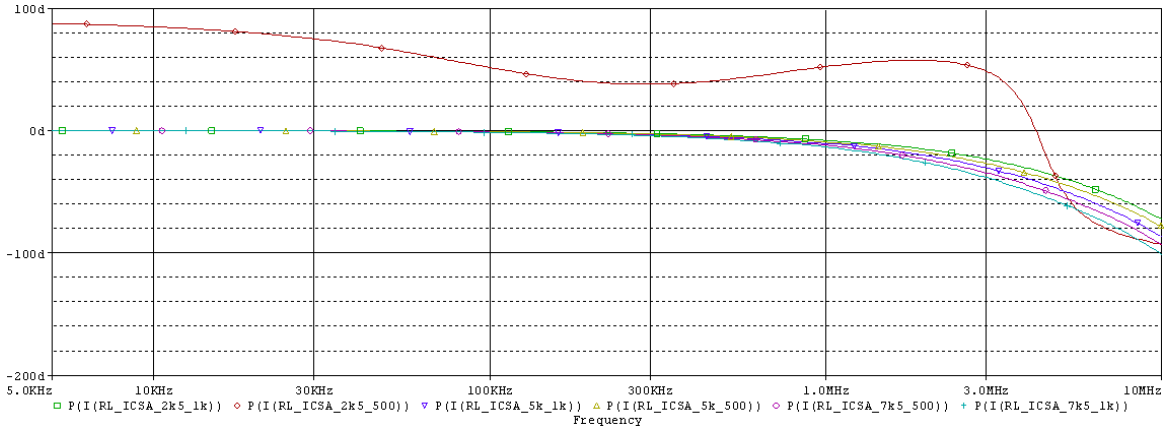

Figure A.7: Phase delay behaviour in the range of 5 to 10000 kHz.

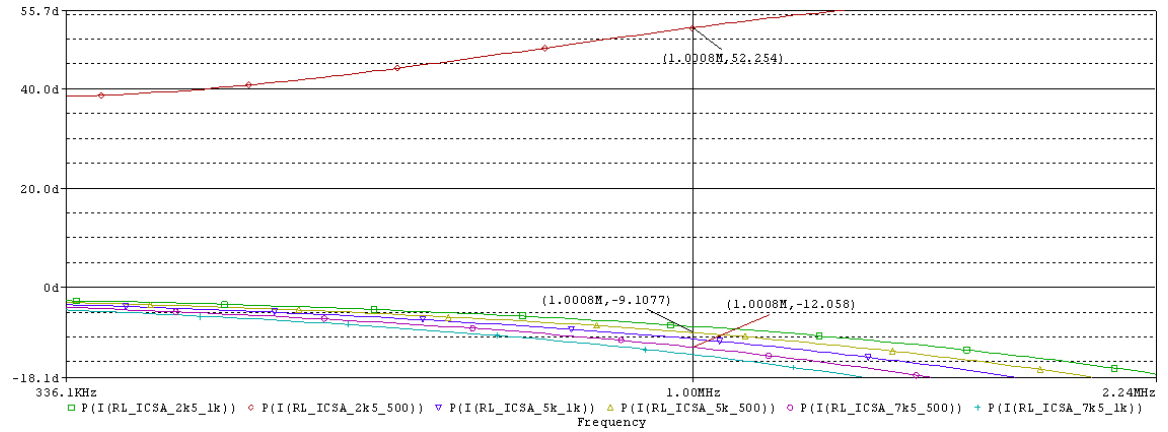

Figure A.8: Phase delay behaviour at 1 MHz.

A.3 ISSB. Improved Howland Current Pump.

The transconductance of the Howland source B is the function A.6:

$$I_{gen} = V_{sg}\frac{R_2R_{4a} + R_3R_{4b} + R_3R_2}{R_3R_{4b}(R_2 + R_1)} + V_{out}\frac{R_1R_{4a} - R_3R_{4b} - R_3R_2}{R_3R_{4b}(R_1 + R_2)} \tag{A.6}$$

Although if the condition $R_1 \times R_{4a} = R_3 \times (R_2 + R_{4b})$ is accomplished, the transconductance can be expressed as the function of one resistor and the input voltage, not as well as the configuration A where the transcoductance was in function of three resistors. In this case:

$$I_{gen} = \frac{V_{sg}}{R_{4b}} \tag{A.7}$$

Current Source Resistors Configuration Test The selected resistor configurations accomplish the design equation ($R_1 \times R_{4a} = R_3 \times (R_2 + R_{4b})$). Table A.3 show the selected resistor values. From the simulations one can drawn that the best performance is obtained with the configuration $R_1 = R_{4a} = R_3 = 2.5\ k\Omega$ and $R_2 = 1\Omega$.

R1	R2	R3	R4a	R4b
2k5	1	2k5	2k5	2k5
5k5	3k	5k	5k	2k5
10k5	8k	10k	10k	2k5

Table A.3: Table of Resistor Values for ISSB

Abbreviations used in the following graphics correspond to the next format:

$RL -' namecurrentsource' -' ResistorConfiguration' -' ResistiveLoadValue'$

Simulations

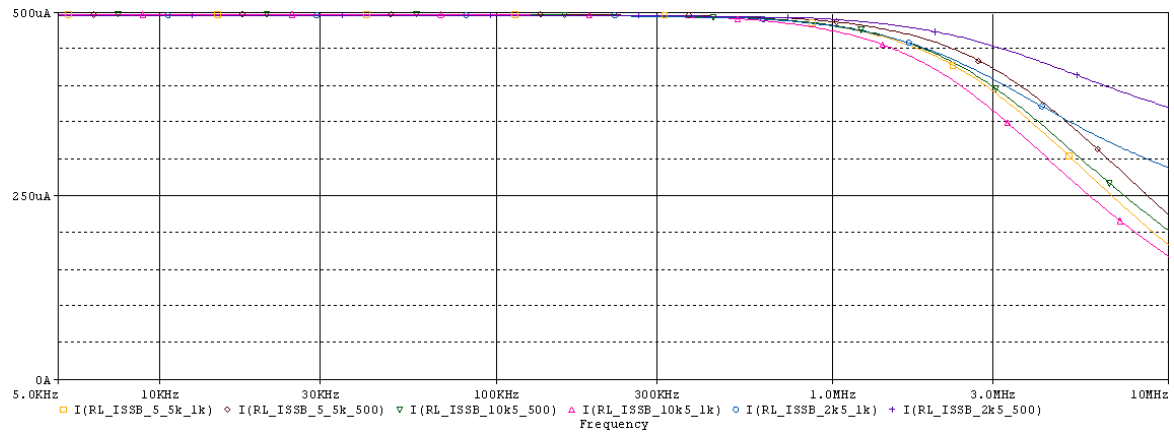

Figure A.9: Current Magnitude behaviour in the range of 5 to 10000 kHz.

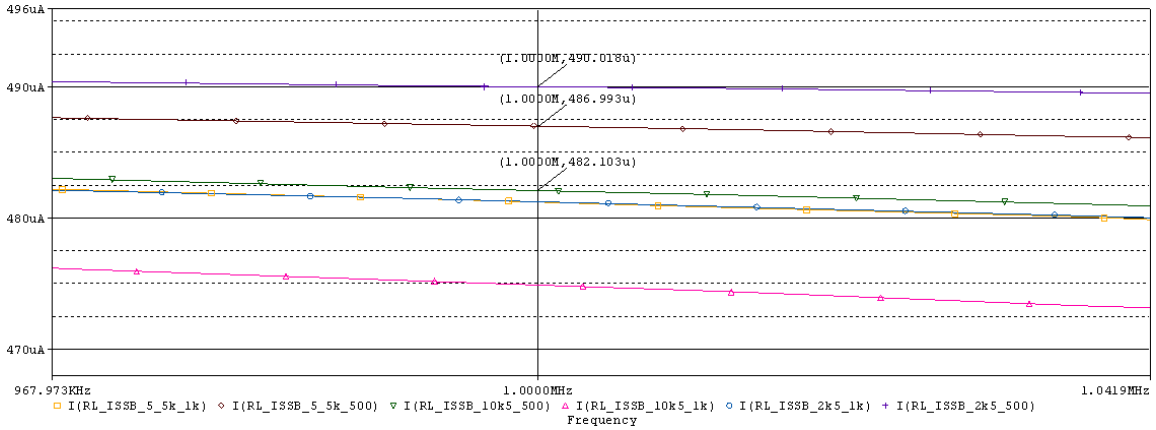

Figure A.10: Current Magnitude behaviour at 1 MHz.

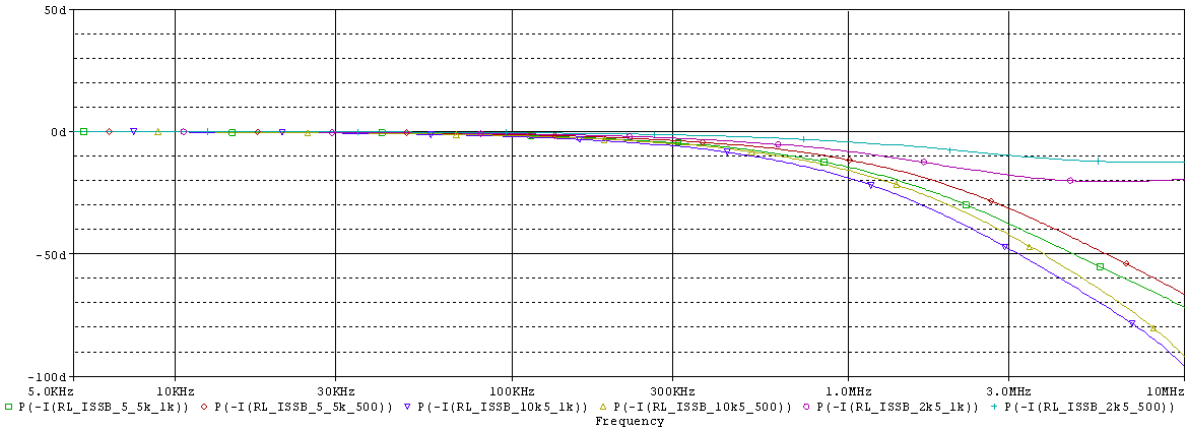

Figure A.11: Phase delay behaviour in the range of 5 to 10000 kHz.

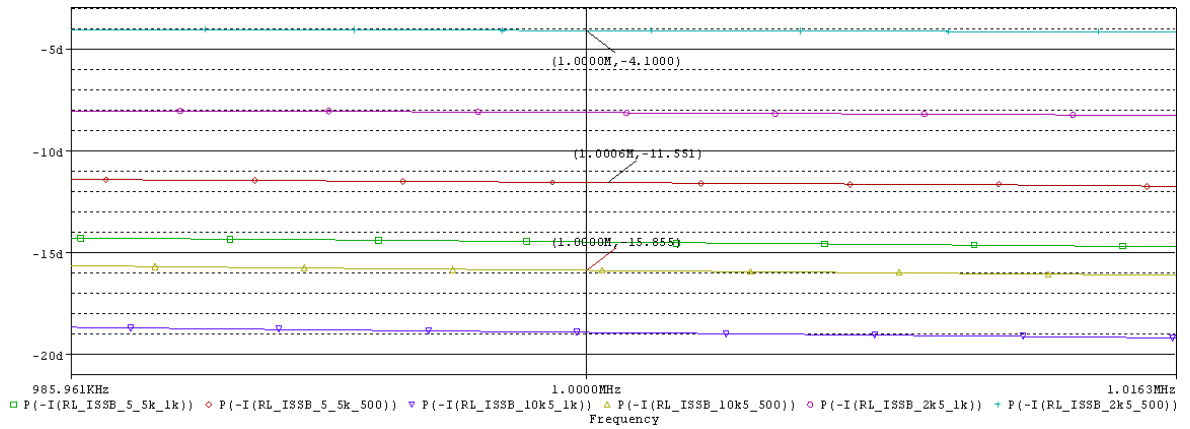

Figure A.12: Phase delay behaviour at 1 MHz.

A.4 ICSB. Improved Howland Current Pump.

The transconductance of the source is the function A.8:

$$I_{gen} = \frac{Vsg}{R4b} \times \frac{R2(R3 + R4a)}{R3(R1 + R2)} + V_{out} \times \frac{R_{4a}R_1 - R_2R_3}{R_3R_{4b}(R_1 + R_2)} \tag{A.8}$$

Although if the condition $R_1 = R_2 = R_3 = R_{4a}$ is accomplished, the transconductance can be expressed as the equation A.9:

$$I_{gen} = \frac{V_{sg}}{R_{4b}} \tag{A.9}$$

Current Source Resistors Configuration Test The selected resistor configurations accomplish the design equation $R_1 = R_2 = R_3 = R_{4a}$. Table A.4 show the resistors values selected for the test. From the simulations one can drawn that the best performance is obtained with the configuration $ICSB_{2k}$ $(R_1 = R_2 = R_3 = R_{4a} = 2k\Omega)$.

R1	R2	R3	R4a	R4b
2k	2k	2k	2k	2k5
4k	4k	4k	4k	2k5
5k	5k	5k	5k	2k5
10k	10k	10k	10k	2k5

Table A.4: Table of Resistor Values for ICSB

Abbreviations used in the following graphics correspond to the next format:

$RL -' namecurrentsource' -' ResistorConfiguration' -' ResistiveLoadValue'$

Simulations

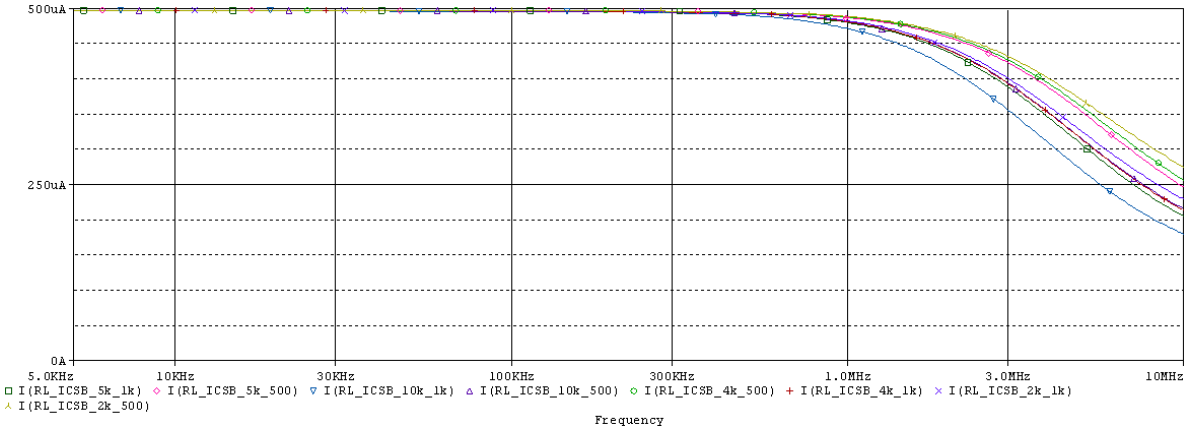

Figure A.13: Current Magnitude behaviour in the range of 5 to 10000 kHz.

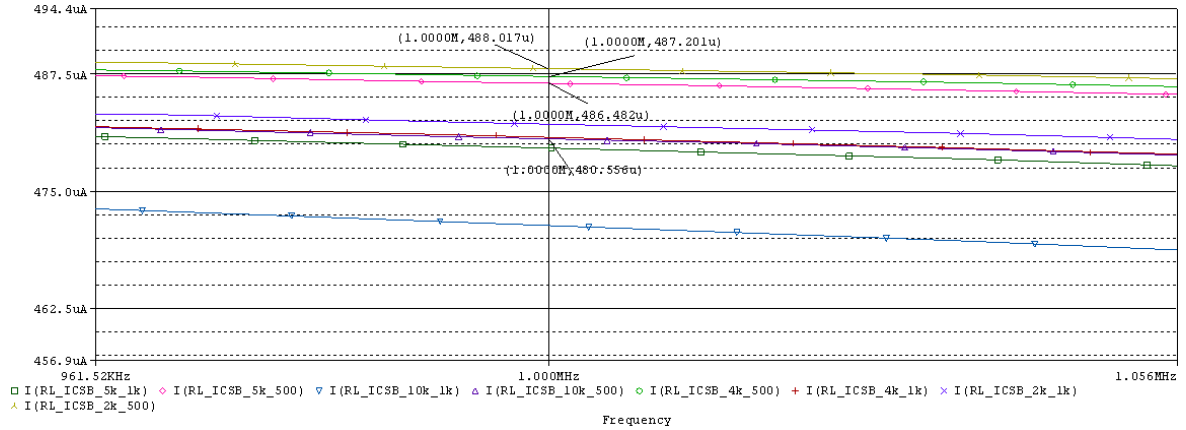

Figure A.14: Current Magnitude behaviour at 1 MHz.

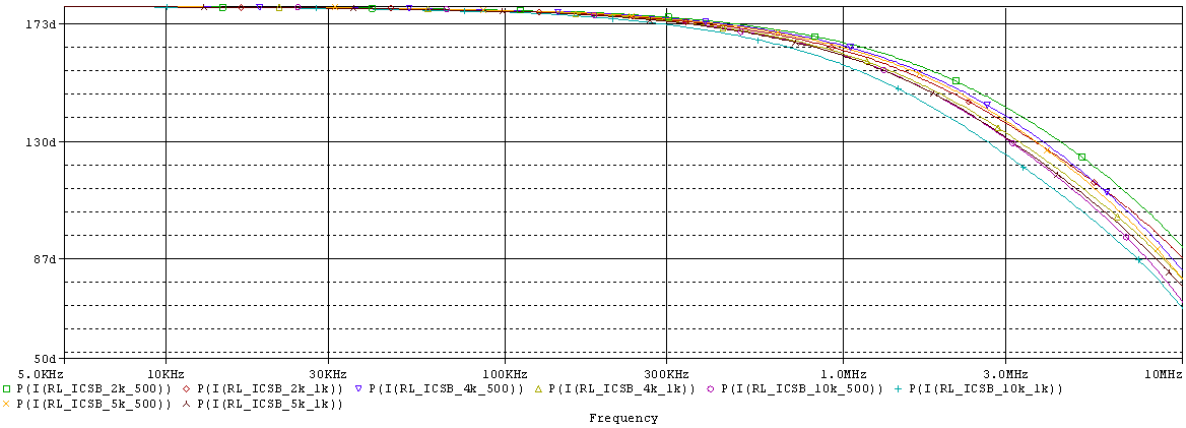

Figure A.15: Phase delay behaviour in the range of 5 to 10000 kHz.

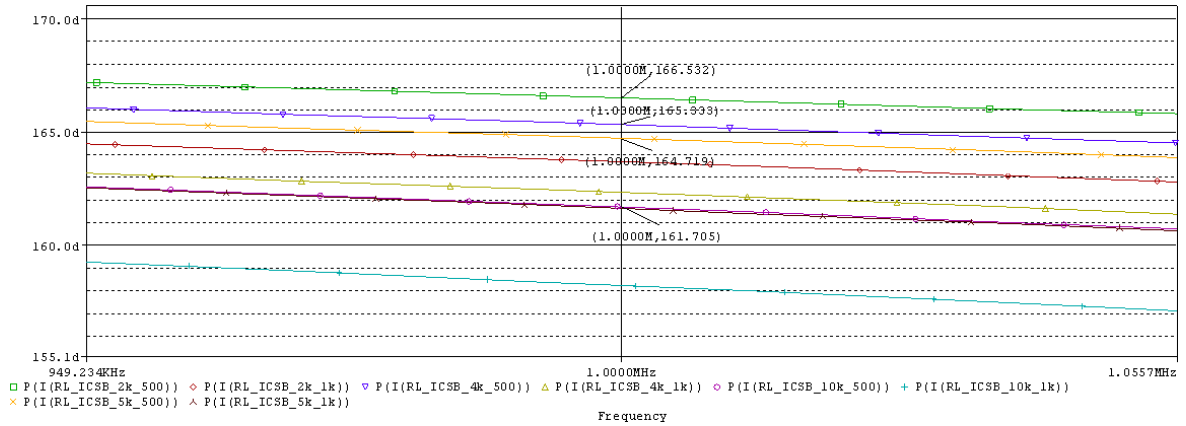

Figure A.16: Phase delay behaviour at 1 MHz.

A.5 Tietze Topology

The transconductance of the source is the function:

$$I_{gen} = \frac{V_{sg}}{R_{4b}} + V_{out}\frac{R_2 - R_3 - R_{4b}}{R_{4b}R_3} \tag{A.10}$$

Although if the condition $R_3 = R_2 - R_{4b}$ is accomplished, the transconductance can be expressed as the function of three resistors:

$$I_{gen} = \frac{V_{sg}}{R_{4b}} \tag{A.11}$$

Current Source Resistors Configuration Test The selected resistor configurations accomplish the design equation $R_3 = R_2 - R_{4b}$. Table A.5 show the resistors selected for the test. From the simulationms one can drawn that the best performance is obtained with the configuration $R_2 = 27\ k\Omega$ and $R_3 = 25.5\ k\Omega$.

R2	R3	R4b
10k	7k5	2k5
17k	14k5	2k5
22k	19k5	2k5
27k	24k5	2k5

Table A.5: Table of Resistor Values for Tietze

Abbreviations used in the following graphics correspond to the next format:

$RL -' namecurrentsource' -' ResistorConfiguration' -' ResistiveLoadValue'$

Simulations

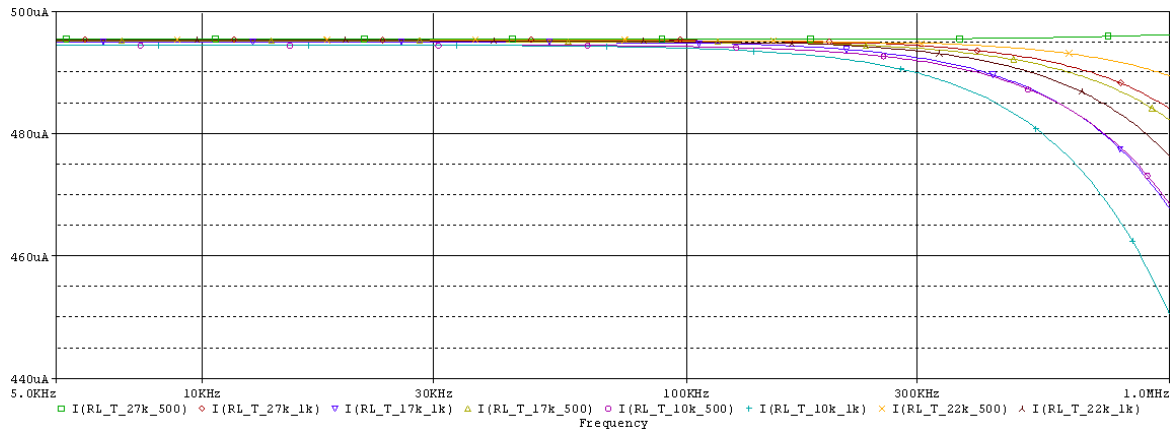

Figure A.17: Current Magnitude behaviour in the range of 5 to 1000 kHz.

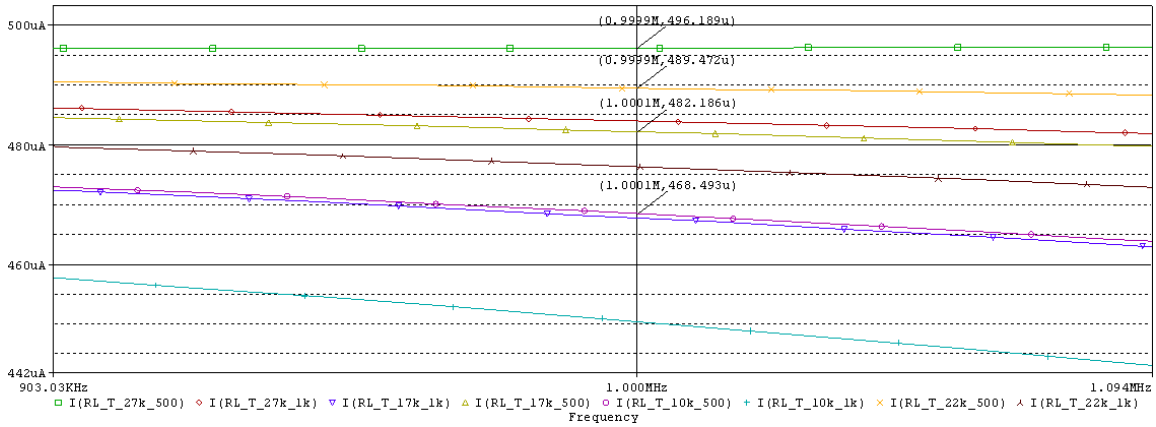

Figure A.18: Current Magnitude behaviour in the range of 1 MHz.

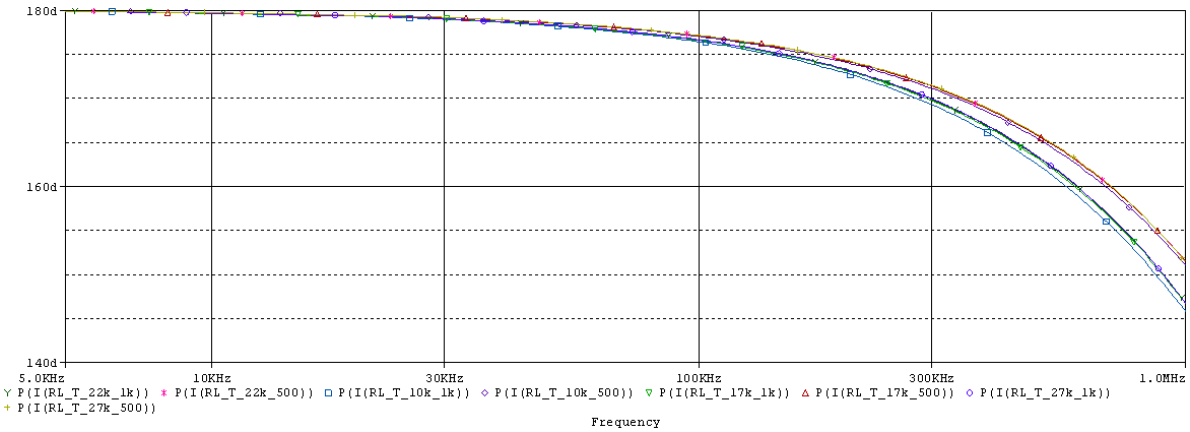

Figure A.19: Phase delay behaviour in the range of 5 to 1000 kHz.

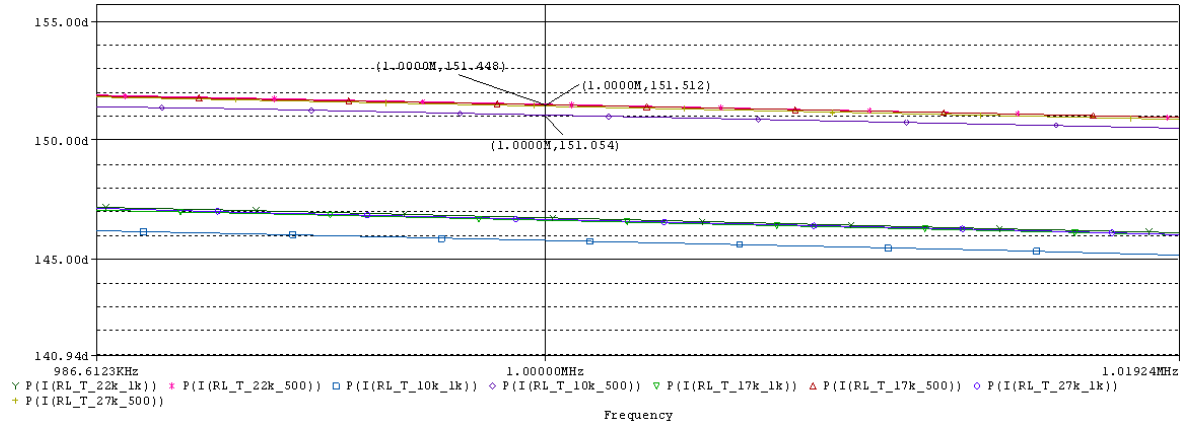

Figure A.20: Phase delay behaviour at 1 MHz.

A.6 Impedance Values for the 'Whole Body' Dummy Model

Frecuency (kHz)	Resistance (Ω)	Reactance (Ω)	Impedance (Ω)	Phase (degrees)
5	667.27	45.29	668.8	3.88
6	665.04	53.53	667.19	4.6
7	661.50	62.14	664.41	5.37
8	657.17	69.98	660.89	6.08
9	652.74	77.76	657.36	6.79
10	648.20	84.46	653.68	7.42
11	642.89	91.25	649.34	8.08
12	637.57	97.49	644.98	8.69
13	631.86	103.01	640.2	9.26
15	620.12	113.33	630.39	10.36
16	614.25	117.85	625.46	10.86
18	602.16	125.39	615.08	11.76
20	589.97	131.54	604.45	12.57
23	572.42	137.99	588.81	13.55
28	545.36	143.32	563.88	14.72
31	530.70	143.97	549.89	15.18
35	513.38	142.91	532.89	15.56
39	498.28	140.22	517.63	15.72
50	466.89	128.93	484.37	15.44
60	447.73	117.31	462.85	14.68
67	437.95	109.54	451.45	14.04
75	429.08	101.50	440.92	13.31
93	415.85	86.17	424.68	11.71
128	402.97	65.56	408.27	9.24
159	397.59	-53.73	401.21	7.7
245	391.48	-35.16	393.06	5.13
273	390.6	-31.44	391.86	4.6
304	389.9	-28.12	390.91	4.13
339	389.39	-25	390.19	3.67
378	389.01	-22.2	389.65	3.27
582	388.15	-12.87	388.37	1.9
649	388.17	-10.85	388.32	1.6
723	388.26	-9.09	388.36	1.34
806	388.43	-7.22	388.5	1.06
1000	388.51	-4.25	388.54	0.63

Table A.6: Impedance Values for the 'Whole Body' Dummy Model

List of Figures

List of Tables

References

[Åbe04] Åberg, P. et a.: Skin cancer identification using multifrequency electrical impedance—a potential screening tool. In: IEEE Trans. Biomed. Eng. 51, no. 12. (2004), S. 2091–2102

[BFA99] Bertemes-Filho, B.H. ; A., Wilson: A comparison of modified Howland circuits as current generators with current mirror circuits. In: Physioloical Measurement. 21 (1999)

[BFBW00] Bertemes-Filho, P. ; Brown, B.H. ; Wilson, A.J.: A comparison of modified Howland circuits as current generators with current mirror type circuits. In: Physiol. Meas. 21 (2000), S. 1–6.

[BFLA04] Bertemes-Filho, P. ; Lima, R.G. ; Amato, M. B. P.: Capacitive-compensated current source used in electrical impedance tomography. In: XII International Conference on Electrical Bio-Impedance, The Gdánsk University of Technology, Poland., 2004

[BH96] Boone, K.G. ; Holder, D.S.: Current Approaches to Analogue Instrumentation Design in Electrical Impedance Tomography. In: Physiol. Meas. 17 (1996), S. 229–247

[BKZS04] Beetner, D. G. ; Kapoor, S. S.AND M. S.AND Manjunath ; Zhou, X. ; Stoecker, W. V.: Differentiation among basal cell carcinoma, benign lesions, and normal skin using electric impedance. In: IEEE Trans. Biomed. Eng. 50, no. 8. (2004), S. 1020–1025

[BRR94] Bragos, R. ; Rosell, J. ; Riu, P.J.: A wide-band AC-coupled current source for electrical impedance tomography. In: Physiol. Meas. 15 (1994), S. A91–A99.

[CAP09] ; Wikimedia Foundation, Inc. (Veranst.): Capacitor. `http://en.wikipedia.org/wiki/Capacitor`. Version: June 2009

[CRB+96] Casas, O. ; Rosell, J. ; Bragós, R. ; Lozano, A. ; Riu, P.J.: A parallel broadband real-time system for electrical impedance tomography. In: Physiol. Meas. 17 (1996), S. A1–A6

[DLAMW97] De Lorenzo, A. ; Andreolli, A. ; Matthie, J. ; Withers, P. J.: Predicting body cell mass with bioimpedance by using theoretical methods: a technological review. In: Appl. Physiol. (1997)

[DP72] David, R.M. ; Portnoy, W.M.: Insulated Electrocardiogram Electrodes. In: Medical and Biological Engineering and Computing 10 (1972), S. 742–751

[DP88] D., Murphy ; P., Rolfe: Aspects of instrumentation design for impedance imaging. In: Clin. Phys. Physiol. Meas., 1 (1988), S. 5–14

[Fou08] FOUSSIER, J.: Entwicklung und Evaluierung einer spannungsgesteuerten Stromquelle für die EIT. Studienarbeit. Lehrstuhl für medizinische informationstechnik., February 2008

[Gar07] GARCÍA, Elena M.: On the Way to a Portable Thirst Sensor. Electronic. CHAIR FOR MEDICAL INFORMATION TECHNOLOGY., August 2007

[Gen05] GENESCA, M. et a.: Electrical bioimpedance measurement during hypothermic rat kidney preservation for assessing ischemic injury. In: Biosens. Bioelectron. 15, no.20. (2005), S. 1866–1871

[GFRH98] GOOVAERTS, H. G. ; FAES, T. J. ; RAAIJMAKERS, E. ; HEETHAAR, R. M.: An electrically isolated balanced wideband current source: basic considerations and design. In: Medical & Biological Engineering & Computing 36 (1998), S. 598–603

[GH74] GUYTON, D.J. ; HAMBRECHT, F.T.: Theory and design of capacitor electrodes for chronic stimulation. In: Medical and Biological Engineering (1974)

[GY84] GRISHANOVICH, A. P. ; YARMOLINSKII, V. I.: Development and trial experience with capacitive electrodes. In: Meditsinskaya Tekhnika. (Lenin Belorussian University, Minsk) 1 (1984), S. 35–39.

[HAN68] HANAI, T. ; DH., Sherman (Hrsg.): Electrical properties of emulsion. Emulsions Science. 1968

[HF09] HOCHBERG, J. ; FOSTER, P.: Four Point Probe I-V Electrical Measurements Using the Zyvex Test System Employing a Keithley 4200. / Zyvex Instruments. 2009. – Forschungsbericht

[Hof08] HOFFMANN, T.: Anwendbarkeit von kapazitiven, isolierten Elektroden in Bioimpedanzspektroskopie-Messungen. Studienarbeit. Lehrstuhl für medizinische informationstechnik., July 2008

[HR07] HERNÁEZ RIOJA, I.: Procesado de señal en comunicaciones: modulación QAM. `http://bips.bi.ehu.es/inma/psc/tema3.pdf`. Version: 2007

[IEE63] IEEE., Proceedings of t. (Hrsg.): A double-balanced modulator. Bd. 51. 1963

[ins00] INSTRUMENTS:, PerkinElmer: Technical note 1000: What is a Lock-in Amplifier. `http://www.cpm.uncc.edu/programs/tn1000.pdf`. Version: 2000

[JEO03] A Precision constant current source for electrical impedance tomography. IEEE, September 2003 (25th Annual International Conference of the IEEE EMBS.). – Jeong Whan Lee, Tong In Oh, Sang Min Paek, Jae Sang Lee, Eung Je Woo.

[JTJ94] JOSSINEC, J. ; TOURTEL, C. ; JANY, R.;: Active current electrodes for in vivo electrical impedance Tomography. In: Physiol. Meas. 15 (1994), S. A83–A90

[Jun05] JUNGBAUER, S: Evaluation con konstantstromquellen für die Medizintchnik. Lehrstuhl für medizinische informationstechnik. Dezember 2005

[Kir99] KIRKHORN, J.: Introduction to IQ-demodulation Of RF-data. In: IFBT, NTNU. 15 (1999)

[KUE06] A Multi-Frequency Current Source for Bioimpedance Application. 2006 (International Special Topic Conference on Information Technology in Biomedicine.). – Kue-Sheng Cheng, Cheng-Yu Chen, Min-Wei Huang, Chien-Hung Chen.

[Kus92] KUSHNER, R.F.: Bioelectrical impedance analysis: a review of principles and applications. In: J Am. Col.l Nutr. 2 (1992), S. 199–209

[LDH+03] LINGWOOD, B.E. ; DUNSTER, K.R. ; HEALY, G.N. ; WARD, L.C. ; COLDITZ, P.B.: Cerebral impedance and neurological outcome following a mild or severe hypoxic/ischemic episode in neonatal piglets. In: Brain Research 969 (2003), S. 160

[Mat05] MATTHIE, J.: Second generation mixture theorie equation for estimating intracellular water using bioimpedance spectroscopy. (2005)

[MB06] MEDRANO, G. ; BECKMANN, L.: Portable Bioimpedance Spectroscopy System. Prague, May 18. 2006.. – Dept. Of Medical Information Technology, Aachen University.

[MBZ+] MEDRANO, G. ; BECKMANN, L. ; ZIMMERMANN, N. ; GRUNDMANN, T. ; GRIES, T. ; LEONHARDT, S.: Bioimpedance Spectroscopy with textile Electrodes for a continuous Monitoring Application.

[MDK67] MONTES, L. F. ; DAY, J. L. ; KENNEDY, L.: The response of human skin to long-term space flight electrodes. In: J. Invest. Dermatol 49 (1967), S. 100–102

[MED07] Skin Electrode Impedance of Textile Electrodes for Bioimpedance Spectroscopy. 2007 (IFMBE Proceedings. 17). – Medrano, G. AND Ubl, A. AND Zimmermann, N. AND Gries, T. AND Leonhardt, S.

[MOD07] Modeling the Influence of Body Position in Bioimpedance Measurements. 2007 (29th Annual International Conference of the IEEE EMBS.). – Medrano, G. AND Leonhardt, S. AND Zhang, P.

[OV70] OLSSON, T. ; VICTORIN, L.: Transthoracic impedance, with special reference to newborn infants and the ratio air-to-fluid in the lungs. In: Acta Paediatr. Scand. 207 (1970)

[Pea08] PEASE, R.A.: A comprensive study of Howland current pump. / National Semiconductor. 2008. – Forschungsbericht

[Pin] PINDADO, R.: Phase Locked-Loop (PLL): Fundamento y aplicaciones. / Departament d'Enginyeria Electrònica. Universitat Politècnica de Catalunya. E.U.E.T.I.T.. – Forschungsbericht

[Pol99] Poletto, C.L.; C.J.; Van D. C.J.; Van Doren: A High Voltage, Constant Current Stimulator for Electrocutaneous Stimulation Though Small Electrodes. 1999

[RCR+98] ROSELL, J. ; COLOMINAS, J. ; RIU, P. ; PALLAS-ARENY, P. ; WEBSTER, J.G.: Skin Impedance From 1 Hz to 1 MHz. In: IEEE TRANSACTIONS ON BIOMEDICAL ENGINEERING 35 (1998)

[RMPAR88] Rosell, J. ; Murphy, D. ; Pallas-Areny, R. ; Rolphe, P.: Analysis and assessment of errors in a parallel data acquisition system for electrical impedance tomography. In: Clin. Phys. Physiol. Meas., 01.9 (1988), S. 98–99

[RSNI03] Ross, A.S. ; Saulnier, G.J. ; Newell, J.C. ; Isaacson, D.: Current source design for Electrical Impedance Tomography. In: Physiol. Meas. 24 (2003), S. 509–516

[SB87] Seagar, A.D. ; Brown, B.H.: Limitations in hardware design in impedance imaging. In: Clin. Phys. Physiol. Meas. 8 (1987), S. 85–90.

[SDSH04] Shröder, J. ; Doerner, S. ; Schneider, T. ; Hauptmann, P.;: Analogue and digital sensor interfaces for impedance spectroscopy. In: Measurement Science and Technology 15 (2004), S. 1271–1278

[Seo05] Seoane, F. et a.: Spectroscopy study of the dynamics of the transencephalic electrical impedance in the perinatal brain during hypoxia. In: Physiol. Meas. 26 (2005), S. 849–863

[SEO06] Current Source for Multifrequency Broadband Electrical Bioimpedance Spectroscopy Systems. A Novel Approach. New York City, USA., 2006 (28th IEEE EMBS Annual International Conference.). – Seoane, F. AND Bragós, R. AND Lindecrantz, J.

[SG92] Steele, J. ; Green, T: Tame those versatile current source circuits. In: Electrical Design. (1992), S. 61–62

[SHSP04] Skourou, C. ; Hoopes, P. J. ; Strawbridge, R. R. ; Paulsen, K. D.: Feasibility studies of electrical impedance spectroscopy for early tumor detection in rats. In: Physiol. Meas. 25 (2004), S. 335–346

[Sis07] Sistemas, Universidad Polit´ecnica de M. Se˜nales y Comunicaciones d. Se˜nales y Comunicaciones C. Se˜nales y Comunicaciones: Electronica y comunicaciones. `http://www.gr.ssr.upm.es/elcm/actual/pdf`. Version: 2007

[Smi90] Smith, R.W.M.: Design of a real-time impedance imaging system for medical application., Department of Electrical and Electrical Engineering, University of Sheffield, UK., Diss., 1990

[Tie02] Tietze, C.; Gamm E. U.; Schenk S. U.; Schenk: Halbleiter-Schaltungstechnik. Springer, 2002

[TSU04] Variable Frequency Bioimpedance Instrumentation. San Francisco, CA, USA., September 2004 (26th Annual International of the IEEE EMBS.). – Tsunami, D. AND McNames, J. AND Colbert, A. AND Pearson, S. AND Hammerschlag, R.

[VK01] Van Kreel, B. K.: Multi-frequency bioimpedance measurements of children in intensive care. In: Med. Biol. Eng. Comput. 39 (2001), S. 551–557

[Whe62] Wheelwright, D. C.: Physiological sensors for use in project Mercury. / NASA Manned Spacecraft Centre. 1962. – Forschungsbericht

[Xit01] Xitron Technologies, (San Diego),: Hydra ECF/ICF (Model 4200) Operation Manual: Bioimpedance Spectrum Analyzer. 2001. – Forschungsbericht